

Testing Quantum Physics on the Large Scale

Lecturer: Rainer Kaltenbaek

Faculty of Mathematics and Physics
University of Ljubljana
IQOQI Vienna
Austrian Academy of Sciences

Vienna, Winter Semester 2021/2022

1 The Quantum Measurement Problem

The quantum measurement problem (QMP) lies at the heart of quantum physics, how we understand it, and how we interpret it. In the literature, you can find many different definitions of that the quantum measurement problem is or how to describe the underlying challenge. To illustrate that, let us look at the following examples of definitions of the measurement problem:

1. Angelo Bassi et al, Ref. [1]
 - a) why are macroscopic objects never found in superposition states?
 - b) why does one get random outcomes according to Born's rule?
2. Časlav Brukner, Ref. [2]
 - a) “small problem”: why does one outcome occur and not another?
 - b) “bigger problem”: how does one arrive at an outcome **or** what makes a measurement a measurement?
3. Maximilian Schlosshauer, Ref. [3]
 - a) the problem of the preferred basis - why do we usually observe positions and not superpositions of positions?
 - b) the problem of the nonobservability of interference - why is it so hard to observe quantum interference?
 - c) the problem of outcomes - (a) why do measurements have outcomes at all?
(b) why one particular outcome and not another?

Of course, there are significant overlaps between some of these definitions. Schlosshauer states in his book[3] that the first two issues he mentions in 3 are essentially “solved” by the phenomenon of decoherence, a topic we will discuss in detail later. The third issue he mentions is identical to the issues states in 2, while 1 focuses on point 3b and on the “small problem” 2a.

In the following, we will concentrate on the “problem of outcomes” etc as described in 2 and 3. One should also note, that some of the definitions of the measurement problem already indicate the cause of the “problem” in the sense that, of course, human

observers will always perceive definite “classical” outcomes. It is not possible to perceive superpositions.

First, let us ask a fundamental question: what **is** a measurement? We can summarize this in the following main points:

- a measurement requires a subject and object, and the procedure should provide **definite** outcomes that are **quantifiable**.
- this requires a separation between subject and object – a cut between the object and the measurement device.
- we need to assign “classical” outcomes to measurement results. That means, they have to be macroscopically distinguishable.

There are several implicit requirements in this description:

- we need to separate the object from the environment. This is an essential part of physics, which always focuses on a specific part of the universe and assumes that it can be described, at least to some extent, separate from the rest of the universe.
- we need quantifiable results. This is an essential part of the scientific method.
- results need to be **intersubjective**. That means, if someone else is doing the same experiment (following the same recipe), they will get the “same” result.

1.1 Which-way information and Schrödinger’s cat

The QMP goes back to the very origin of quantum physics, and it has been at the center of famous discussions between Bohr, Einstein, Schrödinger and other influential scientists of those times (see, e.g., Ref. [4]). The core elements of this discussion can be illustrated by the double-slit experiment and Schrödinger’s cat.

1.1.1 Schrödinger’s cat

In 1935, E. Schrödinger illustrated the QMP in a famous gedankenexperiment. This thought experiments illustrates that it is not as simple as saying the microscopic particles behave strangely, but that this could also have counter-intuitive consequences for macroscopic objects. In particular, he assumed that there is a radioactive atom. By that time, it was already well established that such an atom can decay at any time. As long as it is not decayed, it will be in a superposition of decayed ($|0\rangle_a$) or not decayed ($|1\rangle_a$). Schrödinger’s gedankenexperiment coupled such a superposition state with the life or death of a cat (see Fig. 1).

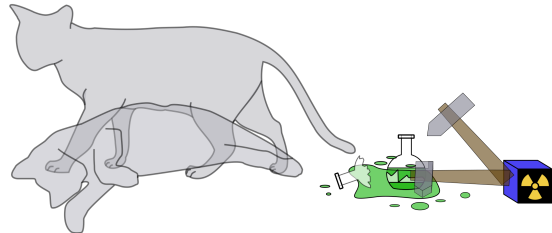


Figure 1: **Schrödinger’s cat.** If a radioactive atom decays, it triggers a “diabolic” mechanism that kills a cat. Because the atom is in a superposition of decayed and not decayed, the cat will be in a superposition of being dead and being alive. The whole setup including the cat is within a box, such that an outside observer will not know the state of the cat unless they open the box[5]. The figure is based on wikimedia, Dhatfield, CC BY-SA 3.0.

If we assume that the cat’s initial state is $|\Psi_0\rangle_c$, the overall initial state will be:

$$\frac{1}{\sqrt{2}}|\Psi_0\rangle_c (|0\rangle_a + |1\rangle_a). \quad (1.1)$$

As long as there is not interaction between the atom and the cat, these states will be separable. If one introduces Schrödinger’s “diabolic mechanism”[5], the decay of the atom will trigger poison that will kill the cat. Because of this interaction, the overall quantum state will become maximally:

$$\frac{1}{\sqrt{2}} (|\text{dead}\rangle_c |0\rangle_a + |\text{alive}\rangle_c |1\rangle_a). \quad (1.2)$$

This superposition state will, of course, only survive as long as there is no interaction with the environment. For that reason, Schrödinger assumed all of that to happen hidden in a box. If one then opens the box, the quantum state will “collapse” in either of the two possibilities due to decoherence.

The state in equation 1.2 is maximally entangled. Based on this, one can get a pure superposition state of the cat being dead and alive if one performs a measurement of the atom state in the diagonal/anti-diagonal basis. Since this is difficult with radioactive atoms, a more convenient approach would be to use an atomic spin state instead. The principle remains the same.

1.1.2 Which-way information and the double-slit experiment

The main prerequisite for seeing matterwave interferometry is that the probability amplitudes leading to interference are indistinguishable. In the case of a double-slit inter-

ferometer, this means that it must be impossible to tell whether a particle detected on the screen passed through one or the other slit. Any information about the path of the particle leaking to the environment will result in a reduction of the interference visibility. We illustrate the two extreme cases of no vs full which-path information in Fig. 2.

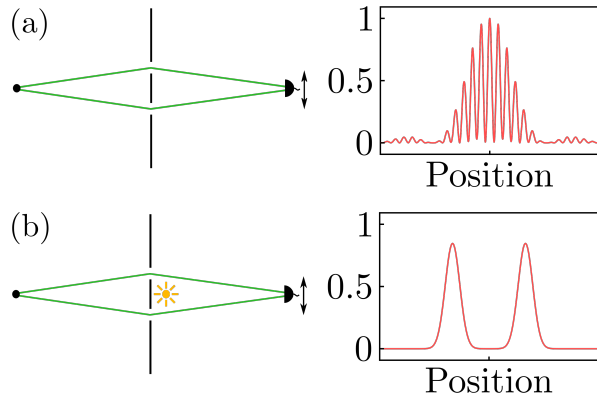


Figure 2: **Double-slit interferometer.** (a) if a particle emitted by the source on the left can go through either of two slits, and if there is no possible way to find out which path the particle took, the distribution of particles on the screen will show an interference pattern. (b) if we put a light source between the slits, then light scattered off the particles can reveal which-path information. How much information is revealed depends on the wavelength of the light. The interference visibility is reduced in accordance with the amount of which-path information that is leaked to the environment. Note that panel (b) is oversimplified because it does not show the diffraction that may occur at each of the individual slits.

As we discuss in the caption of Fig. 2(b), one can in principle tune continuously between seeing no interference and seeing perfect interference by appropriately choosing the wavelength of light scattered off particles passing through the double slit. In order to discuss this continuous tuning of the which-path information and the corresponding reduction of the interference visibility, let us briefly investigate a simpler form of the double-slit experiment.

In particular, let us consider single photons passing through a modified Mach Zehnder interferometer as illustrated in Fig. 3. The modification we do is that we take into account the polarization of the photons passing through the interferometer, and we will put a half-wave plate into one of the interferometer arms. The input state of the interferometer is $|H\rangle_1$, where the index 1 indicates the spatial mode. For simplicity, we will denote this simply with the creation operator $\hat{a}_{H,1}^\dagger$. The beam splitter (BS) acts as

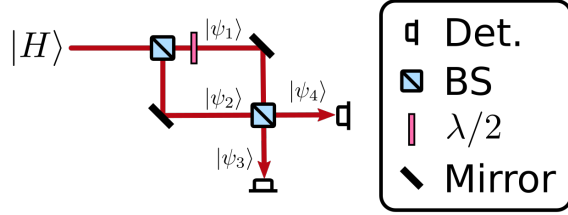


Figure 3: **Modified Mach-Zehnder interferometer.** Consider single photons with horizontal polarization entering the interferometer. At the first beam splitter (BS), the photon can be transmitted or reflected with equal probability. In the transmitted path, the photon travels through a $\lambda/2$ waveplate. When the two paths are mixed again at the second BS, the polarization state of the photon can carry which-path information. The interference visibility will depend on how distinguishable the paths are by if one would measure the polarization.

follows on the creation operator:

$$\hat{a}_{H,1}^\dagger \rightarrow \frac{1}{\sqrt{2}} (\hat{a}_{H,3}^\dagger + i\hat{a}_{H,4}^\dagger), \quad (1.3)$$

where the i results from the reflection at the beam splitter, and 3 and 4 are the output modes of the BS.

The waveplate transforms that into:

$$\frac{1}{\sqrt{2}} (\cos(2\theta)\hat{a}_{H,3}^\dagger + \sin(2\theta)\hat{a}_{V,3}^\dagger + i\hat{a}_{H,4}^\dagger), \quad (1.4)$$

where θ is the angle of rotation of the waveplate. After the second BS, we get:

$$\left[-\sin^2(\theta)\hat{a}_{H,6}^\dagger + i\cos^2(\theta)\hat{a}_{H,5}^\dagger + \frac{1}{2}\sin(2\theta)(\hat{a}_{V,6}^\dagger + i\hat{a}_{V,5}^\dagger) \right], \quad (1.5)$$

with 5 and 6 being the output modes of the second BS. This results in the following probability for getting a horizontally polarized photon in output mode 5:

$$\frac{4\cos^4(\theta)}{3 + \cos(4\theta)}. \quad (1.6)$$

For θ being an integer multiple of π , the polarization in both interferometer arms will be horizontal. That means, there will be no which-path information. Perfect interference will lead to all photons exiting either one or the other output of the interferometer. For θ being an odd multiple of $\pi/4$, the polarization in one of the arm is flipped from H

to V , and there will be no interference. That means, the photons will exit completely randomly at one or the other output of the second BS. For $\theta = \pi$ all horizontal photons exit via output port 6. Why?

1.1.3 Which-way information in more general terms

Let us assume that we have a general superposition like a particle going through a double slit. We will describe that with the following state:

$$|\psi\rangle = \frac{1}{\sqrt{2}} (|\psi_1\rangle + |\psi_2\rangle). \quad (1.7)$$

If our system interacts with an environment that is initially in state $|\chi\rangle$, this interaction can change the state of the environment (information leaks out). If we assume that this interaction leaves our system unchanged, we can describe the change of our overall state as:

$$|\psi\rangle|\chi\rangle \rightarrow \frac{1}{\sqrt{2}} (|\psi_1\rangle|\chi_1\rangle + |\psi_2\rangle|\chi_2\rangle) = |\phi\rangle, \quad (1.8)$$

where we denoted the changed states of the environment as $|\chi_{1,2}\rangle$.

If we now perform a measurement of our system, we will still treat our state as separate from its environment because we cannot perform a measurement on the whole universe but only on the system we are dealing with. To describe the resulting state we are dealing with, we have to **trace out** the environment. This yields the following state:

$$\begin{aligned} \langle\chi_1|\phi\rangle\langle\phi|\chi_1\rangle + \langle\chi_2|\phi\rangle\langle\phi|\chi_2\rangle &= \\ = \frac{1}{2} (|\psi_1\rangle\langle\psi_1| + |\psi_2\rangle\langle\psi_2| + |\psi_1\rangle\langle\psi_2|\langle\chi_2|\chi_1\rangle + |\psi_2\rangle\langle\psi_1|\langle\chi_1|\chi_2\rangle), \end{aligned} \quad (1.9)$$

which we can write as:

$$\frac{1}{2} [|\psi_1(x)|^2 + |\psi_2(x)|^2 + \text{Re}(\psi_1(x)\psi_2^*(x)\langle\chi_2|\chi_1\rangle)]. \quad (1.10)$$

In the last step, we used wave functions as a function of x to better illustrate the situation in a double slit, where we measure the particle distribution as a function of x .

We can see that the interference visibility is proportional to the modulus of the scalar product $\langle\chi_2|\chi_1\rangle$ between the two states of the environment. That means there will be **no interference** iff these two states are orthogonal, which corresponds to perfect distinguishability of the two paths in the interferometer.

If we did not trace out the environment, we would have an “ideal von-Neumann measurement. In general terms, such a measurement works as follows. Instead of a general environment, let us assume that we have a system that is initially in the state $|\psi\rangle$ and a

measurement apparatus that is initially in the state $|a_r\rangle$. To describe the measurement procedure, we will assume that the initial state of the system is a superposition of some basis states $|s_i\rangle$, and that the interaction with the apparatus will change the state of the measurement device to state $|a_i\rangle$. Then the overall state evolves as:

$$|\psi\rangle|a_r\rangle = \left(\sum_i c_i |s_i\rangle \right) |a_r\rangle \rightarrow |\Psi\rangle = \sum_i c_i |s_i\rangle |a_i\rangle. \quad (1.11)$$

As before, we assume that the interaction changes the environment, but that it does not change the state of our system. This is why we call this an “ideal” von-Neumann measurement.

However, this does not yet describe a “collapse” of our state into an eigenstate of the measurement operator, nor is it clear why we should choose a specific basis to describe the system state in. In principle, we could just as well use different basis states $|s'_i\rangle$ and coefficients c' to describe the state of our system, which would result in correspondingly different states $|a'\rangle_i$ of our measurement apparatus:

$$|\Psi\rangle = \sum_i c_i |s_i\rangle |a_i\rangle = \sum_i c'_i |s'_i\rangle |a'_i\rangle. \quad (1.12)$$

This brings us back to one of the parts of the quantum measurement problem we described in the beginning: why do we observe macroscopic states usually rather in the position basis than in some other basis consisting of superpositions of position states - e.g. in the basis of momentum states?

An attempt to explain the appearance of a preferred basis has been made by Zurek, Zeh and others with the concept of pointer states and “superselection”[6, 7] as well as “quantum darwinism”[8]. The central idea is that some basis states are more robust against decoherence than others. For example, we can describe the state of the Schrödinger cat in the basis of states $|\text{dead}\rangle$ and $|\text{alive}\rangle$, but we could also describe the cat’s state in the basis consisting of the states:

$$\frac{1}{\sqrt{2}} (|\text{dead}\rangle \pm |\text{alive}\rangle). \quad (1.13)$$

Obviously, these basis states will not be very long lived if our cat interacts with its environment.

This approach is consistent with an essential **cut** between subject an object and with the isolation of the system under investigation from the rest of the universe because a good measurement device will be such that the result-states remain well distinguishable even when it interacts with the environment.

The “preferred basis” consists of states that are often referred to as **pointer states**.

1.2 Why is it so difficult to observe macroscopic superpositions?

Already in the last sections, we implicitly assumed what we can call an “operational explanation”: the reason it is difficult to observe macroscopic superpositions is that more massive and more complex quantum systems will have even more ways to interact with the environment, which will lead to **decoherence**.

We saw earlier that we will have no interference (complete decoherence) if the coupling to the environment leads to changes in the state of the environment such that those states of the environment will be orthogonal ($\langle \chi_1 | \chi_2 \rangle = 0$ in equation 1.10). We will see in a later lecture that this scalar product often does not vanish immediately but that it will decay exponentially. That means, we will have something like:

$$\langle E_i(t) | E_j(t) \rangle \propto e^{-t/\tau_d}, \quad (1.14)$$

where t is the elapsingtime, τ_d is the characteristic decoherence timescale, and $|E_{i,j}\rangle$ are different states of the environment. This also means, that can increase the lifetime of our superposition if we better isolate our system from its environment. This exponential decay of superposition states then also explains why some bases that are less prone to decoherence will seem to be preferred with respect to others (superselection).

Decoherence explains the following:

- why it is hard to observe macroscopic superpositions.
- why there are preferred bases for measurements.

Decoherences **does not** explain:

- why there are definitive outcomes in the first place.
- why we see one outcome instead of another.

1.3 Interpretations of Quantum Physics

The quantum measurement problem, the quantum superposition principle, and the very formal way in which quantum physics tells us what we can say about the physical world are some of the main reasons why there are so many different interpretations of quantum physics. For that reason, let us now look at some common examples of interpretations of quantum physics in the present context.

1.3.1 Shut up and calculate

While this is not an interpretation, it is a possible approach. Quantum physics is one of the most successful physical theories we have. Proponents of this **operational approach** essentially say that we have a very good theory, so let us simply use it and not worry about any philosophical implications as long as they do not affect what the theory predicts and how well it agrees with the experimental results. In other words: we do not really need an interpretation - the theory works well without it.

1.3.2 The appearance of the classical world due to decoherence

In the strict sense, this is also not an interpretation - it is more an operational approach similar to subsection 1.3.1. It assumed that we live in a classical world because quantum superpositions decohere rapidly due to interactions with the environment (especially macroscopic superpositions). **But** this does not “solve” the measurement problem. It just keeps steadily increasing the parts of the universe entangled with a system that is interacting with its environment.

Also:

- this does not explain “why” we get specific outcomes (the “small” and in my opinion irrelevant outcome problem).
- this does not explain a “completely classical” world because it simply means that we would eventually end up having entanglement between pretty much everything. However, see our later discussion of “for all practical purposes” (FAPP) in subsection 1.3.7.

1.3.3 The Copenhagen Interpretation

One could say that this is the “standard” interpretation of quantum physics. It is called “Copenhagen” interpretation because it is based on the views expressed by Niels Bohr in his famous letter exchanges with Einstein[4].

Let us summarize this interpretation with the following postulates:

1. measurement devices are “classical” devices. That means, they have definite outcomes, and there are no superpositions.
2. deterministic (unitary) evolution according to Schrödinger’s equation **before** the measurement
3. probabilistic “collapse” into a distinct classical outcome according to Born’s rule.

Postulate one is sometimes interpreted as the division between the microscopic and the macroscopic world (see, e.g., Ref. [1]).

1.3.4 Bohmian mechanics

This is essentially a non-local hidden-variable theory that exactly reproduces the results of non-relativistic quantum mechanics. Note that “non-relativistic” in principle also means that there are, e.g., also no photons because one would need quantum electrodynamics for that. However, one needs to keep in mind that we also often simply use standard non-relativistic quantum mechanics to describe experiments done with photons. An example are tests of Bell’s inequality using photons.

The central idea behind Bohm’s interpretation is that the wavefunction is a **real** physical quantity that essentially act as guiding waves for particles. Measurements collapse a wavefunction **immediately**. That is why the Bohmian model is inherently nonlocal. The collapse of the wavefunction exerts a force on the guided particle that will result in the perceived measurement outcome.

Because the Bohmian model is based on the evolution of the wavefunction following the laws of quantum physics, the predictions of the Bohmian model are necessarily identical with the predictions of quantum physics. However, one can hope that measurements involving relativistic observers might some day allow for a decisive test of the Bohmian model.

1.3.5 The many-worlds interpretation

This interpretation assumes that there **is no collapse**. Instead, observers themselves are treated as quantum systems. Consider the following situation, where an observer that is initially in the state $|O\rangle$ interacts with a measurement apparatus that, in turn, interacts with a quantum system that is initially in a quantum superposition of two states. The measurement will then entangle the state of the observer with the measured system depending on the outcome of the measurement:

$$\begin{aligned} |\Psi\rangle &= |O\rangle \otimes |A\rangle \left[\frac{1}{\sqrt{2}} (|\psi_1\rangle + |\psi_e\rangle) \right] \\ &\rightarrow \frac{1}{\sqrt{2}} (|O_1\rangle |A_1\rangle |\psi_1\rangle + |O_2\rangle |A_2\rangle |\psi_e\rangle), \end{aligned} \quad (1.15)$$

where the state $|A_i\rangle$ corresponds to the measurement apparatus showing result i , and $|O_i\rangle$ corresponds to the state of the observer having seen outcome i on the apparatus.

Whenever an observer interacts with the environment, they will perceive a specific outcome, and they will perceive to exist in a world where that outcome has occurred. Since our world contains many observers, and because each observer constantly interacts with the environment in a multitude of ways, this effectively means that there exist essentially infinitely many “perceived” worlds.

This does not necessarily mean that there are infinitely many universes, but there are infinitely many perceived universes. You can find recent considerations about the many-

world interpretation in Refs. [9, 10]. You can also read more about this interpretation in Ref. [11].

Often interpretations of quantum physics are considered to be just a “matter of taste” in the sense that one cannot experimentally distinguish between those interpretations. This might not be strictly correct. For example, we mentioned in the previous section that it is conceivable that experiments with relativistic observers might be able to test the Bohmian interpretation. While it might seem to be even more difficult to test the many-worlds interpretations, D. Deutsch proposed a gedankenexperiment (thought experiment) that could, in principle, test the many-worlds interpretation[12]. This gedankenexperiment is also described in Ref. [2], and we will follow their description.

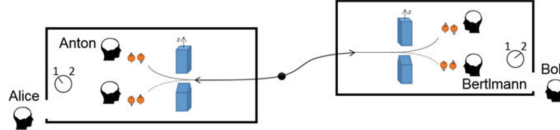


Figure 4: **Deutsch’s test of the many-world interpretation.** Superobservers Alice and Bob perform a Bell-type experiment involving observers Anton and Bertlmann. The experiment tests whether there is a “co-existence” of facts between the various observers or not. The figure is from Ref. [2]

The idea of the gedankenexperiment is illustrated in Fig. 4. In two spatially separated boxes that are shielded from their environment, two observers Anton and Bertlmann perform experiments on particle pairs entangled in their spin. They do so by performing Stern-Gerlach measurements. Let us assume that the shared entangled pairs are in the state

$$|\phi\rangle = \frac{1}{\sqrt{2}} (| \uparrow \rangle | \downarrow \rangle - | \downarrow \rangle | \uparrow \rangle). \quad (1.16)$$

We will index the states of observers Anton and Bertlmann depending on whether they observe the result “up” or “down”. Then our superobservers will ascribe the following state to the two observers ($|A, B\rangle$ for Anton and Bertlmann):

$$|\psi_{AB}\rangle = \frac{1}{\sqrt{2}} (|A_{\text{up}}\rangle |B_{\text{down}}\rangle - |A_{\text{down}}\rangle |B_{\text{up}}\rangle). \quad (1.17)$$

Our superobservers can now decide to measure the states of Anton and Bertlmann in

one of the two following basis:

$$\begin{aligned} A_z &= |A_{\text{up}}\rangle\langle A_{\text{up}}| - |A_{\text{down}}\rangle\langle A_{\text{down}}| \\ A_z &= |A_{\text{up}}\rangle\langle A_{\text{down}}| + |A_{\text{down}}\rangle\langle A_{\text{up}}| \\ B_1 &= \frac{1}{2}(B_z + B_x) \\ B_2 &= \frac{1}{2}(B_z - B_x), \end{aligned} \tag{1.18}$$

where $B_{z,x}$ with Bertlmann bases equivalently as we defined $A_{z,x}$ for Anton.

If Alice and Bob can randomly choose between these measurements, they can test if the corresponding results violate a Bell-type inequality. If they violate the inequality, this shows that there were no local hidden variables. In this case, the local hidden variables would be the knowledge of Anton and Bertlmann. That means, a violation of that Bell-type inequality would show that there is no common reality between these observers. This would confirm the many-world interpretation (or rule it out).

Admittedly, it is unlikely that this gedankenexperiment will performed some day, but it shows that an experimental test would, in principle, be possible.

1.3.6 Collapse models

The idea behind collapse models is to add nonlinear modifications to the Schrödinger equation that will eventually lead to an actual “collapse” of the wave function and “solve” the measurement problem in this way. The deviations from the Schrödinger equation are chosen such that they depend on the mass of the observed system and on the size of superposition states. The parameters are chosen such that the predictions of the collapse model agree with quantum physics for microscopic superpositions, but that superpositions will quickly decohere if they involve massive objects we perceive in our everyday experience. We will discuss these collapse models in more detail later.

1.3.7 FAPP irreversibility

The concept of attempting to solve the quantum measurement problem because decoherence will destroy macroscopic superpositions irreversibly **for all practical purposes** (FAPP) is, e.g., described by Č. Brukner[2].

In subsection we said that decoherence alone does, in principle, not solve some elements of the measurement problem. The argument was that the time evolution according to quantum physics is unitary. That means, while our quantum system will become more and more entangled with the environment, this evolution is in principle reversible. That means, we could in principle reverse the time evolution and recover the original quantum state. The superposition will not “collapse”.

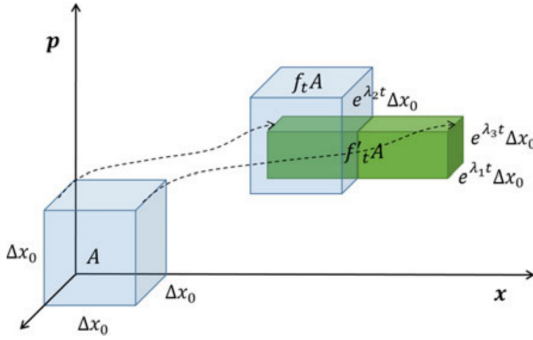


Figure 5: **Evolution in phase space.** A is the phase space volume before an evolution in time. Under deterministic conditions, the phase space volume will evolve to $f_t A$. If there are small fluctuations in the evolution, the phase space will evolve to $f'_t A$. If we try to reverse this evolution, additional errors will occur because of additional fluctuations and because we can never **exactly** know and implement the Hamiltonian determining the evolution. The figure is from Ref. [2]

This concept is illustrated in Fig. 5. The general idea is that, if a system and its interaction with the environment is sufficiently long and/or complicated, it will soon become **effectively** impossible to reverse the evolution occurring due to the interaction of a system with its environment.

While quantum evolution is, in principle, reversible, this is a very theoretical concept. The more and the longer our quantum system interacts with its environment, the more the system becomes entangled with ever more parts of our universe. This entanglement will not only become more and more diluted, there will also be more and more fluctuations influencing that evolution. We will often, even in principle, not be able to know in detail about each quantum fluctuation.

That means we would not be able to apply an exact inverse of the total Hamiltonian that acted on our system. Even if we did, there would again be additional quantum fluctuations disturbing that inverse evolution. That is the reason why, if a superposition has interacted long and/or strongly enough with the environment, this evolution will become **irreversible FAPP**.

1.4 Summary

Let us briefly summarize what we have learned so far about which aspects of the quantum measurement problem (QMP) are solved by decoherence:

- solved: problem o the preferred basis → decoherence-induced **pointer states**

- solved: problem of non-observability of macroscopic
- unclear: problem of outcomes → not solved by decoherence *unless* one accepts that it is sufficient that environmental decoherence is irreversible for all practical purposes (FAPP). This boils down to an interpretational or philosophical issue.

2 A formal description of environmental decoherence

After discussing earlier how decoherence can help us to address most (if not all) aspects of the quantum measurement problem (QPM), we now want to give a more detailed description how to describe the occurrence and the effects of decoherence in a more formal way.

Let us begin by describing the interaction between the state of a quantum system and its environment in terms similar to the ideal von-Neumann measurement. If the initial states of the quantum system and the environment are $|\psi\rangle$ and $|\chi\rangle$, respectively, then we can approximate the change of the states due to the interaction as:

$$|\psi\rangle|\chi\rangle = (a_u|\phi_i\rangle)|\chi\rangle \rightarrow \sum a_i|\phi_i\rangle|\chi\rangle. \quad (2.1)$$

Here, we assumed that we can write our quantum state in a basis $|\phi_i\rangle$, and that the interaction will not change the state of our system, such that the a_i and the $|\phi_i\rangle$ remain the same. While this is a strong assumption, in principle, it is also one that typically works rather well. A more general treatment is possible but way more complicated.

The main point of equation 2.1 is that the interaction between system and environment will entangle system and environment. If we trace out the environment, this will cause decoherence.

2.1 Decoherence via elastic scattering

We will now aim to describe this effect in more detail, and we will use the formalism we develop to describe the effects of decoherence due to some typical interactions:

- the scattering of gas particles
- the emission, absorption and the scattering of (thermal) photons.

These effects are important because one always has to take them into account because one never has perfect vacuum, and one never can avoid thermal radiation. We can cool down the environment temperature, but there will always be thermal photons present - only their wavelength will change.

These two examples will also help us to distinguish between two limiting cases. In the case of gas collisions, the de Broglie wavelength can often be small compared to the size

of macroscopic superpositions. In that case, a single scattering event will already carry away sufficient information to the environment to cause significant decoherence. In the other extreme, the wavelength of thermal photons λ_{th} often can be very large compared to the characteristic dimensions of our system. That means:

$$\Delta x \ll \lambda_{\text{th}} \text{ and } r \ll \lambda_{\text{th}}, \quad (2.2)$$

where Δx denotes the size of our superposition, and r denotes the size of our system (e.g. the radius of a spherical particle). In this case, we can say that the scattering interaction is in the **Rayleigh regime**.

In order to formally describe decoherence, let us first consider the effect of a single scattering event. Let us describe the state of our system by a position eigenstate $|\mathbf{x}\rangle$, which denotes that our system is at position \mathbf{x} , and let us assume that the environment is in the initial state $|\chi_i\rangle$. We can describe the action of the scattering event via a **scattering operator** \hat{S} . This is sometimes referred to as the “S-matrix”. Then the scattering will change the initial state according to:

$$|\mathbf{x}\rangle|\chi_i\rangle \rightarrow \hat{S}|\mathbf{x}\rangle|\chi_i\rangle. \quad (2.3)$$

Let us now rewrite the position eigenstate using the translation operator:

$$|\mathbf{x}\rangle = e^{-i\hat{\mathbf{p}}\cdot\mathbf{x}}|\mathbf{x}=0\rangle = e^{-i\hat{\mathbf{p}}\cdot\mathbf{x}}|0\rangle, \quad (2.4)$$

where we use $|0\rangle$ to denote the position eigenstate for the origin of our coordinate system.

Then we can write the action of the scattering event as:

$$\hat{S}_0 e^{-i\hat{\mathbf{p}}\cdot\mathbf{x}}|0\rangle|\chi_i\rangle \rightarrow \hat{S}_0 e^{-i(\hat{\mathbf{p}}+\hat{\mathbf{q}})\cdot\mathbf{x}}|0\rangle e^{+i\hat{\mathbf{q}}\cdot\mathbf{x}}|\chi_i\rangle, \quad (2.5)$$

where we defined:

- $\hat{\mathbf{p}}$...the momentum operator for our system
- $\hat{\mathbf{q}}$...the momentum operator for the scattered particle
- $\hat{\mathbf{P}} = \hat{\mathbf{p}} + \hat{\mathbf{q}}$...the momentum operator for the composite system,

and we used an index 0 on the scattering operator because it describes scattering from a particle at position 0.

Because the interaction will not change the total momentum, we can assume that the scattering operator and the operator for the composite momentum commute: $[\hat{S}, \hat{\mathbf{P}}] = 0$, and we can rewrite equation 2.1 as:

$$e^{-i(\hat{\mathbf{p}}+\hat{\mathbf{q}})\cdot\mathbf{x}}\hat{S}_0|0\rangle e^{i\hat{\mathbf{q}}\cdot\mathbf{x}}|\chi_i\rangle = |\mathbf{x}\rangle e^{-i\hat{\mathbf{q}}\cdot\mathbf{x}}\hat{S}_0 e^{i\hat{\mathbf{q}}\cdot\mathbf{x}}|\chi_i\rangle = |\mathbf{x}\rangle \hat{S}_{\mathbf{x}}|\chi_i\rangle. \quad (2.6)$$

Here we made the implicit and important assumption that the scattering does **not** affect the momentum of our system. This is, e.g., okay if the mass of the scattered particles is much less than the mass of our system. A more general approach is described in Ref. [13]. In equation 2.6, we first exchanged the order of the translation operator for the scattered particle and scattering operator with the state $|0\rangle$, and then we defined the translated scattering operator

$$\hat{S}_{\mathbf{x}} = e^{-i\hat{\mathbf{q}} \cdot \mathbf{x}} \hat{S}_0 e^{i\hat{\mathbf{q}} \cdot \mathbf{x}}. \quad (2.7)$$

Think: why can we do that?

The scattering operator now acts on the environment state, and overall we can write:

$$|\mathbf{x}\rangle |\chi_i\rangle \rightarrow |\mathbf{x}\rangle \hat{S}_{\mathbf{x}} |\chi_i\rangle = |\mathbf{x}\rangle |\chi(\mathbf{x})\rangle. \quad (2.8)$$

Now that we know how a single scattering event affects a position basis state, we can also write down how it will affect a more general state. In particular, let us look at the action on a product state of density matrices - one for our quantum system, one for the environment. Initially (for time $t = 0$), we can write this as:

$$\hat{\rho}(0) = \hat{\rho}_S(0) \otimes \hat{\rho}_E(0) = \int d^3x \int d^3x' \rho_s(\mathbf{x}, \mathbf{x}', 0) |\mathbf{x}\rangle \langle \mathbf{x}'| \otimes |\chi_i\rangle \langle \chi_i|, \quad (2.9)$$

where we assumed that the initial state of the environment is pure.

The scattering event will transform this into:

$$\hat{\rho} = \int d^3x \int d^3x' \rho_s(\mathbf{x}, \mathbf{x}', 0) |\mathbf{x}\rangle \langle \mathbf{x}'| \otimes |\chi(\mathbf{x})\rangle \langle \chi(\mathbf{x}')|, \quad (2.10)$$

and if we trace out the environment, we get:

$$\hat{\rho}_S = \text{Tr}_E(\hat{\rho}) = \int d^3x \int d^3x' \rho_s(\mathbf{x}, \mathbf{x}', 0) |\mathbf{x}\rangle \langle \mathbf{x}'| \langle \chi(\mathbf{x}') | \chi(\mathbf{x}) \rangle. \quad (2.11)$$

The scalar product $\langle \chi(\mathbf{x}') | \chi(\mathbf{x}) \rangle$ is analogue to the scalar product between environmental states that we already saw reducing the visibility of quantum interference. Let us denote this scalar product as the **decoherence factor**. We will now aim to calculate it.

In order to simplify the calculation in the momentum eigenbasis, let us express \hat{S}_0 in terms of \hat{T} (the T -Matrix):

$$\hat{S}_0 = \hat{I} + i\hat{T}. \quad (2.12)$$

\hat{I} is the identity operator. One can write the matrix element of \hat{T} in the momentum basis as:

$$\langle \mathbf{q} | \hat{T} | \mathbf{q}' \rangle = \frac{i}{2\pi\hbar q} \delta(q - q') f(\mathbf{q}, \mathbf{q}') = \frac{i}{2\pi\hbar m} \delta(E - E') f(\mathbf{q}, \mathbf{q}'). \quad (2.13)$$

Here, the Dirac delta between E and E' ensures energy conservation, which will be fulfilled if we assume elastic scattering. m is the mass of the scattered particle, and $f(\mathbf{q}, \mathbf{q}')$ is the **scattering amplitude**. Its modulus squared is the **scattering cross section**, which one can determine experimentally:

$$|f(\mathbf{q}, \mathbf{q}')|^2 = \frac{d\sigma}{d\Omega} \equiv \frac{\text{scattered flux}}{\text{incident flux}}. \quad (2.14)$$

We will now try to relate that to the decoherence factor following the description of M. Schlosshauer[3] (starting on page 123). First, we assume that the scattered particle is restricted to a “box-normalization” volume V , which allows us to introduce normalized momentum eigenstates, and we can then later take the continuum limit again:

$$|\tilde{q}\rangle \equiv \left[\frac{(2\pi\hbar)^3}{V} \right]^{1/2} |\mathbf{q}\rangle. \quad (2.15)$$

In this basis, we can write $\hat{\rho}_E$ as:

$$\rho_E(0) = \frac{(2\pi\hbar)^3}{V} \sum_{\mathbf{q} \in Q_V} \mu(\mathbf{q}) |\tilde{q}\rangle \langle \tilde{q}|, \quad (2.16)$$

where Q_V are all states fulfilling the boundary conditions of volume V . We will use that \hat{T} is diagonal in the normal **and** in the normalized momentum basis.

First, let us write down our decoherence factor:

$$\begin{aligned} \langle \chi(\mathbf{x}' | \chi(\mathbf{x}) \rangle &= \frac{(2\pi\hbar)^3}{V} \sum_{\mathbf{q} \in Q_V} \mu(\mathbf{q}) e^{i\mathbf{q} \cdot (\mathbf{x} - \mathbf{x}')/\hbar} \langle \tilde{q} | \hat{S}_0^\dagger e^{-i\mathbf{q} \cdot (\mathbf{x} - \mathbf{x}')/\hbar} \hat{S}_0 | \tilde{q} \rangle = \\ &= \frac{(2\pi\hbar)^3}{V} \sum_{\mathbf{q} \in Q_V} \mu(\mathbf{q}) [1 - \langle \tilde{q} | \hat{T} \hat{T}^\dagger | \tilde{q} \rangle + e^{i\mathbf{q} \cdot (\mathbf{x} - \mathbf{x}')/\hbar} \langle \tilde{q} | \hat{T}^\dagger e^{-i\mathbf{q} \cdot (\mathbf{x} - \mathbf{x}')/\hbar} \hat{T} | \tilde{q} \rangle], \end{aligned} \quad (2.17)$$

where we used $\hat{S}_0 = \hat{I} + i\hat{T}$, and that \hat{T} commutes with the scattering momentum operator.

If one uses the completeness relation on our quantization volume:

$$\sum_{\mathbf{q} \in Q_V} |\tilde{q}\rangle \langle \tilde{q}| = \hat{I}_V, \quad (2.18)$$

one can rewrite equation 2.17 as:

$$\langle \chi(\mathbf{x}' | \chi(\mathbf{x}) \rangle = \frac{(2\pi\hbar)^3}{V} \sum_{\mathbf{q} \in Q_V} \mu(\mathbf{q}) \left[1 - \sum_{\mathbf{q}' \in Q_V} \left(1 - e^{i(\mathbf{q} - \mathbf{q}') \cdot (\mathbf{x} - \mathbf{x}')/\hbar} \right) \left| \langle \tilde{q} | \hat{T} | \tilde{q} \rangle \right|^2 \right]. \quad (2.19)$$

One can then take the continuum limit

$$\frac{(2\pi\hbar)^3}{V} \sum_{\mathbf{q} \in Q_V} \rightarrow \int d^3q \quad (2.20)$$

and get:

$$\langle \chi(\mathbf{x}') | \chi(\mathbf{x}) \rangle = 1 - \int d^3q \left(1 - e^{(\mathbf{q}-\mathbf{q}') \cdot (\mathbf{x}-\mathbf{x}')/\hbar} \right) |\langle \tilde{q} | \hat{T} | \tilde{q} \rangle|^2. \quad (2.21)$$

The expectation value of \hat{T} modulus squared gives:

$$|\langle \tilde{q} | \hat{T} | \tilde{q} \rangle|^2 = \frac{1}{(2\pi\hbar m)^2} \delta^2(E - E') |f(\mathbf{q}, \mathbf{q}')|^2. \quad (2.22)$$

A potentially big issue here is, of course, the square of the Dirac delta, but if one uses the relation

$$\delta(E - E') = \lim_{T \rightarrow \infty} \frac{1}{2\pi\hbar} \int_{-T/2}^{T/2} dt e^{i(E-E')t\hbar}, \quad (2.23)$$

one can write the square of the Dirac delta as:

$$\delta^2(E - E') = \delta(E - E') \lim_{T \rightarrow \infty} \frac{T}{2\pi\hbar}. \quad (2.24)$$

While this, of course, does not converge, one does not need to let T go to infinity. It is sufficient to choose a fixed value for T that is much longer than the time scale of the scattering event and much shorter than the characteristic time scale of decoherence of many particles are scattered.

Then one can write:

$$\delta^2(E - E') \approx \delta(E - E') \frac{T}{2\pi\hbar} = \delta(q - q') \frac{m}{q} \frac{T}{2\pi\hbar}. \quad (2.25)$$

This approximation is invalid if a few scattering events already destroy the coherence. The Dirac delta with the momenta again indicates that we are dealing with elastic scattering.

Using approximation 2.25, we can now write how a single scattering event changes our density matrix:

$$\begin{aligned} & \rho_S(\mathbf{x}, \mathbf{x}', T) - \rho_S(\mathbf{x}, \mathbf{x}', 0) \\ &= -\rho_S(\mathbf{x}, \mathbf{x}', 0) \frac{T}{V} \int d^3q \mu(\mathbf{q}) v(\mathbf{q}) \int d^3\hat{\mathbf{n}}' \left(1 - e^{i(\mathbf{q}-\mathbf{q}') \cdot (\mathbf{x}-\mathbf{x}')/\hbar} \right) |f(\mathbf{q}, q\hat{\mathbf{n}}')|^2. \end{aligned} \quad (2.26)$$

Here, we introduced $\hat{\mathbf{n}}' = \mathbf{q}'/q'$, and the speed of particles with momentum q . This speed is q/m for massive particles and c for photons.

Equation 2.26 gives the change of the density matrix due to a single scattering event. If there are N particles scattered, we multiply the right-hand side with N . Then the ratio N/V appears, which is simply the particle density.

We can simplify our description if the particle distribution is isotropic - e.g., for an ideal gas. Then we can write:

$$\mu(\mathbf{q}) = \frac{1}{4\pi} \xi(q) dq d\hat{\mathbf{n}}. \quad (2.27)$$

Here, $\xi(q)$ is the probability density to get q momentum, independent of the direction. ξ should be chosen such that $\int dq \xi(q) = N/V$.

If we divide equation 2.26 by T and then take the limit of $T \rightarrow 0$, we get the time derivative of the density matrix:

$$\frac{\partial \rho_S(\mathbf{x}, \mathbf{x}', t)}{\partial t} = -F(\mathbf{x} - \mathbf{x}') \rho_S(\mathbf{x}, \mathbf{x}', t). \quad (2.28)$$

Here, we defined the localization rate F as:

$$F(\mathbf{x} - \mathbf{x}') = \int dq \xi(q) v(q) \int \frac{d^3 n d^3 n'}{4\pi} [1 - e^{iq(\hat{\mathbf{n}} - \hat{\mathbf{n}}') \cdot (\mathbf{x} - \mathbf{x}')/\hbar}] |f(q\hat{\mathbf{n}}, q\hat{\mathbf{n}}')|^2. \quad (2.29)$$

It destroys coherent spatial coherences (superpositions) between different positions.

After this relatively general description of decoherence due to scattering, we can now apply it to specific scenarios by properly choosing the scattering amplitude f , the momentum distribution ξ as well as $v(q)$.

To summarize, Schlosshauer states that his derivation, which we followed here, is based on five assumptions:

1. the initial states ρ_S, E are uncorrelated
 2. the scattering interaction is invariant under translation of the complete system (environment + quantum system)
 3. the center of mass of our quantum object is not disturbed by the scattering event
 4. the rate of scattering is much faster than any internal dynamics of the object
 5. the scattered particles are distributed isotropically (assumption towards the end)
- An additional assumption was the replacement of δ^2 with $\delta \times T$.

2.2 Full versus partial which-path information

How strongly a scattering event decoheres our quantum system depends on how much information the event carries away into the environment. For example, let us assume

that we have a massive, spherical **test particle** with radius r in a superposition state of being either at position \mathbf{x} or at position \mathbf{x}' . Let $\Delta x = |\mathbf{x} - \mathbf{x}'|$ denote the size of our superposition.

If our system is now subjected to scattering events with particles of a wavelength λ_0 , we need to compare λ with the characteristic dimensions r and Δx of our quantum system. Based on this comparison, we can now distinguish between two extreme cases:

1. the **short-wavelength limit**, where $\lambda_0 \ll r, \Delta x$
2. the **long-wavelength limit**, where $\lambda_0 \gg r, \Delta x$

We will discuss how our formal treatment simplifies in these two cases.

2.2.1 The short-wavelength limit

If $\lambda_0 \ll \Delta x$ each scattered particle will carry away significant information about the position of our test particle. The de Broglie wavelength associated to the scattered particle is $q_0 = 2\pi\hbar/\lambda_0$, and $\lambda_0 \ll \Delta x$ results in:

$$\frac{q_0 \Delta x}{\hbar} \gg 1. \quad (2.30)$$

Because we are dealing with elastic scattering, this will also be true for q'_0 , and then the exponent on the right-hand side of equation 2.29 will oscillate very rapidly and average out to good approximation.

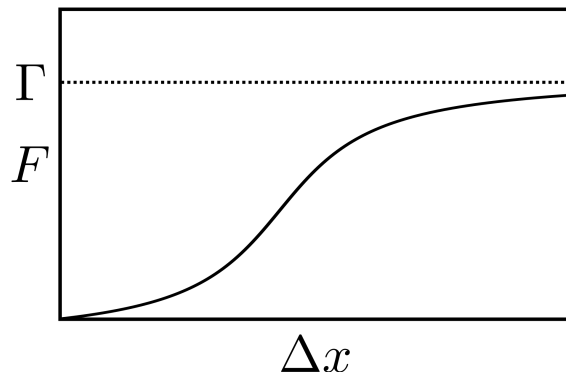


Figure 6: **Saturation of the localization rate.** The localization rate F changes as a function of the size of our superposition. For large Δx , the localization rate will eventually saturate and take a constant value Γ .

What is left in that integral will yield:

$$\int \frac{d^3 n d^3 n'}{4\pi} |f(q\hat{\mathbf{n}}, q\hat{\mathbf{n}}')|^2 = \sigma_{\text{tot}}(q), \quad (2.31)$$

which is the total scattering cross section for environmental particles of momentum q .

Then we can write our localization rate as:

$$F(\mathbf{x} - \mathbf{x}') = \int dq v(q) \sigma_{\text{tot}}(q) = \Gamma_{\text{tot}}. \quad (2.32)$$

That means, our localization rate is a constant. The convergence of the localization rate F as a function of the size of our superposition Δx is illustrated in Fig. 6.

In the short-wavelength limit, the equation 2.28 will become:

$$\frac{\partial \rho_S(\mathbf{x}, \mathbf{x}', t)}{\partial t} = -\Gamma_{\text{tot}} \rho_S(\mathbf{x}, \mathbf{x}', t). \quad (2.33)$$

That means, off-diagonal (coherent) elements of the density matrix will decay exponentially:

$$\rho_S(\mathbf{x}, \mathbf{x}', t) = \rho_S(\mathbf{x}, \mathbf{x}', 0) \exp(-\Gamma_{\text{tot}} t). \quad (2.34)$$

2.2.2 The long-wavelength limit

The other extreme is if we have $\lambda_0 \gg \Delta x$. In this case, a single scattering event carries very little information, and it will take many such events to fully decohere our quantum system. If we again look at the momentum associated with the scattered particles, this means the opposite of what we had in the short-wavelength regime:

$$\frac{q_0 \Delta x}{\hbar} \ll 1. \quad (2.35)$$

Using this, we can again look at the exponent on the right-hand side of equation 2.29 and expand it to first order in q :

$$1 - e^{iq(\hat{\mathbf{n}} - \hat{\mathbf{n}}') \cdot (\mathbf{x} - \mathbf{x}')/\hbar} \approx -\frac{i}{\hbar} q (\hat{\mathbf{n}} - \hat{\mathbf{n}}') \cdot (\mathbf{x} - \mathbf{x}') + \frac{1}{2\hbar^2} q^2 [(\hat{\mathbf{n}} - \hat{\mathbf{n}}') \cdot (\mathbf{x} - \mathbf{x}')]^2. \quad (2.36)$$

This simplifies the integral in F because the first term is antisymmetric in $\hat{\mathbf{n}}$ and $\hat{\mathbf{n}}'$, but it is multiplied with a symmetric term. This results in:

$$F(\mathbf{x} - \mathbf{x}') = \int dq \xi(q) v(q) q^2 \int \frac{d^3 n d^3 n'}{8\pi\hbar^2} [(\hat{\mathbf{n}} - \hat{\mathbf{n}}') \cdot (\mathbf{x} - \mathbf{x}')]^2 |f(q\hat{\mathbf{n}}, q\hat{\mathbf{n}}')|^2. \quad (2.37)$$

We can simplify this even further with the following assumptions:

- the orientation of our quantum system does not influence the scattering process (for example, a spherical test particle, or a test particle in the Rayleigh regime). Then we can average $[(\hat{\mathbf{n}} - \hat{\mathbf{n}}') \cdot (\mathbf{x} - \mathbf{x}')]^2$ over all directions.
- the scattering cross section is isotropic.

While these are, of course, strong assumptions, they are valid in several relevant cases. Then F simplifies to:

$$F(\mathbf{x} - \mathbf{x}') = (\mathbf{x} - \mathbf{x}')^2 \int dq \xi(q) v(q) q^2 \frac{2\pi}{3\hbar^2} \int d\cos(\theta) \cdot (1 - \cos(\theta)) |f(q, \cos(\theta))|^2. \quad (2.38)$$

Now, let us define the effective cross section:

$$\sigma_{\text{eff}}(q) \equiv \frac{2\pi}{3} \int d\cos(\theta) \cdot (1 - \cos(\theta)) |f(q, \cos(\theta))|^2, \quad (2.39)$$

and let us introduce the **decoherence parameter**:

$$\Lambda \equiv \int dq \xi(q) v(q) \frac{q^2}{\hbar^2} \sigma_{\text{eff}}(q). \quad (2.40)$$

Then we can write the time dependence of the density matrix as:

$$\frac{\partial \rho_S(\mathbf{x}, \mathbf{x}', t)}{\partial t} = -\Lambda (\mathbf{x} - \mathbf{x}')^2 \rho_S(\mathbf{x}, \mathbf{x}', t). \quad (2.41)$$

For short time scales, this means:

$$\rho_S(\mathbf{x}, \mathbf{x}', t) = \rho_S(\mathbf{x}, \mathbf{x}', 0) \exp(-\Lambda \Delta x^2 t), \quad (2.42)$$

and this allows us to define a typical decoherence time scale for a superposition of size Δx :

$$\tau_{\Delta x} = \frac{1}{\Lambda \Delta x^2}. \quad (2.43)$$

In contrast to the short wavelength limit, this typical time scale depends explicitly on the size of the superposition.

2.3 Some important decoherence effects

As we promised earlier, we will now give a few important examples of decoherence mechanisms one has to take into account when dealing with macroscopic superpositions.

$T(\text{K})$	$\lambda_{\max}(\mu\text{m})$
4	720.0
20	144.0
300	9.7
1000	2.9

Table 2.1: Examples of peak wavelengths of the blackbody spectrum.

2.3.1 Scattering of blackbody radiation

To get an impression what we are dealing with, let us first get an idea of the typical wavelengths of blackbody radiation. From Planck's law we know the spectral radiance as a function of wavelength:

$$B(\lambda, T) = \frac{2hc^2}{\lambda^5} \left[\exp\left(\frac{hc}{\lambda k_B T}\right) - 1 \right]^{-1}. \quad (2.44)$$

The maximum of this distribution will be at the wavelength $\lambda_{\max} = hc/(\xi_0 k_B T)$, where $\xi_0 \approx 4.965$. Examples for this maximum wavelength are given in table 2.1. We can see from the table that, even at high temperatures, the thermal wavelength is much longer than superpositions on a sub-micron length scale.

To formally describe the scattering of blackbody radiation, let us begin by finding the correct momentum density $\xi(q)$. The average number of photons with an energy $q \cdot c$ is:

$$\langle n(q) \rangle_T = \frac{2}{e^{\frac{cq}{k_B T}} - 1}. \quad (2.45)$$

The factor of two on the right-hand side results from the fact that each photon can have two polarizations. We get the number density by multiplying this with the number of states per unit volume with momenta between \mathbf{q} and $\mathbf{q} + d\mathbf{q}$:

$$\xi(q) = \frac{1}{\pi^2 \hbar^3} \left(\frac{q^2}{e^{\frac{cq}{k_B T}} - 1} \right). \quad (2.46)$$

Now, we still have to estimate what the scattering cross section will be. Like we indicated above, the wavelength of blackbody radiation will typically be much larger than quantum superpositions with $\Delta x \lesssim 1\mu\text{m}$. For that reason, let us assume that we are dealing with Rayleigh scattering. In that case, the scattering cross section will be:

$$|f(q\hat{\mathbf{n}}, q\hat{\mathbf{n}}')|^2 = \left(\frac{q}{\hbar} \right)^4 \frac{a^6}{2} \operatorname{Re} \left[\frac{\epsilon - 1}{\epsilon + 2} \right]^2 (1 + \cos^2 \theta). \quad (2.47)$$

This assumed the following:

- the test particle is a sphere with radius a
- the material is homogeneous with a wavelength-independent dielectric constant ϵ .

Under these assumptions, the scattering cross section will be[14]:

$$\sigma_{\text{eff}}(q) = \frac{8\pi}{9} \left(\frac{q}{\hbar}\right)^4 a^6 \text{Re} \left[\frac{\epsilon - 1}{\epsilon + 2} \right]^2, \quad (2.48)$$

and our decoherence parameter becomes:

$$\Lambda_{\text{bb,sca}} = 8! \frac{8}{9\pi} a^6 c \text{Re} \left[\frac{\epsilon - 1}{\epsilon + 2} \right]^2 \left(\frac{k_B T}{\hbar c} \right)^9 \zeta(9). \quad (2.49)$$

Here, ζ is the Riemann Zeta function, and $\zeta(9) \approx 1.002$.

2.3.2 Emission and absorption of blackbody radiation

These two effects lead to the same expression for the decoherence parameter, but the values will differ, because in one case the relevant temperature is the temperature of the environment ($T = T_{\text{env}}$), and in the other case, it is the internal temperature of our test particle ($T = T_i$). We get:

$$\Lambda_{\text{bb,em./abs.}} = \frac{16\pi^5 a^3 c}{189} \text{Im} \left[\frac{\epsilon - 1}{\epsilon + 2} \right]. \quad (2.50)$$

2.3.3 Scattering of gas molecules

We already hinted earlier that this decoherence effect has to be treated in the short-wavelength limit. The reason is that the de-Broglie wavelength of gas particles usually is very short. To get an impression, let us give two examples.

If the gas particles are air molecules, then the mass of each gas particle is about 29 atomic mass units (amu). If the gas is following Maxwell Boltzmann statistics, the root mean square velocity of these gas particles will be:

$$v_g = \sqrt{\frac{3k_B T}{m_g}} \approx 508 \text{ m/s.} \quad (2.51)$$

The corresponding de-Broglie wavelength then is 27 pm.

If we go to a cryogenic environment at 4 K, the residual gas will most likely be Helium with a molecular weight of 4 amu, and the gas velocity will be $v_g \approx 158 \text{ m/s}$. This results in a de-Broglie wavelength of 0.6 nm.

In both cases, the de-Broglie wavelength is very short compared to the dimensions of anything we might call a macroscopic superposition. For that reason, the scattering of gas molecules will have to be treated in the short-wavelength limit, and even a few scattering events can completely decohere superposition states. Ideally, we want to **avoid even single collisions**.

Given some residual gas pressure, what collision frequency will we get? The simplest estimate is to assume a geometric cross section for our test particle: $\sigma = \pi a^2$. Then we can treat the cross section $|(|qmathbf{f}, qmathbf{f}')|^2$ as a constant $|f|^2$. In this approximation, we should then have:

$$\int d\hat{\mathbf{n}} |f|^2 = 4\pi |f|^2. \quad (2.52)$$

From this, we can conclude that $|f|^2 = a^2/4$.

Schlosshauer then puts this into his expressions for the long-wavelength limit and arrives at[3]:

$$\Lambda_{\text{Schlosshauer}} = \frac{8}{3\hbar^2} \frac{N}{V} \sqrt{2\pi m} a^2 (k_B T)^{3/2}. \quad (2.53)$$

On the other hand, O. Romero-Isart takes a similar approach but arrives at different expressions - e.g. in Ref.[15]:

$$\gamma_g = \frac{16\pi\sqrt{2\pi}}{\sqrt{3}} \frac{Pa^2}{\sqrt{m_g k_B T}}. \quad (2.54)$$

A very different treatment was given by K. Hornberger and J. Sipe[16]. They arrived at the following scattering rate:

$$\gamma_g \approx \frac{4\pi\Gamma(0.9)}{5\sin(\pi/5)} \left(\frac{3\pi C_6}{2\hbar} \right)^{2/5} \frac{P v_g^{3/5}}{k_B T}, \quad (2.55)$$

where Γ is the Gamma function with $\Gamma(0.9) \approx 1.07$, and C_6 characterizes the van der Waals coupling[17]. Hornberger and Sipe calculated how the gas particles would interact with a macroscopic test particle via van-der-Waals interaction. While there result looks rather complicated, these interactions can lead to significant deviations from a purely geometric approach in certain size-ranges of test particles. For large test particles, the actual cross section is most likely a combination of the geometric cross section and such a cross section depending on particle-particle interactions. According to a private communication with Benjamin Stickler (around 2018), it should probably be a safe estimate to double the geometric cross section.

3 Master equation approach to decoherence

Our goal here is to find a simpler way to describe the evolution of the density matrix of a system interacting with the environment via a unitary operator $\hat{U}(t)$. So far, we have described that as:

$$\hat{\rho}_S(t) = \text{Tr}_E(\hat{\rho}_{SE}(t)) = \text{Tr}_E(\hat{U}(t)\hat{\rho}_{SE}(0)\hat{U}^\dagger(t)). \quad (3.1)$$

Instead of that, the master-equation approach aims to write this as:

$$\hat{\rho}_S(t) = \hat{V}(t)\hat{\rho}(0), \quad (3.2)$$

where $\hat{V}(t)$ is a “superoperator”. That is, an operator acting on operators. The goal is to define $\hat{V}(t)$ such that it (at least approximately) describes the effect of the environment on our system.

In particular, we will consider master equations that can be described via a first-order differential equation of the form:

$$\frac{d}{dt}\hat{\rho}_S(t) = \hat{\mathcal{L}}[\hat{\rho}(t)] = -i[\hat{H}'_S, \hat{\rho}_S(t)] + \hat{\mathcal{D}}[\hat{\rho}_S(t)]. \quad (3.3)$$

Here, we split the superoperator $\hat{\mathcal{L}}$ in two parts: (1) a (coherent) unitary evolution, but possibly with some slight modifications due to the environment. For example, the energy levels may shift in the presence of the environment. (2) a term describing decoherence. We assume that the evolution of the system is “local” in time. That means, the density matrix and its derivative only depend on values at time t .

If there is no decoherence, we get something very similar to the usual Liouville-von Neumann equation:

$$\frac{d}{dt}\hat{\rho}_S(t) = -i[\hat{H}'_S, \hat{\rho}_S(t)]. \quad (3.4)$$

The system’s Hamiltonian is slightly modified due to the environment.

3.1 The Born-Markov master equation

Given a few assumptions, one can derive a pretty general form of $\hat{\mathcal{L}}$. Because that derivation is pretty technical, we will only give a rough description and instead focus on the Born-Markov approximation.

The Born-Markov approximation actually consists of two approximations:

- **Born approximation:**

the interaction of the system with the environment is weak enough and the environment is big enough such that the overall state remains approximately in a product state, i.e.: $\hat{\rho}(t) \approx \hat{\rho}_S(t) \otimes \hat{\rho}_E$.

- **Markov approximation:**

there is no “memory” in the interactions with the environment. That means, self-correlations in the environment decay quickly compared to the time scale the system evolves noticeably.

We will describe the interaction between environment and system via the interaction Hamiltonian \hat{H}_i , and the internal evolution of the system via the Hamiltonian \hat{H}_S .

One can always write the interaction Hamiltonian in a diagonal of the form

$$\hat{H}_i = \sum_{\alpha} \hat{S}_{\alpha} \otimes \hat{E}_{\alpha}, \quad (3.5)$$

where the two operator sets consist of unitary but not necessarily Hermitian operators. Intuitively, if the \hat{S}_{α} are Hermitian, this decomposition means that the \hat{S}_{α} correspond to “physical quantities of the system” (M. Schlosshauer) that are continuously monitored by the environment. This is the basis for the definition of pointer states, which we mentioned in lecture 2.

In particular, if the set $\{|s_i\rangle\}$ are simultaneous eigenvectors of the \hat{S}_{α}

$$\hat{S}_{\alpha}|s_i\rangle = \lambda_i^{(\alpha)} |s_i\rangle \quad (3.6)$$

for all α and i , then they are pointer states of our system. The time evolution of these states will be given by:

$$e^{-i\hat{H}_i t} |s_i\rangle |E_0\rangle = |s_i\rangle e^{-i(\sum_{\alpha} \lambda_i^{(\alpha)} \hat{E}_{\alpha}) t} |E_0\rangle = |s_i\rangle |E_i(t)\rangle. \quad (3.7)$$

That means, the interaction does not entangle the pointer states with the environment.

Now, if we use equation 3.5 in our master equation, we get the **Born-Markov master equation**:

$$\frac{d}{dt} \hat{\rho}_S(t) = -i[\hat{H}_S, \hat{\rho}_S(t)] - \sum_{\alpha} \left\{ [\hat{S}_{\alpha}, \hat{B}_{\alpha} \hat{\rho}_S(t)] + [\hat{\rho}_S(t) \hat{C}_{\alpha}, \hat{S}_{\alpha}] \right\}, \quad (3.8)$$

where we introduced the system operators:

$$\begin{aligned}\hat{B}_\alpha &= \int_0^\infty d\tau \sum_\beta \mathcal{C}_{\alpha\beta}(\tau) \hat{S}_\beta(-\tau), \\ \hat{C}_\alpha &= \int_0^\infty d\tau \sum_\beta \mathcal{C}_{\beta\alpha}(-\tau) \hat{S}_\beta(-\tau).\end{aligned}\quad (3.9)$$

The operators $S_\alpha(\tau)$ are taken to be in the interaction picture. The quantity

$$\mathcal{C}_{\alpha\beta}(\tau) = \langle \hat{E}_\alpha(\tau) \hat{E}_\beta(\tau) \rangle_{\hat{\rho}_E} \quad (3.10)$$

can be understood as environment self-correlation functions. In the above equation, the average is taken over the initial state of the environment, and we assumed that the \hat{E}_α to be Hermitian. We can then think of the \hat{E}_α as “measurements” on the environment, and then the $\alpha\beta$ represents correlations between such “measurements” being performed at different times. These correlations are interesting at this point because the Markov approximation states that any such correlations should decay rapidly compared to the evolution of our system.

The Born-Markov master equation looks very complicated, but it can often be simplified a lot. Now, we will have a quick look at how one arrives at that master equation. The derivation of the Born-Markov equation can be found in Ref. [3].

3.2 The master equation in the Lindblad form

A special case of the Born-Markov master equation is the master equation in the Lindblad form. It was shown by Lindblad (Comm. Math. Phys. 48, 119 (1976)) as well as by Gorini, Kossakowski and Sudarshan (J. Math. Phys. 17, 821 (1976)) that the most general master equation that ensures that the positivity of the reduced density matrix at all times (i.e., $\langle \psi | \hat{\rho}_S(t) | \psi \rangle \geq 0$) is of the following form:

$$\frac{d}{dt} \hat{\rho}_S(t) = -i[\hat{H}_S, \hat{\rho}_S(t)] + \frac{1}{2} \sum_{\alpha, \beta} \gamma_{\alpha\beta} \left\{ [\hat{S}_\alpha, \hat{\rho}_S(t) \hat{S}_\beta^\dagger] + [\hat{S}_\alpha \hat{\rho}_S(t), \hat{S}_\beta^\dagger] \right\}, \quad (3.11)$$

where the operators \hat{S}_α are again the same as earlier in equ. 3.5. The coefficients $\gamma_{\alpha\beta}$ are time dependent and comprise all the information about decoherence and possible dissipation effects. They define a coefficient matrix $\Gamma = (\gamma_{\alpha\beta})$.

One should note that the Lindblad master equation is “local in time”, and it is Markovian. To get the Born-Markov master equation 3.8 into Lindblad form, one also has to assume the **rotating-wave approximation**. Here, this means that the system evolves much faster than it decoheres.

One can simplify equ. 3.11 by diagonalizing Γ , which is always possible because all eigenvalues of Γ are positive. If one also assumes the \hat{S}_α to be Hermitian, one can further simplify the master equation to:

$$\frac{d}{dt}\hat{\rho}_S(t) = -i[\hat{H}'_S, \hat{\rho}_S(t)] - \frac{1}{2} \sum_\mu \kappa_\mu [\hat{L}_\mu, [\hat{L}_\mu, \hat{\rho}_S(t)]] . \quad (3.12)$$

3.2.1 Environmental decoherence in the Lindblad form

Equation 3.12 is already of the same form as the time evolution we get in the case of environmental decoherence. In order to see that, let us assume that we only sum μ to 1, and that we set $\hat{L} = \hat{L}_1 = \hat{x}$, and let us assume that the system Hamiltonian is that for a free massive particle: $\hat{H}_S = \hat{p}^2/2m$. If we set $\kappa = \kappa_1 = 2\Lambda$ the Lindblad master equation becomes:

$$\frac{d}{dt}\hat{\rho}_S(t) = -\frac{i}{2m}[\hat{p}^2, \hat{\rho}_S(t)] - \Lambda[\hat{x}, [\hat{x}, \hat{\rho}_S(t)]] . \quad (3.13)$$

This is the Lindblad master equation for decoherence in the long-wavelength regime with the scattering constant Λ . In the position representation, this becomes:

$$\frac{\partial \rho_S(x, x', t)}{\partial t} = -\frac{i}{2m} \left(\frac{\partial^2}{\partial x'^2} - \frac{\partial^2}{\partial x^2} \right) \rho_S(x, x', t) - \Lambda(x - x')^2 \rho_S(x, x', t) . \quad (3.14)$$

This is identical to our expression for long-wavelength decoherence. The only difference is that the present equation also includes the free evolution of the center of mass.

4 How do we test quantum physics and decoherence?

We discussed several ways how decoherence affects the evolution of a quantum system. How can we check these theoretical predictions experimentally? One example is to test the influence of decoherence on the interference visibility in a matter-wave interferometer. For example, that was done in two experiments by the Arndt group where they tested the influence of collisions with background gas[18] and of blackbody radiation[19]. We will discuss interferometric tests in more detail later.

Here, we will discuss an easier way of performing such tests, in principle. While it is less sensitive than interferometry, it is instructive to consider this approach. It can also act as a calibration measurement for interferometers and to determine the rough level of decoherence one deals with before making more accurate measurements.

4.1 Heating of the center-of-mass motion

Let us describe decoherence in the long-wavelength limit by the following master equation of the Lindblad form:

$$\frac{\partial \rho_S(x, y, t)}{\partial t} = -\frac{i\hbar}{2m} \left(\frac{\partial^2}{\partial y^2} - \frac{\partial^2}{\partial x^2} \right) \rho_S(x, y, t) - \Lambda(x - y)^2 \rho_S(x, y, t). \quad (4.1)$$

The scattering constant Λ determines the strength of the decoherence.

Following Joos and Zeh[20], let us assume that the density matrix can be described as a Gaussian of the general form:

$$\rho_S(x, y, t) = \exp \{ -A(t)(x - y)^2 - iB(t)(x^2 - y^2) - C(t)(x + y)^2 - D(t) \}. \quad (4.2)$$

We then try to determine the time-dependent coefficients $A(t)$, $B(t)$, $C(t)$, and $D(t)$ to describe the evolution and the decoherence of this density matrix in time. The intuitive meaning of the coefficients is the following: the width of our wave-packet in the off-diagonal direction where $x = -y$ is inversely proportional to $\sqrt{A(t)}$ and the width of the wave packet on the diagonal where $x = y$ is inversely proportional to $\sqrt{C(t)}$.

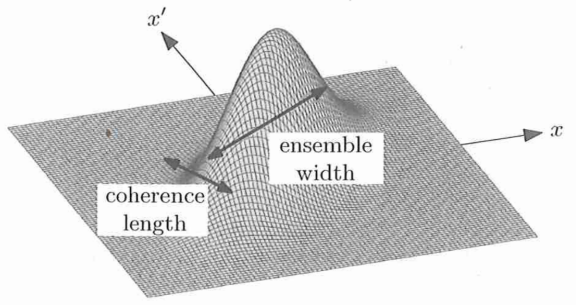


Figure 7: **Coherence length and ensemble width.** The figure represents a Gaussian density matrix. Its width along the diagonal is the ensemble width, and its width along the anti-diagonal we denote as the coherence length. If there is no decoherence and we start from a pure state, these two will be equal. The figure is taken from M. Schlosshauer's book[3]. Instead of y he uses x' .

In particular, we can introduce a characteristic **coherence length**:

$$l_c(t) = \frac{1}{\sqrt{8A(t)}} \quad (4.3)$$

and the **ensemble width** or “wave-packet width”:

$$\Delta X(t) = \frac{1}{\sqrt{8C(t)}}. \quad (4.4)$$

$D(t)$ is used for normalizing the density matrix. The momentum distribution is given by:

$$\Delta P(t) = \sqrt{2}\hbar \left[A(t) + \frac{B^2(t)}{4C(t)} \right]^{\frac{1}{2}}. \quad (4.5)$$

Then the product of $\Delta X \Delta P$, which is important for the uncertainty relation, becomes:

$$\Delta X(t)\Delta P(t) = \frac{\hbar}{2} \left[\frac{A(t)}{C(t)} + \frac{B^2(t)}{4C^2(t)} \right]^{\frac{1}{2}}. \quad (4.6)$$

In figure 7, we illustrate what the coherence length and the ensemble width correspond to in relation to our density matrix.

Let us assume that the initial state is a pure Gaussian state described by the density matrix

$$\rho_S(x, y, t) = (2\pi b^2)^{-1/2} \exp \left(-\frac{x^2 + y^2}{4b^2} \right), \quad (4.7)$$

then we have $A(0) = C(0) = 1/8b^2$ and $B(0) = D(0) = 0$. Because we have a pure state, the density matrix is symmetric around the origin. As our density matrix evolves in time, decoherence can destroy this symmetry. If we put our Gaussian density matrix into the master equation 4.1, we get a system of coupled differential equations for the coefficients $A(t)$ etc. For $\mathcal{A}(T)$, one gets the solution:

$$A(t) = \frac{\Lambda t^3 \hbar^2 + 3m^2 b^2/2 + 2\hbar^2 \Lambda^2 b^2 t^4 + 12\Lambda m^2 b^4 t}{3t^2 \hbar^2 + 8\Lambda \hbar^2 b^2 t^3 + 12m^2 b^4}, \quad (4.8)$$

and for $C(t)$ we get:

$$C(t) = \frac{1}{2} \left[\frac{t^2 \hbar^2}{m^2 b^2} + \frac{8}{3} \frac{\Lambda t^3 \hbar^2}{m^2} + 4b^2 \right]^{-1}. \quad (4.9)$$

We see that these two coefficients are equal for $\Lambda = 0$.

Then the coherence length becomes:

$$l_c(t) = \frac{1}{\sqrt{8A(t)}} = \frac{1}{2} \left[\frac{3t^2 \hbar^2 + 8\Lambda \hbar^2 b^2 t^3 + 12m^2 b^4}{2\Lambda \hbar^2 t^3 + 3m^2 b^2 + 4\Lambda^2 \hbar^2 b^2 t^4 + 24\Lambda m^2 b^4 t} \right]^{\frac{1}{2}}. \quad (4.10)$$

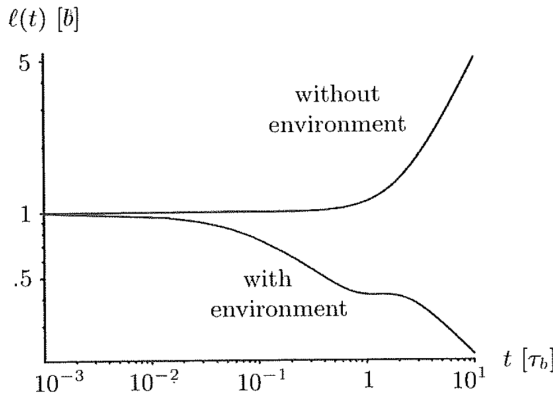


Figure 8: **Coherence length as a function of time.** In the presence of decoherence the coherence length quickly decays with time, whereas it would increase in the absence of decoherence. The time is given in units of τ_b . I took the figure from M. Schlosshauer's book[3].

In the absence of decoherence, this spreads in time just as the width of the wave packet. If there is decoherence, the coherence length will quickly decay. Figure 8 shows a comparison of these two cases.

For times that are short compared to the localization time scale $\tau_b \equiv 1/\Lambda b^2$ the time

dependence of the coherence length is:

$$l_c(t) \approx b(1 - 4\Lambda b^2 t). \quad (4.11)$$

That means for short times the coherence length decreases linearly in time proportional to the scattering constant Λ . For very large times compared to τ_b , we get:

$$l_c(t) \rightarrow \frac{1}{\sqrt{2\Lambda t}}, \quad (4.12)$$

so the coherence length will be inversely proportional to the square root of Λ and t .

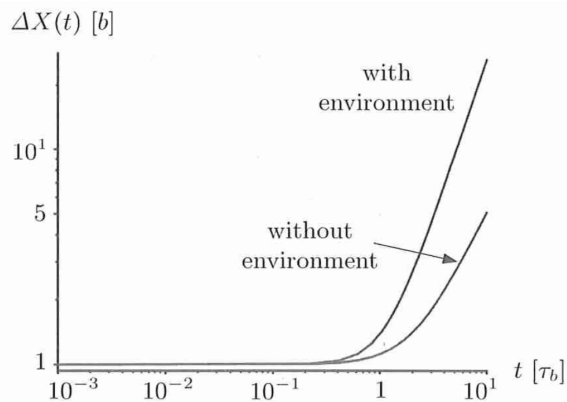


Figure 9: **Ensemble width as a function of time.** Even in the absence of decoherence, the ensemble width will spread due to the wave-packet dispersion for massive particles. In the presence of decoherence this spreading happens even more quickly. The figure is taken from M. Schlosshauer's book[3].

The interesting thing is that decoherence also affects the ensemble width ΔX . This is illustrated in figure 9. In the presence of decoherence the ensemble width will increase with time more quickly than it would in the absence of decoherence:

$$\Delta X(t) = \frac{1}{\sqrt{8C(t)}} = \frac{1}{2} \left[\frac{t^2 \hbar^2}{m^2 b^2} + \frac{8 \hbar^2 \Lambda t^3}{3 m^2} + 4b^2 \right]^{\frac{1}{2}}. \quad (4.13)$$

Where does this additional increase in the ensemble width come from? We can understand it as an increase in the mean energy of our system due to the continuous monitoring by the environment. This increase in the energy is a consequence of our assumption that no momentum is transferred to our system in scattering events.

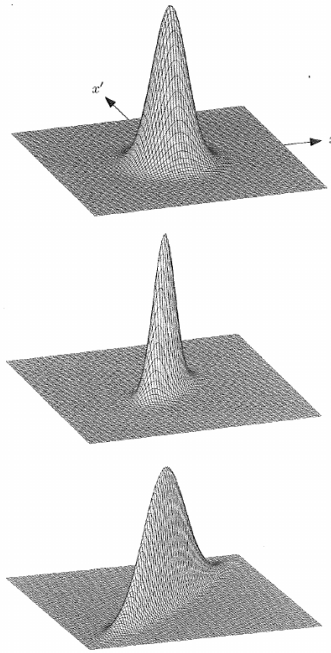


Figure 10: **Evolution of a Gaussian density matrix in the presence of decoherence.** Decoherence will lead to a reduction of the coherence length and at the same time to an increase in the ensemble spread. The figure is taken from M. Schlosshauer's book[3].

For a free particle, the mean energy is simply related to the momentum spread:

$$E(t) = \langle \hat{H}_{\text{free}}(t) \rangle = \left\langle \frac{\hat{p}^2(t)}{2m} \right\rangle = \frac{1}{2m} (\Delta P(t))^2 = \frac{\hbar^2}{m} \left(\frac{1}{8b^2} + t\Lambda \right). \quad (4.14)$$

From this, we can see that the mean energy of our system increases linearly in time, proportional to the scattering constant.

That means while decoherence will lead to a decrease in the coherence length, it will lead to an increase in the ensemble width. Roughly speaking, the interaction with the environment constantly resolves differences $|x - y|$ while it is insensitive to the sum of the positions $(x + y)$. This effect will lead to a “squeezing” of our Gaussian wave packet over time as illustrated in figure 10.

In order to quantify this effect, we can introduce the following dimensionless quantity:

$$\delta(t) \equiv \frac{l_c(t)}{\Delta X(t)} = \frac{C(t)}{A(t)}. \quad (4.15)$$

This ratio quantifies the level of coherence of our density matrix. Figure 11 shows a

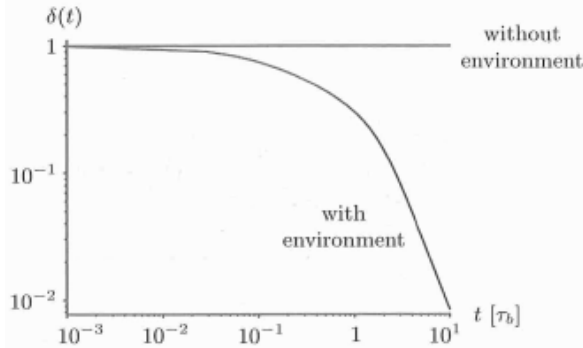


Figure 11: **Time dependence of $\delta(t)$.** The figure is taken from M. Schlosshauer's book[3].

plot of δ over time, which illustrates how δ drops rapidly with time in the presence of decoherence, while it stays constant in the case of no decoherence.

The ratio $\delta(t)$ is not only a measure of the coherence of our state, it also represents the purity of our density matrix because for a Gaussian state, we have $\delta(t) = \text{Tr}(\hat{\rho}^2(t))$. That means, the purity of our density matrix rapidly decreases in the presence of decoherence, which reflects the fact that the interaction with the environment keeps entangling our system with the environment while we only consider the reduced density matrix or our system.

To illustrate the effect of decoherence more clearly, let us consider a Gaussian “cat state”, i.e., the superposition of a Gaussian state being at position x_0 or at position $-x_0$. Let us assume a pure state for time $t = 0$:

$$\Psi(x, 0) = \psi_{x_0}(x, 0) + \psi_{-x_0}(x, 0). \quad (4.16)$$

The corresponding density matrix will initially consist of four Gaussian peaks of equal height. In the presence of decoherence, the two off-diagonal peaks that represent the coherence of our state will vanish over time. This is illustrated in figure 12.

4.2 Experimental tests

Earlier I stated that experimental tests of quantum physics and decoherence effects by measuring the expansion of the wave packet may be simpler than looking for deviations in the visibility of matter-wave interference patterns. This is only correct under specific circumstances. It is a fact that, so far, the record-holding experiments in terms of observing quantum effects for massive objects have been matter-wave interferometers. This started with the demonstration of matter-wave interferometry of C_{60} molecules[21], and the Arndt group has continued demonstrating matter-wave interferometry for in-

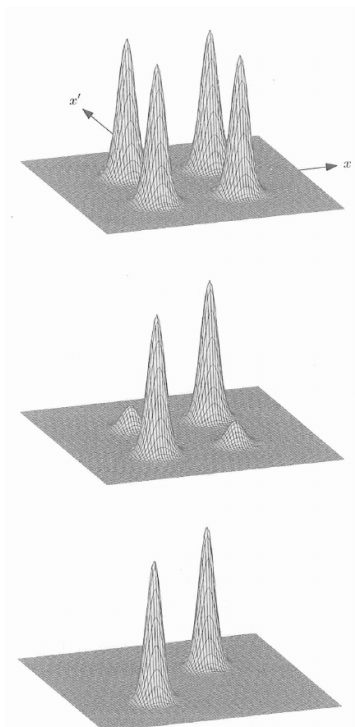


Figure 12: **Evolution of a Gaussian cat state in the presence of decoherence.**

At time $t = 0$, our density matrix shows four Gaussian peaks of equal height. Decoherence will quickly result in the vanishing of the two off-diagonal peaks. In the end, only a classical mixture remains, which corresponds to two peaks positions on the diagonal. The figure is taken from M. Schlosshauer's book[3].

CHAPTER 4. HOW DO WE TEST QUANTUM PHYSICS AND DECOHERENCE?

creasingly massive objects.

The big practical advantage in doing matter-wave interferometry with molecules like C_{60} is that there existed “bright” sources. In particular, in the C_{60} experiment and similar ones, the source was an oven containing the molecules, and the molecules then evaporated out of an aperture.

One could, in principle, use the same source to observe not matter-wave interferometry but molecule diffraction at a single slit. The advantage of doing matter-wave interferometry in this case is that one can use all the molecules coming out of the oven. If one places a single slit there, it will greatly diminish the overall number of molecules detected.

In this sense, my earlier assessment that it would be simpler to test quantum physics by observing the expansion of a wave packet was based on the assumption that one has a bright source of well initialized (approximately pure) quantum states.

Given recent progress in the optical trapping and optomechanical cooling of single dielectric particles [22, 23, 24, 25, 26], it has become increasingly likely that it will soon be feasible to create pure states of center-of-mass motion with a sufficient rate and fidelity that one can use them for observations of wave-packet expansion.

At the same time as these potential sources of pure-state single particles have become increasingly feasible, it has become imperative to achieve control on the single-particle level if one wants to perform matter-wave interferometry with particles of a mass far beyond the current record of 10^4 atomic mass units (amu)[27].

Effectively, this leads to a situation where the sources required to perform matter-wave interferometry with high-mass test particles will also be well suited to observe the expansion of wave packets. My claim that it would be easier to observe wave-packet expansion is based on this assumption.

Now assume that we have a source of particles with a reasonably pure quantum state - similar to the Gaussian state we assumed earlier. How will we then proceed to test the predictions of quantum physics?

Assume that we simply want to compare the pure, coherent evolution of a quantum state to what we actually see in the experiment. In order to observe the expansion of the wave packet, we have to observe it at at least two points in time. If we assume that we know the initial quantum state, that counts as one point in time, and we only have to observe our system again at any later time T .

But, how do we measure the width of our wave packet? Earlier on, we referred to the “width of the wave packet” as ensemble width. This is a more accurate description because the width of the wave packet is not an observable - it really just describes the statistical distribution of the results of position measurements.

In essence, an experiment of this type would look as follows: (1) prepare a particle in a (reasonably) pure Gaussian state, (2) measure its position again after some time T . (3) repeat steps 1 and 2 many times. The standard deviation of all these measurement results will correspond to the “width of the wave packet” or rather the ensemble width.

Now, if one want to use this method to test quantum physics, one has to compare

this experimental result to the ensemble width one would expect theoretically. That means that the uncertainty in our determination of the ensemble width had to be much smaller than the difference between the mean of the measured result and the theoretical prediction.

If we look at the ensemble width given in equation 4.13, we see that (under the square root) it comprises two contributions, On the one hand, we have the “normal” expansion of the wave packet according to Schrödinger’s equation:

$$w_s(t) = \sqrt{\frac{\hbar^2 t^2}{4m^2 b^2} + b^2}. \quad (4.17)$$

And added to that (beneath the square root), we have a contribution due to decoherence:

$$\frac{1}{3} \frac{\hbar^2 \Lambda t^3}{m^2}. \quad (4.18)$$

Now, in order for us to be able to distinguish this accelerated expansion from the “normal” expansion due to Schrödinger’s equation. Let us consider more closely how we would experimentally determine the ensemble width. After N times measuring the position of our test particle after an expansion time t , we would estimate our ensemble width w with a relative error of[28]:

$$\frac{\Delta w}{w} = [2(N - 1)]^{-\frac{1}{2}}. \quad (4.19)$$

Now, if we assume that the square of our deviation from normal Schrödinger evolution as given in equation 4.18 is much smaller than the square of the ensemble width according to Schrödinger, then we get:

$$\Delta X(t) - w_s(t) \approx \frac{1}{3} \frac{\hbar^2 \Lambda t^3}{m^2}. \quad (4.20)$$

For us being able to distinguishing this from normal unitary evolution, this deviation has to be larger than the accuracy with which we can determine the ensemble width. That means:

$$\frac{1}{3} \frac{\hbar^2 \Lambda t^3}{m^2} > \Delta w = \frac{w}{\sqrt{2(N - 1)}} \approx \frac{w_s(t)}{\sqrt{2(N - 1)}}. \quad (4.21)$$

Given the integration time t and the number N of data points measured, we can therefore estimate the minimum discernible scattering constant as:

$$\Lambda_{\min}(N, t) \equiv \frac{3m^2 w_s^2(t)}{\sqrt{2(N - 1)} \hbar^2 t^3}. \quad (4.22)$$

5 Collapse models and gravitational Decoherence

Until now, we mainly focused on decoherence, and we used the phrase that the coherence will get lost “for all practical purposes”, as : Schlosshauer is paraphrasing Bell[29, 3].

Collapse models, on the other hand, aim to achieve a “proper” collapse of the wavefunction. To allow for a “breakdown”[1] of superposition states, these models introduce a non-linear modification to the standard unitary evolution of quantum mechanics. The goal is that the non-linear modification will lead to an exponential decay of all terms except one in any quantum superposition $\sum_i c_i |\phi_i\rangle$ where the $|\phi_i\rangle$ are preferred basis states. In repeated measurements of an ensemble of identical states, the frequency with which a particular basis state “survives” obeys Born’s rule in accordance with quantum physics.

Both environmental decoherence and collapse models predict the loss of coherence for macroscopic superpositions, but there are two **central** distinctions between these two approaches:

- if the only limitation is environmental decoherence, it is in principle possible to isolate our quantum system well enough to preserve even macroscopic superpositions
- both approaches result in pure superposition states becoming mixed states. However, in the case of collapse models, these will be “proper” mixed states: that means, statistical mixtures of distinct, separable states. Environmental decoherence results in “improper” mixed states. The coherence is still there, but due to our lack of knowledge/control we trace out the environment and focus on a subsystem that is strictly speaking not separable from the environment.

Another central point of all collapse models is that they have to take into account that the predictions of quantum mechanics agree very well with experiments on microscopic systems. This holds true even in matter-wave experiments with test masses of by around 3×10^4 amu[30] and superposition sizes of hundreds of nanometers. For that reason, any nonlinear effects leading to a wavefunction collapse need to be sufficiently weak to only affect the predictions of quantum physics for very massive test particles in large superpositions. The effect of these nonlinear corrections to quantum physics therefore has to be cumulative - that means, increasing with the mass of the test particle or, equivalently, with the number of its microscopic constituents.

In the context of collapse models, this is typically referred to as collapse models providing “universal dynamics”. That means, they aim to define master equations that describe the unitary evolution of microscopic systems as well as the nonlinear evolution resulting in classical measurement outcomes and the classical behaviour of macroscopic systems. This is based on the assumption that quantum physics fails to describe macroscopic “reality”.

In my description of collapse models, I will closely follow the review of A. Bassi et al.[1] and the description in Schlosshauer’s book[3]. The reason behind this choice of literature is that A. Bassi is a proponent of continuous spontaneous localization models whereas the treatment of M. Schlosshauer is more critical towards such models. Since I tend to side more with Schlosshauer’s point of view, it seemed appropriate to adhere to A. Bassi’s work to reduce my bias. If you have read this far, you have seen that I am still failing miserably in remaining objective.

5.1 Collapse models

In order to “break” quantum superpositions, one necessarily needs to introduce some form of nonlinearity. In quantum mechanics, this is included in the postulate that a measurement “collapses” the wavefunction into an eigenstate of the corresponding measurement operator.

In 1976, Pearle proposed replacing the standard Schrödinger evolution with a stochastic nonlinear equation during the measurement process[31]. The stochasticity allows to account for the randomness of measurement outcomes and because deterministic nonlinear theories can result in superluminal effects (see, e.g., [32]). A drawback with the approach by Pearle was that one had to ad-hoc define the nonlinear dynamics such that they would reproduce Born’s rule.

Other drawbacks of such early stochastic nonlinear collapse models were that they did not explain why the state of a system would collapse in a preferred basis and what triggered that collapse. According to A. Bassi, the work of Ghirardi, Rimini and Weber (GRW)[33] overcame these limitations[1].

The GRW model was based on two principles:

- the preferred basis is chosen to guarantee a definite position in space for macroscopic objects
- the nonlinear dynamics must have little effect on microscopic systems to ensure compatibility with known experimental results confirming quantum physics.

They fulfilled these guidelines with the following assumptions:

- each of n distinguishable particles comprising an object experiences a sudden spontaneous localization process with a mean rate λ_{GRW}
-

- at other times the system evolves according to Schrödinger's equation.

In the context of GRW, the rate λ_{GRW} is a new constant of nature. A second novel fundamental constant of nature is the length scale r_c , which determines how accurately a particle is localized during a collapse event. GRW chose these parameters to be $\lambda_{\text{GRW}} \sim 10^{-16} \text{ Hz}$ and $r_c \sim 100 \text{ nm}$. They chose the values such that a typical dust grain would be localized within a very short time. The argument was that objects the size of dust grains are already visible, in principle, to the bare human eye, so objects of this size should already behave in accordance with our perceived macroscopic reality.

Because the GRW model only dealt with the very classical concept of objects consisting of distinguishable particles, the model was later generalized into the **continuous spontaneous localization** model (CSL)[34] to allow for indistinguishable particles. In this model, a fluctuating classical field couples to the particle number density operator in the process leading to the collapse into spatially localized eigenstates[1].

Three things should be noted: (1) because in CSL the localization process is continuous in time one can describe it by modifying the Schrödinger equation. (2) because the process narrows the wavefunction, it leads to a small violation of energy conservation. There are on-going efforts to include dissipative terms in collapse models in order to overcome this issue (for example Ref. [35]). (3) typical collapse models are non-relativistic. In the review of A. Bassi et al.[1], they describe various efforts where people tried to devise relativistic collapse models. This is ongoing research.

IMPORTANT NOTE: the violation of the energy conservation in many collapse models like CSL leads to the heating of the center-of-mass motion of particles. However, this is **different** from what we discussed in the last lecture in the context of the accelerated spreading of the wavefunction in the presence of environmental decoherence. This accelerated spreading results from an increase of the entropy of the reduce density matrix. Here, it is indeed added energy due to a physical collapse process.

While there exist collapse models that collapse states in the energy or momentum basis, we will concentrate on collapse models that decohere quantum superpositions in the position basis. Only in this way can one ensure that macroscopic objects cannot be in a superposition of being in two different positions in space. That means that usual collapse models like GRW or CSL are designed to ensure the selection of **position as the preferred basis** and to provide random outcomes according to Born's rule. That means collapse models solve the measurement problem per definition. Drawbacks are: (1) because the wavefunctions collapse instantaneously, collapse models are inherently non-relativistic. (2) while collapse models “solve” the measurement problem, there is no clear reason **why** collapses occur. We will later discuss models, where the collapse is assumed to result from gravitational effects. (3) even in collapse models, quantum superpositions do not collapse into pure quantum states because the localization is approximate[3]. Otherwise the heating due to the collapses would become too strong. There is a finite width to each collapse (r_c), and after the collapse the wavefunction will begin expanding again. For that reason, even macroscopic states in collapse models have small Gaussian

“tails” and the resulting macroscopic state will only approximately be pure[3]. Still, these approximately pure macroscopic states are of course significantly more satisfying to proponents of the emergence of a macroscopically realistic world than the improper mixtures resulting from environmental decoherence.

5.1.1 The formal description of collapse models

Collapse models modify the Schrödinger equation such that the modifications fulfill the following properties:

- they are nonlinear such that superpositions are “broken” on the macroscopic level.
- they are stochastic to prevent superluminal signalling, and to allow for random measurement outcomes according to Born’s rule.
- the effects are amplified for increasingly massive objects to allow unitary evolution for microscopic systems while ensuring classical behaviour for macroscopic objects.

The GRW model

Due to the stochastically occurring collapses, the wavefunction ψ_t of a system consisting of N particles will at random times experience jumps of the form[1]:

$$\psi_t \rightarrow \frac{L_n(\mathbf{x})\psi_t(\mathbf{x}_1, \mathbf{x}_2, \dots, \mathbf{x}_N)}{\|L_n(\mathbf{x})\psi_t(\mathbf{x}_1, \mathbf{x}_2, \dots, \mathbf{x}_N)\|} \quad (5.1)$$

$L_n(\mathbf{x})$ is a linear operator of the form:

$$L_n(\mathbf{x}) = \frac{1}{\pi r_c^2} e^{i(\hat{\mathbf{q}}_n - \mathbf{x})^2/2r_c^2}. \quad (5.2)$$

Here, $\hat{\mathbf{q}}_n$ is the position operator of the n^{th} particle.

The probability for a jump occurring is $\|L_n(\mathbf{x})\psi_t(\mathbf{x}_1, \mathbf{x}_2, \dots, \mathbf{x}_N)\|^2$. The jumps are occurring randomly in time with Poissonian statistics and a rate λ_{GRW} . As stated earlier, GRW assume $r_c \sim 100 \text{ nm}$ and $\lambda_{\text{GRW}} \sim 10^{-16} \text{ Hz}$.

An important “conceptual” point is that the GRW model assumes that there are no particles but that even macroscopic objects are very well localized waves. That means, **the wavefunction is assumed to be a real entity**. The mass density of the n^{th} constituent particle of our test particle then is assumed to be:

$$\rho_t^{(n)}(\mathbf{x}_n) = m_n \int d^3x_1 \dots d^3x_{n-1} d^3x_{n+1} d^3x_N |\psi_t(\mathbf{x}_1, \mathbf{x}_2, \dots, \mathbf{x}_N)|^2. \quad (5.3)$$

While the single constituent of a test particle experiences collapse at a very low rate, if any one of its constituents collapses, that will collapse the whole rigid body.

Although the collapse mechanism in GRW is expressed in terms of the wavefunction, it is often more convenient to use the density-matrix formalism. GRW give the following master equation for a single constituent particle:

$$\frac{d}{dt}\hat{\rho}(t) = -\frac{i}{\hbar}[\hat{H}, \hat{\rho}(t)] - T[\hat{\rho}(t)]. \quad (5.4)$$

In the position basis, the operator $T[\cdot]$ is[1]:

$$\langle \mathbf{x}|T[\hat{\rho}(t)]|\mathbf{y}\rangle = \lambda_{\text{GRW}}[1 - e^{-(\mathbf{x}-\mathbf{y})^2/4r_c^2}]\langle \mathbf{x}|\hat{\rho}(t)|\mathbf{y}\rangle. \quad (5.5)$$

If $|\mathbf{x} - \mathbf{y}| \ll r_c$, we can do a Taylor expansion of the exponential and get:

$$\langle \mathbf{x}|T[\hat{\rho}(t)]|\mathbf{y}\rangle \sim -\frac{\lambda_{\text{GRW}}}{4r_c^2}(\mathbf{x} - \mathbf{y})^2\langle \mathbf{x}|\hat{\rho}(t)|\mathbf{y}\rangle = -\Lambda(\mathbf{x} - \mathbf{y})^2\langle \mathbf{x}|\hat{\rho}(t)|\mathbf{y}\rangle. \quad (5.6)$$

In this case, we get a master equation that is formally identical to the long-wavelength limit of environmental decoherence if one sets $\Lambda = \lambda/4r_c^2$. The mechanism behind it is, of course, completely different. If one has a massive, solid test particle consisting of N constituent particles, the decoherence will be amplified by a factor N .

Bassi et al[1] proceed to describe the measurement process according to GRW. In particular, they consider a 2D quantum system (e.g., a spin) coupled to a measurement device with a pointer. Their description is based on earlier work by Bassi and Salvetti[36]. The position of the pointer is coupled via an interaction Hamiltonian to the quantum system. While the quantum system is assumed to evolve coherently, the pointer of the measurement device is treated using the GRW master equation. Because the pointer is macroscopic, it will be localized very quickly due to wavefunction collapse. The localization of the pointer will also collapse the quantum system.

The CSL model

The GRW model is meant for dealing with systems of distinguishable constituent particles. The continuous spontaneous localization model (CSL) overcomes this limitation, and it is so far the most advanced collapse model[1].

The dynamics according to CSL is determined by the following stochastic differential equation in Fock space:

$$\begin{aligned} d\psi_t &= \left[-\frac{i}{\hbar}\hat{H}dt + \frac{\sqrt{\gamma}}{m_0} \int d\mathbf{x}[\hat{M}(\mathbf{x}) - \langle \hat{M}(\mathbf{x}) \rangle_t]dW_t(\mathbf{x}) \right. \\ &\quad \left. - \frac{\gamma}{2m_0^2} \int d\mathbf{x}[\hat{M}(\mathbf{x}) - \langle \hat{M}(\mathbf{x}) \rangle_t]^2 dt \right] \psi_t. \end{aligned} \quad (5.7)$$

Here, \hat{H} is the Hamiltonian, m_0 is a reference mass that is usually taken to be the mass

of a nucleus, γ is a positive coupling constant determining the collapse strength. \hat{M} is a “smeared mass operator”[1]:

$$\hat{M}(\mathbf{x}) = \sum_j m_j \hat{N}_j(\mathbf{x}), \quad (5.8)$$

$$\hat{N}_j(\mathbf{x}) = \int d\mathbf{y} g(\mathbf{y} - \mathbf{x}) \hat{\psi}_j^\dagger(\mathbf{y}) \hat{\psi}_j(\mathbf{y}), \quad (5.9)$$

where $\hat{\psi}_j^\dagger$ and $\hat{\psi}_j$, respectively, are the creation and annihilation operators of a particle of type j at position \mathbf{y} . $g(\mathbf{x})$ is a function to smear out the mass distribution and is taken to be a Gaussian of the form:

$$g(\mathbf{x}) = \frac{1}{(\sqrt{2\pi}r_c)^3} e^{-\mathbf{x}^2/2r_c^2}. \quad (5.10)$$

As in the GRW model, r_c is a second new constant (in addition to γ). $W_t(\mathbf{x})$ is an ensemble of Wiener processes - one for each point in space.

The above formulation of the dynamic equation of for the CSL model is called “mass proportional”. In the original version of the model, it was not mass proportional but instead of the smeared-out mass operator there were number density operators.

The density number operators $\hat{\psi}_j^\dagger(\mathbf{y}) \hat{\psi}_j(\mathbf{y})$ lead to a suppression of coherent superpositions with different numbers of particles in spatially separate positions. This leads to the collapse localizing the wavefunction in space.

If we neglect the normal coherent evolution for now and only concentrate on the decay of coherences according to the CSL model, we get the following master equation for the off-diagonal elements of the density matrix:

$$\frac{\partial}{\partial t} \langle \mathbf{x} | \hat{\rho}_t | \mathbf{y} \rangle = -\Gamma(\mathbf{x}, \mathbf{y}) \langle \mathbf{x} | \hat{\rho}_t | \mathbf{y} \rangle, \quad (5.11)$$

where \mathbf{x} and \mathbf{y} actually represent the sets of coordinates for the N constituent particles of our test particle.

The decay function Γ is given by:

$$\Gamma = \frac{\gamma}{2} \sum_{i,j} [G(\mathbf{x}_i - \mathbf{x}_j) + G(\mathbf{y}_i - \mathbf{y}_j) - 2G(\mathbf{x}_i - \mathbf{y}_j)]. \quad (5.12)$$

The sum in this expression runs over the N constituent particles (nucleons) of our test particle, and

$$G(\mathbf{x}) = \frac{1}{(4\pi r_c^2)^{3/2}} e^{-\mathbf{x}^2/4r_c^2}. \quad (5.13)$$

If one only looks at a single constituent particle, Γ simplifies to:

$$\Gamma(\mathbf{x}, \mathbf{y}) = \frac{\gamma}{(4\pi r_c^2)^{3/2}} [1 - e^{-|\mathbf{x}-\mathbf{y}|^2/4r_c^2}], \quad (5.14)$$

which is identical to the GRW model. The collapse rate in CSL is given by:

$$\lambda_{\text{CSL}} = \frac{\gamma}{(4\pi r_c^2)^{3/2}}. \quad (5.15)$$

In the original paper[34], the authors chose its value as $\lambda_{\text{CSL}} = 2.2 \times 10^{-17}$ Hz, which is lower than in the GRW model.

An interesting effect is the scaling of the decoherence rate with the number of constituent particles. If the constituent particles are within a region of radius r_c , the scaling is different than for constituent particles that are farther apart. This results from the indistinguishability of constituent particles that are close together. For that reason, Γ scales as follows:

$$\Gamma = \lambda_{\text{CSL}} n^2 N, \quad (5.16)$$

where n is the number of particles within a volume of radius r_c , and N is the number of such volumes within our test particle.

If the displacements of our test particle are small, the master equation can again be approximated in a form equivalent to the long-wavelength limit of environmentally induced decoherence with a scattering constant that is given by[37, 38, 39]:

$$\Lambda_{\text{CSL}} = \frac{m^2}{m_0^2} \frac{\lambda_{\text{CSL}}}{4r_c^2} f(r/r_c), \quad (5.17)$$

where m is the test particle mass, r is the radius of the test particle, which we assume to be spherical. f is a function defined by Collett and Pearle[37]:

$$f(x) = \frac{6}{x^4} \left[1 - \frac{2}{x^2} + \left(1 + \frac{2}{x^2} \right) e^{-x^2} \right]. \quad (5.18)$$

5.2 Gravitational decoherence

In contrast to the GRW model, where no reason is given for the collapses occurring, other researchers tried derive causes for a collapse. For example, some assumed this cause to be gravity. Given that collapse models predict a transition from coherent quantum evolution at a microscopic scale to classical behaviour at macroscopic scales, it may seem natural to assume that gravitation plays a role in such a transition. Here, we will focus on essentially two approaches to gravitational decoherence. The model of Károlyházy (K model) and the model of Diósi and Penrose (DP model). It should be noted however, that the K model indeed a model of gravitational decoherence, and not

a collapse model in the strict sense, while the DP model is a collapse model where a nonlinear modification of quantum evolution is introduced that depends on a form of self-gravitation of the wave function.

Let us first summarize why one might be inclined to believe that gravity could play a role in a transition between quantum behavior and classical behavior or why the combination of gravity and macroscopic superpositions may cause uneasiness:

- in a very early attempt[40] to analyse the effect of gravity on macroscopic superpositions, Karolyhazy argued that there has to be a fundamental uncertainty in how well we can know the spacetime. Diósi gave a similar argument in Ref. [41].
- in one of his early papers, Diósi argued[42] that there was “obviously” something wrong with quantum physics: the spreading of wavepackets in combination with the spontaneous collapse of the wave function in a measurement would result in an instantaneous shift in the center of mass. This is, of course, based on the assumption that the wavepacket corresponds to a real mass distribution.
- in CSL and similar models, the collapse is assumed to be mass proportional. In the Diósi-Penrose model, the collapse is *gravity related and not merely mass proportional*[43]. In my words: if we have an unknown collapse mechanism that is mass proportional, would it not make sense that gravity then also would play a role?
- Penrose argues macroscopic superpositions would lead to a superposition of different metrics and a superposition of different time evolutions. He therefore proposes that any such state should be unstable and spontaneously collapse with a rate depending on the gravitational self-energy of the superposition state. He argues that one can also derive that from assuming that the equivalence principle also holds for quantum states in a gravitational field[44].

In a 2005 paper[45], Diósi describes commonalities of four theoretical models that assume that space-time and/or gravitational effects or uncertainties lead to modified dynamics compared to quantum theory. He shows that all these four models can be described with the same master equation that describes the evolution of a quantum system if there is a fundamental uncertainty in time. **Note:** Keep in mind that the physics behind those models can still be fundamentally different. For example, we saw already that we can describe some types of environmental decoherence and the collapse according to CSL using the same master equation. This only reflects the evolution of spatial superpositions. If we performed different measurements, the corresponding master equations could potentially show significant differences between collapse models and environmental decoherence.

5.2.1 The Károlyházy model

We will begin with the earliest attempts to see gravitational effects in the evolution of macroscopic superpositions. The Károlyházy model starts from a simple consideration: how well can we define a world line in spacetime given the uncertainty relation affecting our ability to determine/predict the position and motion of a test particle?

Consider a simple world-line segment $s = cT$ in a flat spacetime. Because the uncertainty principle will not allow a test particle to move along this world line with infinite precision, what we are considering is actually more a tube along the t axis, and now we want to make this tube as narrow as possible. Assume that the width of the wave-packet is Δx_0 in the beginning. Then the uncertainty of the test particle's velocity will be:

$$\Delta v = \frac{\hbar}{2m\Delta x_0}, \quad (5.19)$$

and the uncertainty in the position at the other end of our tube will be:

$$\Delta x = \Delta v T = \frac{\hbar c T}{2m\Delta x_0}. \quad (5.20)$$

We can achieve a minimum width all along the tube if we choose $\Delta x = \Delta x_0$. The higher the mass of our test particle, the narrower our tube. At the same time, Károlyházy assumes that the spread Δx should never become smaller than the gravitational radius of our test particle (similar to the Schwarzschild radius). So the smallest width we can achieve will be:

$$\Delta x \approx \frac{Gm}{c^2}. \quad (5.21)$$

Then the uncertainty of the length of our world-line segment will be[1]:

$$(\Delta s)^2 = (\Delta x)^2 = \frac{G\hbar}{2\Delta s c^3} s, \quad (5.22)$$

and therefore:

$$(\Delta s)^2 = \left(\frac{G\hbar}{2c^3} \right)^{2/3} s^{2/3}. \quad (5.23)$$

This equation giving the minimum uncertainty in the spacetime structure is known as the Károlyházy uncertainty relation.

This minimum uncertainty is then assumed to apply for any measure of spacetime distance. In order to model this, one can introduce a set of metrics $g_{\mu\nu}^\beta$ that only differ very little from the flat Minkowski metric $\eta_{\mu\nu} = \text{diag}(-1, 1, 1, 1)$. In particular, one assumes that changes occur only in the 00 element of the metric:

$$(g_{00}^{(\beta)})(x) = -1 + \gamma^{(\beta)}, \quad (5.24)$$

where $(\beta \neq 0)$.

For the metric with index β , we get the spacetime distance:

$$s_\beta = \int dt \left[g_{\mu\nu}^{(\beta)} \frac{dx^\mu}{dt} \frac{dx^\nu}{dt} \right]. \quad (5.25)$$

The actual spacetime distance we are interested in, however, is the average $\bar{s} = \langle s_\beta \rangle_\beta$ of the distances across our whole set of metrics, such that the variance will be equal to Károlyházy's uncertainty.

One can construct the $\gamma^{(\beta)}$ through their Fourier series[1]:

$$\gamma^{(\beta)}(x) = \frac{1}{L^{3/2}} \sum_{\mathbf{k}} \{ c^{(\beta)}(\mathbf{k}) \exp[i(\mathbf{k} \cdot \mathbf{x} - \omega t) + \text{c.c.}] \}, \quad (5.26)$$

where L is the side length of an arbitrarily large quantization box, resulting in the following modes:

$$\mathbf{k} = \frac{2\pi}{L} \mathbf{n} \text{ and } \omega = c|\mathbf{k}|. \quad (5.27)$$

The Fourier coefficients become:

$$c^{(\beta)}(\mathbf{k}) = f(k) \exp[i\alpha(\mathbf{k})], \quad (5.28)$$

where $\alpha(\mathbf{k})$ is a random variable such that:

$$\alpha(\mathbf{k}) \in \frac{2\pi}{N_{\mathbf{k}}} [0, 1, 2, \dots, N_{\mathbf{k}} - 1], \quad (5.29)$$

and one can show that:

$$f(k) = \left(\frac{G\hbar}{2c^3} \right)^{1/3} k^{-5/6}. \quad (5.30)$$

Because the Károlyházy's uncertainty in equation 5.23 becomes meaningless if s becomes very small, one assumes a cut-off such that $f(k) = 0$ for $k > 10^{15} \text{ m}^{-1}$ and $s < 10^{-15} \text{ m}$. A. Bassi et al[1] achieve the same results as Károlyházy by smearing out the phases of a set of quantum states instead of investigating a set of metrics. The cut-off parameter is then realized in the following way:

The spread in phase becomes comparable to π if the size of the wavepacket reaches a critical size a_c . As long as the size of a wavepacket is smaller than that size, it evolves coherently. If the wavepacket becomes larger, incoherent parts of the wave function evolve in different “coherence volumes” with a critical width of a_c . For a spherical

particle of size r , one can calculate a_c as follows:

$$a_c \approx \left(\frac{r}{\Lambda_p} \right)^{2/3} L \quad \text{if } R > a_c \quad (5.31)$$

$$a_c \approx \left(\frac{L}{\Lambda_p} \right)^2 L \quad \text{if } R < a_c, \quad (5.32)$$

where $L = \hbar/mc$ is the Compton wavelength of a particle of mass m , and

$$\Lambda_p = \left(\frac{G\hbar}{c^3} \right)^{1/2} \quad (5.33)$$

the Planck length. We can calculate an estimate for a_c by setting $r = a_c$ and setting equations 5.31 and 5.32 equal. If we then solve for r , we get a_c :

$$a_c \approx \left(\frac{27\hbar^2}{64G\pi^3\rho^3} \right)^{1/10}, \quad (5.34)$$

where ρ is the mass density of the spherical test particle.

The model of Károlyházy also provides a critical time scale:

$$\tau_c \approx \frac{ma_c^2}{\hbar}. \quad (5.35)$$

This is essentially the time it takes for the wavepacket of a particle of mass m to spread over a distance of a_c . That means, this is the time after which the evolution of the wavepacket will start to decohere very rapidly.

5.3 Superpositions in energy and uncertainty in time

Let us first discuss how time uncertainty leads to a modified master equation. Assume we have a system in a state $|\psi\rangle$ that is a superposition of two different energy eigenstates $|\phi_{1,2}\rangle$ with energies $E_{1,2}$:

$$|\psi(t)\rangle = c_1 e^{-\frac{i}{\hbar}E_1 t} |\phi_1\rangle + c_2 e^{-\frac{i}{\hbar}E_2 t} |\phi_2\rangle. \quad (5.36)$$

The two eigenstates will evolve slightly differently such that a relative phase factor $\exp[i\Delta E t]$ will appear. If we instead look at a slightly different time $t + \delta t$, we will have a slightly different relative phase factor $\exp[i\Delta E(t + \delta t)]$.

Now if there is a fundamental uncertainty of time, we can emulate that by randomly varying δt . In the simplest case, we can assume that this variation is a Gaussian random variable with zero mean[45].

One can then assume that the variance of δt is proportional to the time t . Diósi writes this as[45]:

$$\mathbf{M}[(\delta t)^2] = \tau t, \quad (5.37)$$

where the time scale τ determines the strength of the time uncertainty.

Then one can write the density matrix as a corresponding average over the pure-state density matrix:

$$\rho(t) = \mathbf{M}[|\psi(t)\rangle\langle\psi(t)|] = |c_1|^2|\phi_1\rangle\langle\phi_1| + |c_2|^2|\phi_2\rangle\langle\phi_2| + \quad (5.38)$$

$$+ \left\{ c_1^* c_2 \exp\left(\frac{i}{\hbar}\Delta E t\right) \mathbf{M}[\exp\left(\frac{i}{\hbar}\Delta E \delta t\right)] |\phi_2\rangle\langle\phi_1| + \right. \quad (5.39)$$

$$\left. + \text{h.c.} \right\}. \quad (5.40)$$

The average over the phase factor in the coherence terms results in:

$$\mathbf{M}[\exp\left(\frac{i}{\hbar}\Delta E \delta t\right)] = \exp[-t/t_D], \quad (5.41)$$

that means we get an exponential decay of the coherent terms, where the decoherence time t_D is given by:

$$t_D = \frac{\hbar^2}{\tau} \frac{1}{(\Delta E)^2}. \quad (5.42)$$

The density matrix then evolves according to the master equation[45]:

$$\frac{d\hat{\rho}}{dt} = -i\hbar^{-1}[\hat{H}, \hat{\rho}] - \frac{1}{2}\tau\hbar^{-2}[\hat{H}, [\hat{H}, \hat{\rho}]]. \quad (5.43)$$

Note the formal similarity between this master equation and the one we had for “normal” decoherence in position space.

5.4 Discrete time uncertainty

G. Milburn proposed[46] that there is a principal uncertainty in time on the order of the Planck time

$$t_P \equiv \sqrt{\frac{\hbar G}{c^5}}, \quad (5.44)$$

which is the time needed for light to travel the Planck length

$$l_P \equiv \sqrt{\frac{\hbar G}{c^3}}. \quad (5.45)$$

We have $t_P \approx 5.39 \times 10^{-44}$ s and $l_P \approx 1.62 \times 10^{-35}$ m.

In particular, Milburn proposed that for very short time steps, time would not vary

continuously but in discrete steps. Interesting characteristics of this model are that (1) it conserves constants of motion like momentum and energy in contrast to usual collapse models. (2) the model can be formulated in a Lorentz-invariant way[47].

If one expands the model to zeroth order, one retains Schrödinger's coherent evolution of quantum states. To first order, one gets a modified time evolution in line with equation 5.43 described in Diósi's treatment. For Milburn's model[46], one sets $\tau = t_P$ and gets the decoherence time:

$$t_D = \frac{\hbar^2}{t_P} \frac{1}{(\Delta E)^2}. \quad (5.46)$$

Because the decoherence time depends on the energy difference squared, the decoherence time will be very long as long as the one has tiny energy differences ΔE , but the decoherence will be very rapid for macroscopic energy differences.

For example, if one considers atomic superpositions where the energy difference is on the order of 1 eV, maybe up to a thousand eV, the decoherence time will be between 10^7 s and 10^{13} s. For large superpositions, on the other hand, where the energy difference can be on the order of 1 J, the decoherence time would be $\sim 10^{-25}$ s. That means, macroscopic superpositions would effectively decay immediately.

5.5 The Diósi-Penrose model

Diósi and Penrose proposed independent theoretical models based on rather dissimilar arguments[42, 48, 49, 50]. Eventually these arguments lead to the same predicted deviations from the predictions of quantum theory[45]. Diósi concluded[45]: *The potential dynamics, underlying the Penrose decay of massive superpositions, can not differ from my master equation or, at least, it must build on this master equation..* This is why these models now are usually referred to as a single model denoted as the Diósi-Penrose model (DP model).

For the sake of completeness, we will quickly describe these models separately, but because they result in the same master equation, we will later simply refer to them as the DP model.

5.5.1 The Penrose model

In the case of a macroscopic superposition of a massive object being at two macroscopically distinct positions, the spacetime curvature should, in principle, also be in a superposition of two corresponding states. Penrose argues[50] that this makes it difficult to identify an operator of “time translation”[50], which would be needed in order to define stationary states with definite energy. In other words, maybe one can write down a formal expression for two superposed space times, but how do we describe a physical system evolving inside such spacetimes? In particular, Penrose argues that one would need to at least approximately identify points in one space time with the points

in the other space time. At the same time, such an identification of space time points is incompatible with the gauge variance in general relativity or the principle of general covariance[50].

One way of comparing the two different space times would be to analyze how much the geodesics differ, i.e., how much the world lines of free falling particles differ in the two space times. If one considers the space times in the Newtonian limit, the metric can be written in terms of the Newtonian potential. Penrose then argues that one can quantify the difference in the free fall in the two difference metrics at a given point \mathbf{x} using the quantity:

$$(\mathbf{f} - \mathbf{f}')^2 = (\mathbf{f} - \mathbf{f}') \cdot (\mathbf{f} - \mathbf{f}'), \quad (5.47)$$

where \mathbf{f} is the gravitational force acting on a test particle (in the Newtonian limit). Then the total “incompatibility” in the two space times, or their uncertainty[50] would be given by the integral over the spatial extension of our massive object:

$$\Delta \equiv \int d^3x (\mathbf{f} - \mathbf{f}')^2 = - \int d^3x (\phi - \phi') (\nabla^2 \phi - \nabla^2 \phi'), \quad (5.48)$$

where ϕ and ϕ' are the gravitational potentials for the two different space times and $\mathbf{f} = -\nabla \phi$ and $\mathbf{f}' = -\nabla \phi'$.

Penrose then assumes that the gravitational field due to our massive system is given by Poisson’s formula:

$$\nabla^2 \phi = -4\pi G \sigma, \quad (5.49)$$

where σ is the mass density.

If one then assumes that the two superposed parts of the wavefunctions result in mass densities $\sigma(\mathbf{x})$ and $\sigma'(\mathbf{y})$ that result in gravitational potentials and gravitationally interact with each other, one gets:

$$\phi(x) = - \int d^3y \frac{\sigma(y)}{|\mathbf{x} - \mathbf{y}|}, \quad (5.50)$$

$$\Delta = -4\pi G \int d^3x \int d^3y \frac{(\sigma(x) - \sigma'(x))(\sigma(y) - \sigma'(y))}{|\mathbf{x} - \mathbf{y}|}. \quad (5.51)$$

Penrose then argues that one can use this uncertainty Δ as a fundamental energy uncertainty E_Δ resulting from such a superposition, and that this energy uncertainty then results in a finite lifetime of superpositions proportional to \hbar/E_Δ in the same way that the finite bandwidth of an atomic level is related to the life time of an excited state.

5.5.2 The Diósi model

Instead of a “global” time uncertainty δt as in Milburn’s proposal, Diósi introduces a local time uncertainty $t_{\mathbf{r}} \rightarrow t + \delta t_{\mathbf{r}}$, where \mathbf{r} refers to a given “spatial cell”[45]. In that

case, the average over local time uncertainty gives:

$$\mathbf{M}[\delta t_{\mathbf{r}} \delta t_{\mathbf{r}'}] = \tau_{\mathbf{rr}'} t. \quad (5.52)$$

If one writes the total Hamiltonian as a sum of local Hamiltonians $\hat{H} = \sum_{\mathbf{r}} \hat{H}_{\mathbf{r}}$, the master equation becomes:

$$\frac{d\hat{\rho}}{dt} = -\frac{i}{\hbar} [\hat{H}, \hat{\rho}] - \frac{1}{2\hbar^2} \sum_{\mathbf{r}, \mathbf{r}'} \tau_{\mathbf{rr}'} [\hat{H}_{\mathbf{r}}, [\hat{H}_{\mathbf{r}'}, \hat{\rho}]]. \quad (5.53)$$

This is just a generalized version of master equation 5.43, and it results in a decoherence time $t_D = \hbar/E_{\text{grav}}$, where E_{grav} is defined as[45]:

$$E_{\text{grav}} = \int d^3x \int d^3y \frac{(\sigma(\mathbf{x}) - \sigma'(\mathbf{x}))(\sigma(\mathbf{y}) - \sigma'(\mathbf{y}))}{|\mathbf{x} - \mathbf{y}|}. \quad (5.54)$$

Apart from the numerical factor $4\pi G$, this is identical to Penrose's expression, and since Diósi said that their expressions are identical, I assume that this might just be a question of how the gravitational potential is defined.

5.6 Decoherence due to gravitational time dilation

Let's do a simple gedankenexperiment. Let us assume, we have a beamsplitter for cats - for the sake of completeness, let's call it a cat splitter. Let us send a cat through the cat splitter. If the cat goes one way, we send it to Alpha Centauri with a speed close to the speed of light and then have it return home. If the cat does not take that path, we store it on Earth. After the possible round trip to Alpha Centauri, we overlap the potentially returning cat with the potentially stored cat at our cat splitter. Because of time dilation, the cat remaining on Earth will have aged a lot more than the space-travelling cat. They will be distinguishable and not interfere.

That is a short-hand description of the paper of I. Pikovski et al.[51]. In their case, the time dilation results from a complex system taking either a high path (lower gravity) or a low path (higher gravity). Depending on which path the system takes, it will experience different gravitational time dilation.

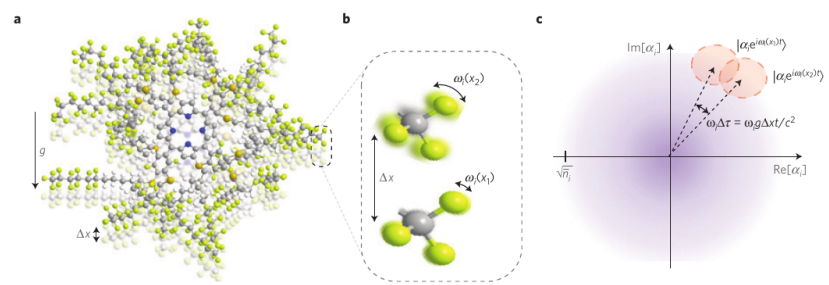


Figure 13: **Decoherence due to time dilation.** Pikovski et al [51] consider matter-wave interferometry with complex systems like molecules, where internal vibrations can be treated as clocks that will run slower or faster depending on which path they take in a gravitational field. This can lead to distinguishability in an interferometer and to decoherence.

6 Experimental tests via CM heating

We will discuss the potential for experimentally testing the foundations of quantum physics - either by looking for spurious heating of the center-of-mass motion or via the observation of matter-wave interferometry and the potential loss of coherence in such experiments.

6.1 CM heating of suspended or trapped objects

We already mentioned the option of testing quantum physics by monitoring the rate with which wavepackets expand. In the presence of decoherence, this expansion is typically quicker due to an additional diffusion of momentum or, in the case of collapse models, due to an actual increase in energy. However, this heating would also affect the CM motion of suspended or trapped objects. This could be seen in the position noise spectrum of trapped particles. Over the last years, researchers looked at existing data where the position noise spectrum of such systems was monitored very accurately for other reasons. In particular, this was done for various gravitational wave detectors like LIGO or AURIGA as shown in Fig.14.

Using these data, M. Carlesso et al.[53] derived bounds for the CSL model that were actually much more restrictive than the bounds set by other methods like matter-wave interferometry. The blue, green and red lines enclose areas of the parameter regime that have been excluded by data from LIGO, LISA Pathfinder and AURIGA, respectively. The Purple line and the purple shaded region is from ultra-cold cantilever experiments. Light-blue line: x-ray experiments. Gray line and gray-shaded region: excluded due to theoretical reasoning: for parameters in this regime, the proponents of the CSL model would deem the model useless because it would not prevent macroscopic superpositions.

There have been several interesting experimental results related to tests of CSL. For example, in an experiment by A. Vinante et al.[54], the authors measured the thermal noise in the motion of a cantilever by monitoring the motion of the cantilever using a superconducting quantum interference device (SQUID).

The noise associated with displacements of the cantilever should be of the form:

$$S_x = \left(\frac{S_{F0}}{k^2} + \frac{4k_B T}{k\omega_0 Q} \right) \frac{f_0^4}{(f_0^2 - f^2)^2 + (ff_0/Q_a)^2}, \quad (6.1)$$

where f_0 is the resonance frequency of the cantilever, k is the spring constant, k_B is

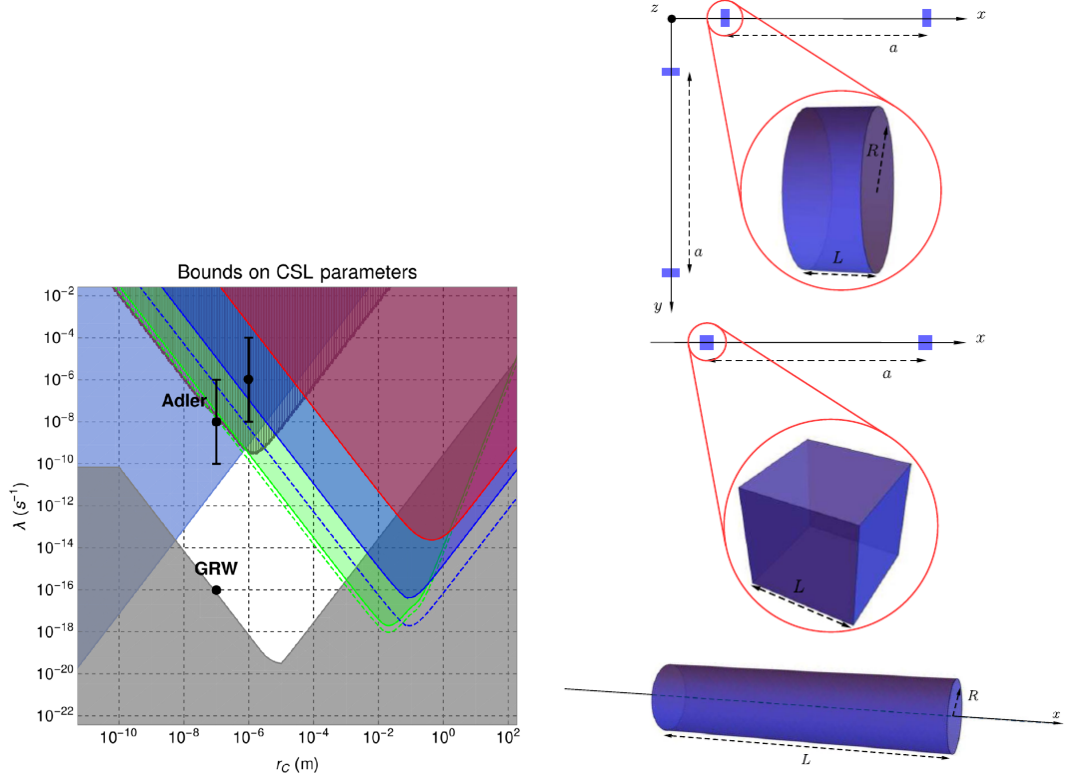


Figure 14: **(left) Bounds on the CSL parameters.** By now the results of many experiments have yielded bounds on the two parameters r_c and λ of the CSL model. The values GRW and Adler correspond to predictions of these parameters due to S. Adler[52] and Ghirardi, Rimini and Weber [33]. The shaded areas show which parameter regimes have been ruled out experimentally. The figure is from Ref. [53]. **(right) Systems analyzed.** In Ref. [53], the authors investigated three experiments (the LIGO and AURIGA gravitational wave detectors and the LISA Pathfinder system) to derive new bounds on CSL. On the top, the test masses in LIGO are indicated, in the middle. The middle shows the test masses in LISA Pathfinder, and the bottom shows the cylindrical test mass in the AURIGA detector.

Boltzmann's constant, T is the temperature, and S_{F0} is the noise spectral density of any non-thermal force noise. If there were effects from CSL, one would expect them to appear in S_{F0} .

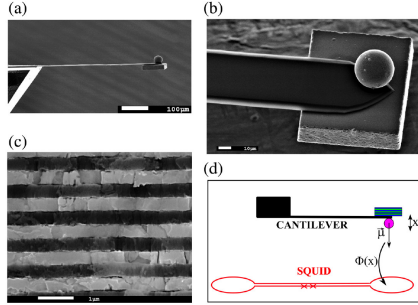


Figure 15: **Setup to measure cantilever heating.** A SQUID is used to monitor the thermal motion of a cantilever.

In the experiment one fits the noise spectral curves with an expression of the form:

$$S_\Phi = A + \frac{Bf_0^4 + C(f^2 - f_1^2)^2}{(f^2 - f_0^2)^2 + (ff_0/Q_a)^2}, \quad (6.2)$$

where A , B and C are fit parameters, and f_1 is an “antiresonance”, which is not relevant here. Q_a is the apparent quality factor, which is different from the “true” quality factor of the cantilever system due to damping introduced by the SQUID feedback electronics. Of particular importance is the Lorentz peak amplitude B because it depends on the temperature of the cantilever system:

$$B = \Phi_x^2 \left(\frac{S_{F0}}{k^2} + \frac{4k_B T}{k\omega_0 Q} \right), \quad (6.3)$$

where $\Phi_x = d\Phi/dx$ us the magnetomechanical coupling factor, S_{F0} is the force noise due to any non-thermal noise, and k is the stiffness of the cantilever.

The CSL model would lead to a heating of that temperature. That means, B would not go to zero as the system is cooled, and T/Q vanishes. The interesting thing is that Vinante's experiment showed a finite offset in the graph on the right-hand side of Fig. 16. This offset could, in principle, indicate a non-thermal heating effect as predicted by CSL. However, of course this offset could also result from experimental imperfections. Efforts over the last 3-4 years since an earlier experiment[55] have not yet identified the cause of this excessive heating.

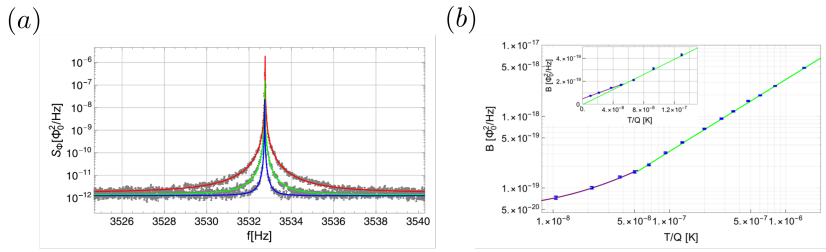


Figure 16: **Results of Vinante’s experiment.** A SQUID is used to monitor the thermal motion of a cantilever. (a) Noise spectra of the flux measured with the SQUID. (b) Temperatures extracted from those measurements.

6.2 Excessive X-ray radiation

Another method use to place bounds on collapse models is to monitor whether test objects emit an excessive amount of X rays. The reasoning behind that is that the momentum diffusion caused by collapses would result in the emission of X-rays if these collapses affect charged particles. For protons and electrons, that would of course be the case.

[17](#) shows a Germanium detector that was used in various experiments in an underground laboratory in Gran Sasso. With this detector, one can measure very low levels of X-rays. The values one can expect can be well simulated, and one can monitor for deviations from that, which could then be attributed to excessive X rays resulting from collapses.

In a recent experiment, where they performed such measurements, they concluded that their measurements ruled out the DP model[\[56\]](#). This is correct for certain versions of the DP model, where a length-scale cut-off parameter R_0 is assumed[\[57, 58\]](#). In particular, this cut-off parameter was introduced to avoid excessive heating being predicted by the DP model. The cut-off parameter defines the size of the mass distribution for each constituent of matter. In particular, if one calculates the self-gravitational potential according to equation [5.54](#), it would diverge if one assumes point-like mass distributions for he nuclei the matter consists of. The same would be true for the excessive heating due to the collapses.

The recent experiment of Donadi et al[\[56\]](#) was sensitive enough to provide a lower bound of $R_0 > 54 \text{ pm}$. Because this is smaller than the radius of the nucleus’ wavefunction, the authors conclude that the DP model is ruled out. I have my doubts about that[\[59\]](#) because it assumes that the mass distribution is given by the wave function. If one instead uses a continuous mass distribution to calculate the self-gravitational potential, one gets no limitation from the experiment of Donadi et al.

Another advantage of this approach is that it provides a lower bound on the gravitational decoherence one can expect from this model without the need for introducing any

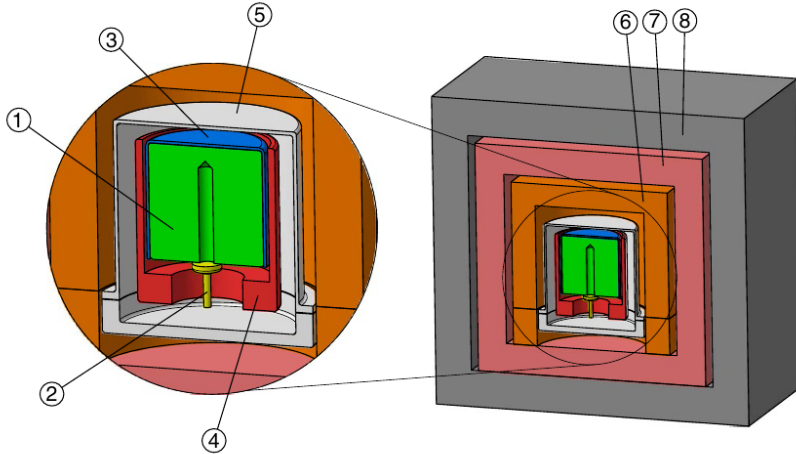


Figure 17: **Germanium detector used for Donadi et al's experiment.** A Germanium test mass is enclosed in various types of shielding, and the whole thing is additionally flushed with nitrogen inside a nitrogen storage tank. The whole thing is deep under ground and well shielded from cosmic radiation. The main background results from γ radiation from various isotopes and their decay products in the surrounding mountains. Picture taken from Ref.[56].

parameters to the DP model. For a continuous mass distribution we get the following spurious heating rate due to the collapses:

$$\frac{d\langle \hat{H} \rangle}{dt} = \frac{1}{2m} \frac{d\langle \hat{p}^2 \rangle}{dt} = \frac{m\hbar G}{2a^3} \quad (6.4)$$

for a particle of radius a and mass m . For a fused silica particle with $a = 200$ nm, this leads to a heating rate of 10^{-18} K/s. For comparison, Donadi et al got 10^{-4} K/s[56].

To calculate the expression above, we used a definition given by Penrose[44] for the gravitational self energy of a spherical test particle of radius a with a uniform mass distribution in a superposition of size $b = |\mathbf{y} - \mathbf{x}|$:

$$E_G = \begin{cases} \frac{m^2 G}{a} \left(2\lambda^2 - \frac{3}{2}\lambda^3 + \frac{1}{5}\lambda^5 \right) & \text{for } 0 \leq \lambda \leq 1 \\ \frac{m^2 G}{a} \left(\frac{6}{5} - \frac{1}{2\lambda} \right) & \text{for } 1 \leq \lambda \end{cases}$$

Here, $\lambda \equiv b/2a$ is a dimension-less parameter describing the size of the superposition.

6.3 CM heating in free evolution

In section 4.2 we gave a brief description of how collapse models would lead to wavepackets spreading more rapidly. Because the width of the wavepacket is **not** an observable but corresponds to the statistical distribution of position measurements, we saw that the accuracy with which we can determine the width of the wavepacket is related to the number of data points N we take. While this is typically not a big concern in lab experiments, it becomes important if we are dealing with very long times of free evolution t .

In particular, consider we have a total amount of time T for collecting our data. If we don't need time for anything but for the measurements, that gives us $N = T/t$. For example, for $t = 100$ s and $T = 30$ days, we get around 26 thousand data points. While this sounds quite a lot, we will see that this will not allow us to put very tight constraints on deviations from the predictions of quantum physics.

Earlier, we expressed this argument in terms of the width we measure for the wavepacket. To look for deviations from the predictions of quantum physics, it is actually more useful to look at the variance Δx^2 of the statistical distribution. This corresponds to the square of the width of the wave function. The fractional uncertainty of that variance will be[59]:

$$\frac{\delta(\Delta x^2)}{\langle \Delta x^2 \rangle} \approx \frac{\delta(\Delta x^2)}{\langle \hat{x}^2(0) \rangle + \frac{t^2}{m^2} \langle \hat{p}^2(0) \rangle} \approx \frac{\delta(\Delta x^2)}{\frac{t^2}{m^2} \langle \hat{p}^2(0) \rangle}, \quad (6.5)$$

where $\delta(\Delta x^2)$ denotes the statistical error of determining the variance. In the first step of approximation, we assumed that the deviations from the predictions of quantum physics are small. As a result, we can neglect them in the denominator compared to the other two summands. In the last step of the approximation, we assumed that t is sufficiently long such that the second summand in the denominator will dominate over the first. This is usually the case for $t \gtrsim 1$ s.

Given this statistical uncertainty, there will be a minimum Λ we will be able to distinguish from pure quantum evolution[59]:

$$\Lambda_{\min} = \sqrt{\frac{1}{2Tt}} \frac{3\langle \hat{p}^2(0) \rangle}{\hbar^2}. \quad (6.6)$$

If we assume that our initial state is a test particle of mass $m = 10^{10}$ amu in the ground-state of a harmonic potential with a trapping frequency $\omega/(2\pi) = 10^5$ Hz, then we have $\langle \hat{p}^2(0) \rangle = 2\hbar m \omega$, and assuming the same T and t we mentioned above, we get $\Lambda_{\min} = 2.61 \times 10^{19} \text{ m}^{-2}\text{s}^{-1}$. For comparison, the DP model for superpositions of such a silicon particle of that mass would be $\Lambda_{\min} = 5.1 \times 10^{10} \text{ m}^{-2}\text{s}^{-1}$. That means, we would be ten orders of magnitude away from being able to see such small deviations. That also means, in order to achieve that statistical accuracy, we would need to collect data for 10^{20} months...

The CSL model, on the other hand, predicts $\Lambda_{\min} = 2.8 \times 10^{16} \text{ m}^{-2}\text{s}^{-1}$. This is “only” three orders of magnitude smaller than Λ_{\min} . That would mean 10^6 months of data acquisition.

Are there other ways to improve this sensitivity? As we saw earlier, Λ_{\min} is proportional to ω . That means, we could reduce the trapping frequency. While this is possible to some extent, it comes with significant drawbacks because noise sources typically become more pronounced at lower frequencies. An attractive alternative was described by Branford et al.[60]. In particular, they found that instead of reducing $\langle \hat{p}^2(0) \rangle$ via tuning ω , one can reduce it by squeezing the initial state using optomechanical methods. Given that one can by now achieve 10 dB or even 20 dB squeezing for optical fields, we will likely be able to achieve something similar for optomechanical systems in the foreseeable future. In other words, this would help us improve the sensitivity Λ_{\min} by up to two orders of magnitude. Given such improvements, it is conceivable that we can test the CSL model for its original parameters λ and r_c , but it will be virtually impossible to test the DP model in this way.

7 Matter-wave interferometry

How do we best test the coherent evolution of increasingly large objects? We already mentioned possible experimental tests of the spreading of matter-wave wavepackets over time[61, 62, 28] and tests monitoring for non-thermal heating in massive objects[53, 55].

Such tests have their advantages, e.g., in order to scan for the presence of unwanted decoherence mechanisms. Nevertheless, the most direct tests of the predictions of quantum theory and the quantum superposition principle are demonstrations of matter-wave interferometry with increasingly massive test particles[63].

These experiments have been spearheaded and pursued by M. Arndt's group. Given that Markus gives a few lectures on this topic himself, I will only provide an overview and concentrate on the details that will be relevant for subsequent topics in our lecture.

7.1 Far-field interferometry vs. near-field interferometry

Let us consider a test particle that we prepare in a superposition of two (or more) spatially separated states. During the subsequent time evolution, the two (or more) parts of our wave function will spread from their original locations, overlap and interfere.

So far we only talked about master equations in general, but how does our state look like, and how does it evolve? Let us start by a simple Gaussian wavepacket in one spatial dimension:

$$\langle x | \phi(t) \rangle = \phi(x, t) = \frac{1}{\pi^{1/4} \sqrt{\sigma_0 + \frac{i t \hbar}{m \sigma_0}}} e^{-\frac{x^2}{2(\sigma_0^2 + i \frac{t \hbar}{m})}}, \quad (7.1)$$

where m is the mass of the test particle, and σ_0 is the width of the wavepacket for $t = 0$.

Because the Schrödinger equation is linear, we can simply add two of such states to get the evolution of a cat state. In particular, let us consider the superposition of two Gaussian states with width σ centered at positions $\pm \Delta/2$, i.e.:

$$|\psi(t)\rangle = \frac{1}{\sqrt{2}} (|\phi_1(t)\rangle + |\phi_2(t)\rangle), \quad (7.2)$$

with:

$$\phi_{1,2}(x, t) = \langle x | \phi_{1,2}(t) \rangle = \quad (7.3)$$

$$= \frac{1}{\pi^{1/4} \sqrt{\sigma + \frac{i\hbar}{m\sigma}}} e^{-\frac{(x \pm \Delta/2)^2}{2(\sigma^2 + i\frac{\hbar}{m})}}. \quad (7.4)$$

Because we are considering a pure state, the density matrix simply is:

$$\rho(x, y; t) = \langle x | \hat{\rho}(t) | y \rangle = \psi(x, t) \psi^*(y, t). \quad (7.5)$$

If one simply enters the expression we have above for $\psi(x; t)$, that works but the expression becomes quite complicated and one does not clearly see what's going on. The situation at time $t = 0$ is still fairly straight forward, and the structure of the density matrix becomes particularly clear if one writes it in terms of new variables $r = x + y$ and $s = x - y$:

$$\rho(r, s; 0) = \frac{e^{-\frac{s^2}{\sigma^2}}}{\sqrt{\pi\sigma}} \left(e^{-\frac{(2r-\Delta)^2}{4\sigma^2}} + e^{-\frac{(2r+\Delta)^2}{4\sigma^2}} \right). \quad (7.6)$$

This shows that the coherence (along s) drops exponentially. So do the diagonal terms (along r), but there the non-zero parts are centered around $\pm\Delta/2$.

How will the density matrix evolve in time from this initial state? In the simple case we mentioned above where we can write down the pure state, the answer is fairly simple, of course, but in general the density matrix will be a mixture of pure states.

As we know, the master equation for free evolution is simply:

$$\frac{d\hat{\rho}}{dt} = -\frac{i}{\hbar} [\hat{H}, \hat{\rho}] = -\frac{i}{2m\hbar} [\hat{p}^2, \hat{\rho}]. \quad (7.7)$$

In position representation, we get:

$$\frac{d\rho(x, y; t)}{dt} = \frac{i\hbar}{2m} \left(\frac{\partial^2}{\partial x^2} - \frac{\partial^2}{\partial y^2} \right) \rho(x, y; t). \quad (7.8)$$

If we use the variables r and s , this becomes:

$$\frac{d\rho(r, s; t)}{dt} = \frac{2i\hbar}{m} \frac{\partial^2 \rho(r, s; t)}{\partial r \partial s}. \quad (7.9)$$

For a general Gaussian state, one can write the density matrix in the form we already gave in equation 4.2[20]:

$$\rho(r, s; t) = \exp [-(\mathcal{A}(t)s^2 + i\mathcal{B}(t)rs + \mathcal{C}(t)r^2 + \mathcal{D}(t))]. \quad (7.10)$$

If one puts this into equation 7.9, one can derive a simple system of differential equations

for the coefficients $\mathcal{A}(t)$ etc like we mentioned earlier, and this then allows to describe the free expansion of a Gaussian wavepacket, even if one takes into account decoherence. In the case of decoherence mechanisms in the long-wavelength limit and using the variables r and s , our master equation becomes:

$$\frac{d\rho(r, s; t)}{dt} = \frac{2i\hbar}{m} \frac{\partial^2 \rho(r, s; t)}{\partial r \partial s} - i\Lambda s^2 \rho(r, s; t). \quad (7.11)$$

If we want to describe interference, however, our density matrix will no longer be of this general Gaussian form, and it becomes less straight forward to write down a simple, explicit expression for the density matrix. It is possible, of course, but from the structure of the density matrix the properties of the state of our system will not be obvious.

To describe the evolution of such states, it is often more helpful to consider the Wigner function or the characteristic function. We will briefly discuss these in the following.

7.1.1 The Wigner function

In a 1932 paper, E. P. Wigner introduced the following function without a particular motivation for this notation[64]:

$$W(x, p) = \frac{1}{2\pi\hbar} \int_{-\infty}^{\infty} d\xi \exp\left(-\frac{i}{\hbar}p\xi\right) \left\langle x + \frac{1}{2}\xi \middle| \hat{\rho} \middle| x - \frac{1}{2}\xi \right\rangle. \quad (7.12)$$

W. P. Schleich motivates this expression as the momentum representation of the transition amplitude from one position $(x - \frac{1}{2}\xi)$ to another $(x + \frac{1}{2}\xi)$ [64].

This motivation by Schleich already gives the hint that the Wigner function might have some nice properties when it comes to the free evolution of a particle. What one finds is that there is a very simple relation between the Wigner function at time t and the Wigner function at time $t = 0$ [65]:

$$W(x, p; t) = W(x - \frac{p}{m}t, p; 0). \quad (7.13)$$

Another useful property of the Wigner function is that its marginals correspond to the position and momentum distributions of the quantum state. Let us, for example, at the marginal when we integrate both sides of equation 7.12 over the momentum variable:

$$\int_{-\infty}^{\infty} dp W(x, p) = \int_{-\infty}^{\infty} d\xi \left\langle x + \frac{1}{2}\xi \middle| \hat{\rho} \middle| x - \frac{1}{2}\xi \right\rangle \int_{-\infty}^{\infty} dp \exp\left(-\frac{i}{\hbar}p\xi\right), \quad (7.14)$$

where we switched the order of the integrals over ξ and p . The integral over p results in

a Dirac delta over ξ , and we get:

$$\int_{-\infty}^{\infty} dp W(x, p) = \int_{-\infty}^{\infty} d\xi \left\langle x + \frac{1}{2}\xi \middle| \hat{\rho} \middle| x - \frac{1}{2}\xi \right\rangle \delta(\xi), \quad (7.15)$$

which yields:

$$\int_{-\infty}^{\infty} dp W(x, p) = \langle x | \hat{\rho} | x \rangle \equiv W(x). \quad (7.16)$$

Here, we introduced $W(x)$ as position distribution, that means the probability of finding our particle at position x .

Similarly, if we integrate the Wigner function over x , we get:

$$\int_{-\infty}^{\infty} dx W(x, p) = \langle p | \hat{\rho} | p \rangle \equiv W(p) \quad (7.17)$$

with the momentum distribution $W(p)$ [64].

Now let us take a look at the Wigner function of the states we introduced earlier. Let us first calculate the Wigner function of a pure Gaussian state. At time $t = 0$, the density matrix is:

$$\rho(x, y; 0) = \frac{1}{\sqrt{pi}\sigma} e^{-\frac{x^2+y^2}{2\sigma^2}}, \quad (7.18)$$

and the Wigner function then is:

$$W(x, p; 0) = \frac{1}{\pi\hbar} e^{-\frac{x^2}{\sigma^2} - \frac{p^2\sigma^2}{\hbar^2}}. \quad (7.19)$$

This shows that our Gaussian state is a state of minimum uncertainty. The width of the momentum distribution is indirectly proportional to the width of the position distribution according to Heisenberg's uncertainty relation: $\sigma_p = \hbar/\sigma_x = \hbar/\sigma$. We also notice that the Wigner function of the Gaussian state is **positive** for all x and p .

We can then simply use the relation $W(x, p; t) = W(x - \frac{p}{m}t, p; 0)$ to calculate the Wigner function at a later time t , and if we want we can use that to get the density matrix at the later time by using the simple relation:

$$\rho(x, y) = \int_{-\infty}^{\infty} dp e^{\frac{i}{\hbar}p(x-y)} W\left(\frac{x+y}{2}, p\right). \quad (7.20)$$

Now, let us calculate the Wigner function of our cat state using the same methods. We get:

$$W(x, p; t) = \frac{1}{\pi\hbar} e^{-\frac{p^2\sigma^2}{\hbar^2}} \left[e^{-\frac{(x - \frac{p}{m}t + \frac{\Delta}{2})^2}{\sigma^2}} + e^{-\frac{(x - \frac{p}{m}t - \frac{\Delta}{2})^2}{\sigma^2}} + e^{-\frac{(x - \frac{p}{m}t)^2}{\sigma^2}} \cos\left(\frac{p\Delta}{\hbar}\right) \right]. \quad (7.21)$$

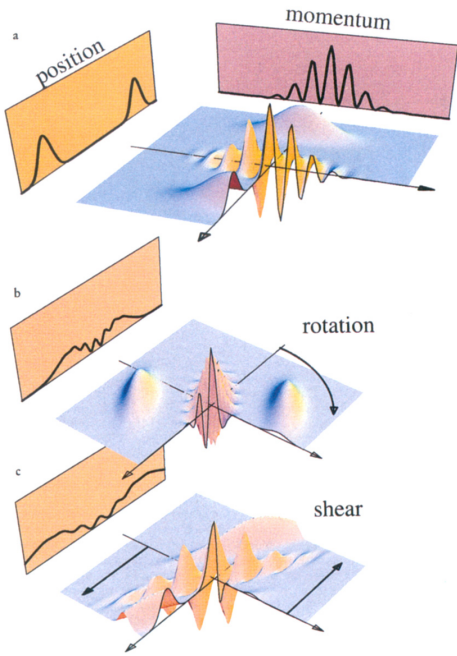


Figure 18: **Wigner function and its evolution.** The image illustrates the Wigner function for the double slit experiment in Ref.[66]. The image is taken from there.

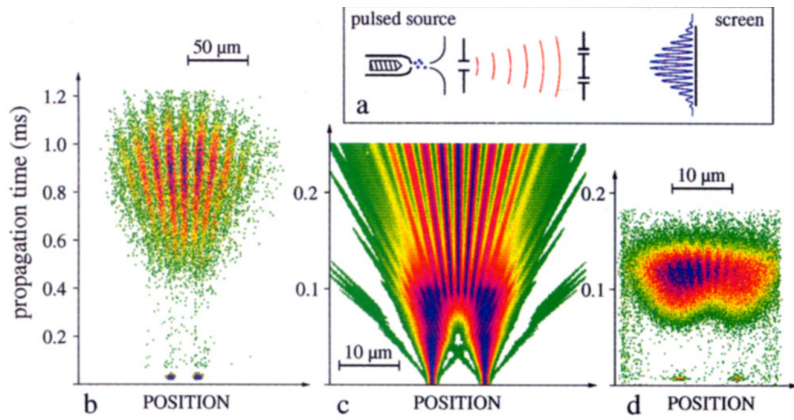


Figure 19: **Double-slit interferometry with atoms.** Image from Ref.[66].

If we look at the position distribution by taking the corresponding marginal, we get:

$$W(x) = (\pi(\sigma^2 + t^2\hbar^2/(m^2\sigma^2)))^{-\frac{1}{2}} \quad (7.22)$$

$$\left[e^{-\frac{(x+\Delta/2)^2}{\sigma^2+t^2\hbar^2/(m^2\sigma^2)}} + e^{-\frac{(x-\Delta/2)^2}{\sigma^2+t^2\hbar^2/(m^2\sigma^2)}} + \right] \quad (7.23)$$

$$2 e^{-\frac{x^2+(\Delta/2)^2}{\sigma^2+t^2\hbar^2/(m^2\sigma^2)}} \cos \left(\frac{t\hbar x \Delta}{m^2\sigma^4 + t^2\hbar^2} \right). \quad (7.24)$$

8 Near-field interferometry

While a double-slit-type interferometer is the conceptually clearest version of tests of the quantum superposition principle, such far-field interferometers can have practical limitations due to vibrations and gravity. For that reason, most matter-wave interference experiments with high masses have been performed using near-field interferometry.



Figure 20: **Talbot carpet with light.** In Ref. [67], the Arndt group used light to demonstrate the Talbot effect. Behind a coherently illuminated grating, a Talbot carpet forms - that means, depending on the distance from the grating, one gets different interference patterns, and at regular distances from the grating, one gets self-images of the grating. The (c) in the image is from the paper[67] and has no meaning here.

8.1 Experiments

In particular, these interferometers used the Talbot-Lau approach. The first of such experiments to demonstrate matter-wave interferometry with large molecules was Ref. [21]. This method is based on using three gratings. The first grating is illuminated by an incoherent source of test particles, and the slits of this first grating will then act as an array of coherent point sources. Each of these point sources coherently illuminates several grating periods of the second grating, where the actual interference takes place. The third grating is only there to analyze the periodicity of the interference pattern.

The central idea behind this approach is the Talbot effect that light (or a matter-wave) from a coherent point source that illuminates a grating will result in an interference pattern behind the grating that is called the Talbot carpet (Fig. 20). At regular distances from the grating, the interference pattern formed has the same period as the grating. This is an interference effect and demonstrates the coherent evolution of the waves

passing through the interferometer. If the test particles behaved classically, one would not see this interference effect but only a shadowing effect that usually has less visibility or at least behaves qualitatively different.

This self-imaging of the grating occurs at multiples of the Talbot length:

$$L_T = \frac{d^2}{\lambda} = \frac{mv^2 d^2}{h} = vt_T, \quad (8.1)$$

where we used the de Broglie wavelength for matter waves defined via $p = \hbar k$, and we introduced the Talbot time t_T , which we will need later. m is the mass of the test particles, and v is their velocity. The Talbot length will determine the size of the interferometer one needs to build and has to keep stable. For that reason, one ideally wants L_T to be sufficiently small to fit on an optical table. This means that one should prepare the test particles with a low initial velocity v and/or choose a grating with a small grating period d .

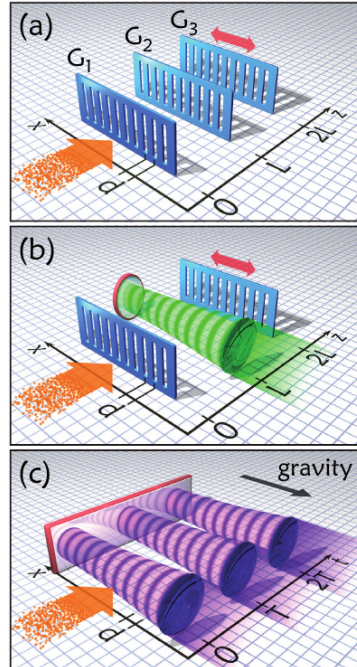


Figure 21: **Wigner function and its evolution.** The image illustrates different ways of realizing a Talbot-Lau interferometer (taken from Ref.[68]). (a) the three gratings are all material gratings. In (b), the central grating is replaced with a standing-wave light grating. (c) shows the approach in OTIMA (optical time-domain matter-wave interferometer[69]).

A simple setup with three gratings would be to use three identical material gratings that are separated by L_T . Then the interference pattern at the position of the third

grating would have the same period as that grating. That means if the maxima of the interference pattern hit the struts of the grating, no or very few particles will pass the third grating. If the interference maxima are at the positions of the opening so the third grating (nearly) all test particles will pass through. Therefore, if one translates the third grating perpendicular to the direction of the particle beam, one should get a periodic modulation in the number of particles detected behind the third grating. This method was often used by the Arndt group, e.g., in Refs. [21, 27]. In Fig. 22, we show the signal recorded by the Arndt group in Ref. 22. In the experiment, the visibility of this pattern is compared to the theoretical predictions of quantum physics and to the expectation if one did not have interference but just classical shadowing effects. The experimental results showed visibilities well beyond what could be expected from classical shadowing and agreed well with the quantum predictions.

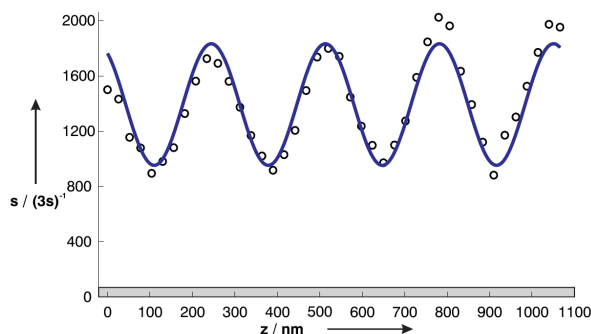


Figure 22: **Molecule flux after third grating.** In ref. [27], the Arndt group demonstrated matter-wave interference with molecules of around 10^4 amu (atomic mass units). This figure taken from their paper shows the number of molecules detected behind the third grating as the grating is translated perpendicular to the beam of molecules.

In the simplest case, one realizes this type of interferometer by using three identical material gratings (e.g., some plate with periodically arranged, narrow slits in it). This is shown in Fig. 21(a). I say “simplest” because nowadays, such gratings can be manufactured using readily available nano-fabrication techniques that allow resolutions down to a few tens of nanometers.

The main disadvantage of using matter-wave gratings is that they interact with the test particles via van-der-Waals interaction.

To overcome this limitation in more recent experiments, the Arndt group replaced the central grating with a standing-wave light grating. The corresponding interferometer was then called a Kapitza-Dirac-Talbot-Lau interferometer[70]. In that case, the light in the grating induces a dipole moment in the test particles, and this dipole moment then interacts with the light field (see, e.g., Ref. [68]). This introduces a phase shift on

the test particles, depending on where they pass through the grating. A schematic of the interferometer can be seen in Fig. 21(b).

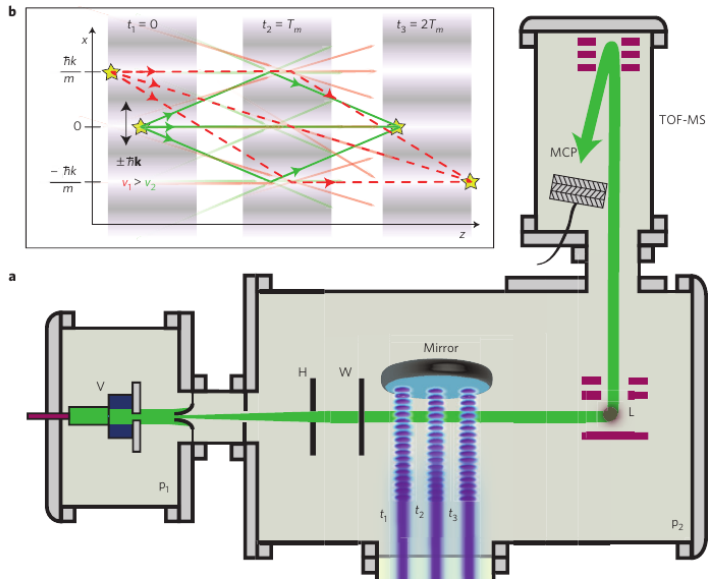


Figure 23: **OTIMA interferometer.** In ref. [69], the Arndt group demonstrated matter-wave interference with ionizing laser gratings. Panel (a) shows the interferometer, where the particles originate from an oven on the left while three ionizing laser beams enter the interferometer from the bottom and are reflected from a common mirror to create standing wave gratings. The gratings were pulsed a time T_m between the pulses. After the third grating, the signal of molecules was measured in a time-of-flight (ToF) spectrometer. By varying the vertical position of the central grating compared to the other two gratings, one could scan the interference pattern and compare the visibility with the predictions of quantum physics.

While standing-wave gratings are free from van-der-Waals interactions or imperfections from fabrication, the test particles can scatter and absorb the light. The absorption can heat up the particles or even break them apart (that may, e.g., be a problem for complex molecules). The scattering becomes a serious problem for very large particles if the scattered photons localize the particle well enough to cause significant decoherence. That means, when the scattered photons localize the test particle to within a distance comparable to the grating period. In addition to these fundamental issues, there is also the practical issue that the Arndt group had to spend a lot of effort into finding and/or designing large molecules that would (a) experience a large enough phase shift in the light gratings used, (b) would not absorb too much light, (c) or break apart due to the absorption of light.

Another disadvantage of such phase gratings is that they can only replace the center grating but not the first and the third grating. The Arndt group solved this by coming up with a new scheme: OTIMA (optical time-domain matter-wave interferometer[69]), the schematic of which is shown in Fig. 21(c), and more detailed schematic of the interferometer is shown in Fig. 23. In this scheme, all three gratings are replaced by light gratings, but in this case the laser wavelength is chosen such that the light will ionize test particles that pass through an anti-node of the grating. One can then get rid of these ionized particles in the case of the first and second grating, and in the case of the third grating, this actually can help to detect the test particles. The big advantage now is that (1) one does not need any material gratings anymore, (2) one can use the same mirror to reflect all three beams (this adds stability), and (3) one actually turns a bug into a feature: if a test particle absorbs “too much” light, it becomes ionized and one can sort it out. In this way, these laser gratings act like material gratings by not only applying a phase shift but by absorbing particles passing through antinodes of the grating. Interferometry could be scanned in two ways: (a) by changing the vertical position of the center grating (out of the plane of Fig. 23) or (b) changing the time delay of the pulse for the third grating. In case (a), one effectively choose different parabolas for the molecules detected, thus changing the path length between the gratings. In case (b), the signal-to-noise ratio (SNR) of the detected molecules varied with the time delay. This variation of the SNR results from the periodicity of the third grating matching or not matching the interference pattern.

8.2 Theoretical description

Here, we will follow the description given in S. Nimmrichter’s PhD thesis[68], which provides a good overview of the theory involved in the work of the groups of K. Hornberger and M. Arndt up to that point (2013).

As we mentioned in the last lecture, it proves to be convenient to describe the quantum evolution using Wigner functions (or characteristic functions). As a reminder, we defined the Wigner function as:

$$W(x, p) = \frac{1}{2\pi\hbar} \int_{-\infty}^{\infty} d\xi \exp\left(-\frac{i}{\hbar}p\xi\right) \left\langle x + \frac{1}{2}\xi \middle| \hat{\rho} \middle| x - \frac{1}{2}\xi \right\rangle. \quad (8.2)$$

We saw last time, that it is very simple to treat free evolution using the Wigner function, and it is also (mathematically) simple to determine the interference pattern by integrating $W(x, p)$ over the momentum.

In order to model the action of the three gratings, let us assume that each grating l has a complex transmission function $t^{(l)}(x) = |t^{(l)}(x)| \exp[i\phi^{(l)}(x)]$, where the possible absorption of the grating results from the modulus of $t^{(l)}$, and the phase $\phi^{(l)}(x)$ imparted on the test particle results from the imaginary factor.

Because the gratings are periodic, one can expand $t^{(l)}(x)$ into a Fourier series:

$$t^{(l)}(x) = \sum_{n=-\infty}^{\infty} b_n^{(l)} \exp\left(i \frac{2\pi n x}{d}\right) \quad (8.3)$$

This representation allows us to see the action of the grating on our state rather clearly. To this end, assume we let a momentum eigenstate $\langle x|p\rangle$ pass through the grating. Each term in the Fourier series will impart an integer multiple of the grating momentum $p_g = h/d$ on our momentum eigenstate:

$$\langle x|p\rangle \rightarrow t^{(k)}\langle x|p\rangle = \sum_{-\infty}^{\infty} b_n^{(k)} \exp\left(i \frac{2\pi n x}{d}\right) \langle x|p\rangle = \sum_{-\infty}^{\infty} b_n^{(k)} \langle x|p + n \frac{h}{d}\rangle. \quad (8.4)$$

This is only valid for thin gratings, i.e., particle movement parallel to the grating during the passage of the particles through the grating can be neglected. The treatment also neglects van-der-Waals interactions between the test particles and the grating.

If we describe our system using the Wigner function, this entails a Fourier transform from position space into phase space. The multiplication with the transition function in the position representation corresponds to a convolution in phase space with a “transmission kernel” T^l :

$$W(x, p) \rightarrow \int d\xi T^{(l)}(x, p - \xi) W(x, \xi). \quad (8.5)$$

To express the kernel in a compact form, we introduce the “Talbot coefficients” $B_n^{(l)}$:

$$B_n^{(l)}(\xi) = \sum_{j=-\infty}^{\infty} b_j^{(l)} \left(b_{j-n}^{(l)}\right)^* \exp[i\pi(n-2j)\xi], \quad (8.6)$$

$$T^{(l)}(x, p) = \sum_{j,n} \exp\left(i \frac{2\pi n x}{d}\right) b_j^{(l)} \left(b_{j-n}^{(l)}\right)^* \delta\left[p - \left(j - \frac{n}{2}\right) \frac{h}{d}\right] \quad (8.7)$$

$$= \frac{1}{2\pi\hbar} \sum_n \exp\left(i \frac{2\pi n x}{d}\right) \int ds e^{ips/\hbar} B_n^{(l)}\left(\frac{s}{d}\right). \quad (8.8)$$

We note that the Talbot coefficients are periodic in ξ , and the addition of multiples of h/d to the momentum reflects what we saw in the action of the grating on momentum eigenstates (equation 8.4). $B_n^{(l)}(0)$ corresponds to the Fourier components of $|t^{(l)}(x)|^2$.

An important property of Talbot-Lau type and similar interferometers is that purely classical particles also lead to a periodic modulation of the signal behind the third grating due to Moiré shadowing. To keep this short, we will not discuss the derivation of the classical shadow pattern, but it is relatively straight-forward to derive[68].

To describe the signal behind the third grating, one first assumes that the particle ensemble before the grating is an incoherent ensemble covering many grating slits. That

means the width of the initial distribution $X_0 \gg d$, and the assumption that the ensemble is incoherent is reflected in the assumption that the initial momentum spread fulfills $P \gg h/d$. If we assume the initial momentum distribution $D(p)$, which will depend on the particle source used, we get the following Wigner function after the first grating:

$$W_1(x, p) = \int d\xi T^{(1)}(x, p - \xi) D(\xi) / X_0. \quad (8.9)$$

After the first grating, one has free evolution for a time t_1 . Then each test particle passes through the second grating, followed by free evolution for a time t_2 and then the passage through the third grating. Then the Wigner function after the third grating is:

$$\begin{aligned} W_3(x, p) &= \frac{1}{X_0} \int d\xi_1 T^{(2)}\left(x - \frac{pt_2}{m}, p - \xi_1\right) \\ &\quad \times \int d\xi_0 T^{(1)}\left(x - \frac{pt_2}{m} - \frac{p_1 t_1}{m}, \xi_1 - \xi_0\right) D(\xi_0). \end{aligned} \quad (8.10)$$

Putting in the expressions for the grating kernels and integrating over p yields the interference pattern:

$$\begin{aligned} w(x) &= \frac{1}{X_0} \sum_{k,n} \tilde{D}\left(\frac{nt_1 + kt_2}{t_T} d\right) B_n^{(1)}\left(\frac{nt_1 + kt_2}{t_T}\right) B_{k-n}^{(2)}\left(\frac{kt_2}{t_T}\right) \\ &\quad \times \exp\left[i\frac{2\pi k}{d}\right], \end{aligned} \quad (8.11)$$

where $\tilde{D}(.)$ is the Fourier transform of $D(p)$, i.e., its characteristic function:

$$\tilde{D}(x) = \int d\xi e^{-i\xi x/\hbar} D(\xi). \quad (8.12)$$

This function is very narrow with its width given by $h/P_0 \ll d$. Because of the narrowness of this function, one can then make the “resonance approximation”[68], which means that only those terms in the Fourier sum in equation 8.11 contribute to the interference pattern where the indices n, k fulfill $|nt_1 + kt_2| \ll t_T$. In practice, this will only hold true for small values of n and k . Specific examples are, of course, $n = k = 0$, which corresponds to the contribution of the constant average particle density transmitted through the first two gratings. Apart from that, usually $|k|$ and $|k - n|$ will be small integer values because otherwise the corresponding Talbot coefficients become very small. We will discuss the resulting pattern in more detail in the next subsection.

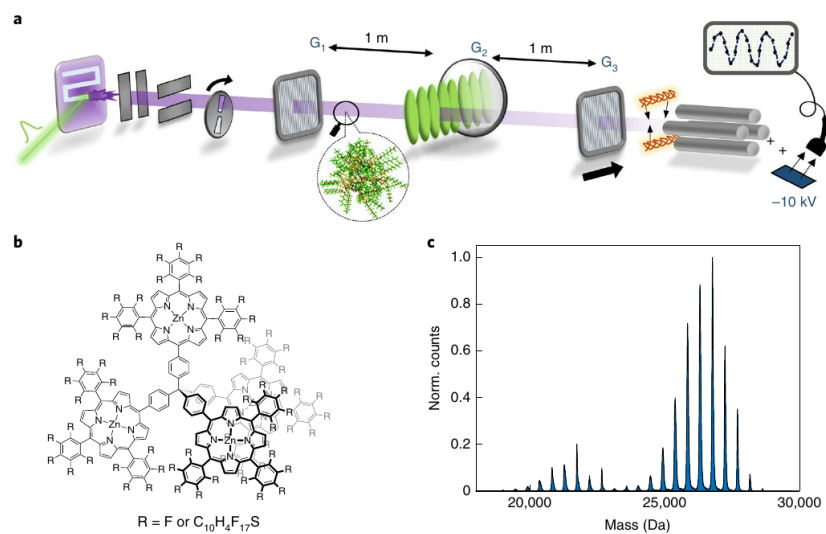


Figure 24: **Interference with molecules with $m \sim 2.5 \times 10^4$ amu.** In Ref. [30], the authors demonstrated matter-wave interferometry with the largest molecules so far (panel b). The interferometer (panel a) uses two material gratings and one optical grating. The molecules are charged and then characterized by a time-of-flight mass spectrometer.

8.3 State-of-the-art, challenges and the future

Why don't we simply perform matter-wave interferometry with arbitrarily large particles? One of the most obvious reasons is, of course, **decoherence** as we discussed earlier in this course. The finite temperatures of the test particles and of the environment will lead to decoherence due to the scattering, the emission and the absorption of blackbody radiation. In addition to that, we will have collisions with residual gas molecules. In addition to these unavoidable effects, there are also practical limitations. On the one hand, there are practical difficulties one has to deal with:

- **high-mass test particles:** the Arndt group has spent a lot of effort over the last two decades on finding or designing increasingly large molecules with the right properties to be used in their interferometers.
- **source:** if one finds fitting test particles, one has to have a method to bring them into the gas phase or to desorb them from a substrate surface. Challenges are for the particles to have clearly defined properties (mass, charge, ...) and for the particles to have low velocities to keep the Talbot length short.

Fig. 24 shows the setup and additional information about an experiment published by the Arndt group in 2019. They successfully demonstrated quantum superpositions with test particles with a mass of $\sim 2.5 \times 10^4$ amu. This is still the world record today (10.12.2021).

In 2014, Bateman et al published a proposal where they also suggested to use optomechanical cooling to prepare the initial quantum state of a test particle before using it for matter-wave interferometry. In their proposal, instead of three gratings, only one phase grating would be required. The proposed setup is shown in Fig. 25.

We will quickly describe the theory behind this approach, because we will refer to it later. To describe the phase grating acting on the test particle, let us assume that the light has the angular frequency $\omega = 2\pi c/\lambda$. If the particle radius R is much smaller than λ , we can operate in the Rayleigh regime, and the linear response of our dielectric particle will be described by the polarizability:

$$\alpha = 4\pi\epsilon_0 R^3 \frac{\epsilon(\omega) - 1}{\epsilon(\omega) + 2}, \quad (8.13)$$

where $\epsilon(\omega)$ is the relative permittivity of the material, which will in general depend on the frequency of the light. If R is significantly larger than an atom, one is typically safe in assuming that the material constants will be the same as in bulk material[14].

The light induces a dipole in the material, and the resulting potential due to the interaction between the dipole and the electromagnetic field will be (in one dimension):

$$V(x, t) = -\frac{1}{4} \text{Re}(\alpha) |\mathbf{E}(x, t)|^2 = -\frac{2\pi R^3}{c} I(x, t) \text{Re} \left(\frac{\epsilon(\omega) - 1}{\epsilon(\omega) + 2} \right). \quad (8.14)$$

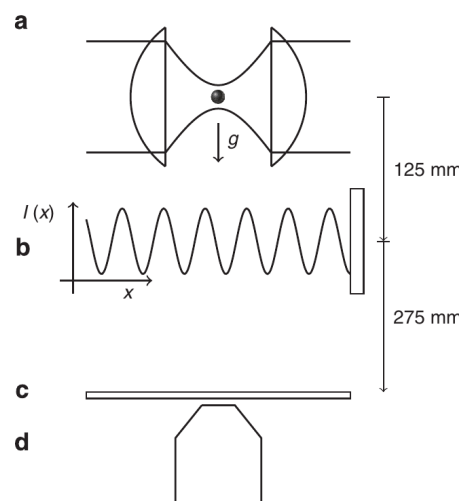


Figure 25: Near-field interferometry with optomechanical preparation. In the proposal of Bateman et al.[17], the authors propose to optomechanically (1) cool the motion of an optically trapped dielectric nanoparticle, (2) switch off the trap and let the particle drop through a standing-wave phase grating, (3) let the particle drop on a microscope slide. Repeating this procedure many times would result in a particle distribution on the microscope slide that should form an interference pattern depending on the power of the phase grating and the distances chosen between the trap, the grating and the microscope slide.

Now Bateman et al assumed that the light grating is only on for a short time (or that the particle passes quickly through a constant field), so the laser power experienced by the test particle will be a function of time $P_G(t)$. If the light is focused to an area a_G , then the corresponding intensity of the standing-wave grating will be:

$$I(x, t) = 4P_G(t)\cos^2(2\pi x/\lambda)/a_G \quad (8.15)$$

along the beam axis.

The phase shift experienced by a particle passing through the grating is:

$$\phi(x) = -\frac{1}{\hbar} \int dt V(x, t) = \frac{2\text{Re}(\alpha)E_G}{\hbar c \epsilon_0 a_G} \cos^2\left(\frac{2\pi x}{\lambda}\right), \quad (8.16)$$

where $E_G = \int dt P_G(t)$ is the integrated energy of the grating pulse.

Some of the grating power will be absorbed by the test particle: $P_{\text{abs}}(x, t) = \sigma_{\text{abs}} I(x, t)$, where the absorption cross section is $\sigma_{\text{abs}} = \omega \text{Im}(\alpha)/c\epsilon_0$. The number of photons absorbed on average then is[17]:

$$n(x) = n_0 \cos^2\left(\frac{2\pi x}{\lambda}\right) \equiv 2\beta\phi(x), \quad (8.17)$$

where we introduced

$$\beta = \frac{n_0}{2\phi_0} = \frac{\text{Im}(\alpha)}{\text{Re}(\alpha)} = \frac{3\text{Im}[\epsilon(\omega)]}{|\epsilon(\omega)|^2 + \text{Re}[\epsilon(\omega)] - 2}. \quad (8.18)$$

This is a parameter that only depends on the test particle's material.

Apart from photons being absorbed by the particle, they will also be scattered. The scattering cross section in the Rayleigh regime is given by $\sigma_{\text{sca}} = (2\pi/\lambda)^4 |\alpha|^2 / 6\pi\epsilon_0^2$, and the scattered number of photons will be $n_{\text{sca}} \equiv 2\eta\phi(x)$, where we introduced the parameter

$$\eta = \left(\frac{2\pi}{\lambda}\right)^3 \frac{|\alpha|^2}{6\pi\epsilon_0 \text{Re}(\alpha)} = \frac{2}{3} \left(\frac{2\pi R}{\lambda}\right)^3 \frac{|\epsilon(\omega) - 1|^2}{|\epsilon(\omega)|^2 + \text{Re}[\epsilon(\omega)] - 2}, \quad (8.19)$$

which depends on the size and the material of the test particle.

Because the discussion also includes the prediction of how decoherence effects the interference pattern, it is convenient to describe the evolution of our quantum state using the characteristic function - that is the Fourier transform of the Wigner function:

$$\chi(s, q; t) = \int dx dp W(x, p; t) e^{i(qx - ps)/\hbar} = \text{tr} \left(\hat{\rho} \exp \left[\frac{i}{\hbar} (q\hat{x} - \hat{p}s) \right] \right). \quad (8.20)$$

Now let us describe the original quantum state of the optomechanically cooled test

particle as a Gaussian:

$$\chi_0(s, q) = \exp\left(-\frac{\sigma_x^2 q^2 + \sigma_p^2 s^2}{2\hbar^2}\right), \quad (8.21)$$

which corresponds to the Wigner function

$$W_0(x, p) = \frac{1}{2\pi\sigma_x\sigma_p} \exp\left(-\frac{x^2}{2\sigma_x^2} - \frac{p^2}{2\sigma_p^2}\right). \quad (8.22)$$

σ_x and σ_p are the widths of the initial Gaussian distribution in position and momentum, respectively. If the initial state is thermal, these widths are given by[64, 17]:

$$\begin{aligned} \sigma_x^2 &= \frac{\hbar}{2m\omega_m} \coth\left(\frac{\hbar\omega_m}{2k_B T}\right) \\ \sigma_p^2 &= \frac{\hbar m \omega_m}{2} \coth\left(\frac{\hbar\omega_m}{2k_B T}\right), \end{aligned} \quad (8.23)$$

where ω_m is the mechanical frequency of our optically trapped test particle.

In order to see reasonable interference, the quantum state should cover many grating periods. This corresponds to the initial momentum spread being much larger than the grating momentum. That means: $\sigma_p \gg \hbar/d$. In that case, the initial characteristic function can be simplified to[17]

$$\chi_0(s, q) \approx \frac{\sqrt{2\pi}\hbar}{\sigma_p} \exp\left(-\frac{\sigma_x^2 q^2}{2\hbar^2}\right) \delta(s). \quad (8.24)$$

This assumption significantly simplifies the calculation of the interference pattern.

The authors include a decoherence effects by adding a time-dependent generator to the von Neumann equation:

$$\frac{\partial \hat{\rho}}{\partial t} = \frac{1}{i\hbar} [\hat{H}(t), \hat{\rho}] + \mathcal{L}(t)\rho. \quad (8.25)$$

In the position representation, they assume:

$$\langle x | \mathcal{L}(t) | y \rangle = \Gamma(t) [g(x - y) - 1] \langle x | \hat{\rho} | y \rangle, \quad (8.26)$$

where $g(0) = 1$. $\Gamma(t)$ is the rate of random jumps $\langle x | \hat{\rho} | y \rangle \rightarrow g(x - y) \langle x | \hat{\rho} | y \rangle$ occurring. g describes how well such a jump localizes the test particle.

After a time of free evolution t , the quantum state becomes:

$$\chi_t(s, q) = \chi_0\left(s - \frac{qt}{m}, q\right) \exp\left\{\int_0^t d\tau \Gamma(\tau) \left[g\left(s - \frac{q\tau}{m}\right) - 1\right]\right\}. \quad (8.27)$$

As in the theoretical description of the standard Talbot-Lau interferometer, we can describe the action of the phase grating using the Talbot coefficients:

$$\chi(s, q) \rightarrow \sum_n B_n\left(\frac{s}{d}\right) \chi\left(s, q + n\frac{h}{d}\right), \quad (8.28)$$

where we again note the addition of integer multiples of the grating momentum.

For a simple standing-wave grating as the one proposed in Ref. [17], the Talbot coefficients take on the simple form $B_n(\xi) = J_n[\phi_0 \sin(\pi\xi)]$, where $J_n(x)$ are the Bessel functions of the first kind. In order to get the classical pattern due to Moiré shadowing, one can simply replace the Talbot coefficients $B_n(\xi)$ with $C_n(\xi) = J_n[\phi_0 \pi\xi]$. Because $\sin(x) \approx x$ for small x , this already shows that we can only get interference patterns clearly distinct from the classical prediction if $\pi\xi$ is **not** small.

As we mentioned earlier, the use of laser gratings has the drawback that the test particles may scatter and absorb laser photons. This can potentially lead to significant decoherence, especially for large test particles or for particles consisting of a material with significant absorption at the laser wavelength.

For particles very small compared to the grating wavelength, the dominant decoherence effect resulting from these processes is the absorption of grating photons. This is a stochastic process that can be described by adding the following term to the master equation[17]:

$$\mathcal{L}_{\text{abs}}\hat{\rho} = \gamma_{\text{abs}} \left[\cos\left(\frac{\pi\hat{x}}{d}\right) \hat{\rho} \cos\left(\frac{\pi\hat{x}}{d}\right) - \frac{1}{2} \left\{ \cos^2\left(\frac{\pi\hat{x}}{d}\right), \hat{\rho} \right\} \right]. \quad (8.29)$$

The effect of the absorption can be taken into account similarly to equation 8.28, but in this case, the Talbot coefficients are replaced by[17]:

$$R_n^{(\text{abs})}(\xi) = \exp\left(-n_0 \frac{1 - \cos\pi\xi}{2}\right) I_n\left(n_0 \frac{1 - \cos\pi\xi}{2}\right), \quad (8.30)$$

where the I_n are modified Bessel functions.

If one combines this absorption effect with the coherent evolution we discussed earlier, one can still describe the evolution the same way, but one has to replace the Talbot

coefficients with the following modified coefficients:

$$B_n(\xi) = e^{-\zeta_{\text{abs}}(\xi)} \left[\frac{\zeta_{\text{coh}}(\xi) + \zeta_{\text{abs}}(\xi)}{\zeta_{\text{coh}}(\xi) - \zeta_{\text{abs}}(\xi)} \right]^{n/2} \times J_n \left[\text{sgn}\{\zeta_{\text{coh}}(\xi) - \zeta_{\text{abs}}(\xi)\} \sqrt{\zeta_{\text{coh}}^2(\xi) - \zeta_{\text{abs}}^2(\xi)} \right]. \quad (8.31)$$

Here, $\zeta_{\text{coh}}(\xi) = \phi_0 \sin \pi \xi$ and $\zeta_{\text{abs}}(\xi) = n_0 \sin^2(\pi \xi / 2) = \beta \phi_0 (1 - \cos \pi \xi)$ as in Ref. [17].

In order to also take into account the scattering of grating photons by the test particle, one has to do the following replacement of Talbot coefficients[17]:

$$\begin{aligned} B_n(\xi) &\rightarrow \sum_j B_{n-j}(\xi) R_j(\xi), \text{ where} \\ R_n^{(\text{sca})}(\xi) &= \exp \left[-\frac{n_R}{2} \left(1 - 3 \cos \pi \xi \frac{\sin \pi \xi - j_1(\pi \xi)}{2 \pi \xi} \right) \right] \\ &\times I_n \left[\frac{n_R}{2} \left(3 \frac{\sin \pi \xi - j_1(\pi \xi)}{2 \pi \xi} - \cos \pi \xi \right) \right], \end{aligned} \quad (8.32)$$

where $j_1(\pi \xi)$ is a spherical Bessel function, and $n_R = 2\eta\phi_0$.

A **central challenge** is the time-of-flight in the interferometer:

- the Talbot time $t_T = md^2/h$ approximately determines time of flight inside a near-field interferometer. On Earth, this limits test particle masses to $m \lesssim 10^8$ amu.
- long Talbot times are also a challenge for **vibration isolation**.

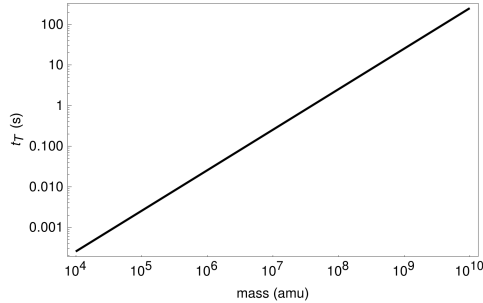


Figure 26: **Talbot time as a function of mass.** The Talbot time increases with mass.

We assumed a grating period of 100 nm. With realistically achievable grating wavelengths, we reach Talbot times on the order of 1 s for masses in the range of 5×10^7 amu to at most 5×10^8 amu. For Earth-bound experiments, free fall times on the order of several seconds are the limit.

9 Alternative ground-based tests of macroscopic superpositions

So far, we heard about ground-based tests of macroscopic superpositions using near-field interferometry (see e.g. Refs. [30, 17]), and why long free-fall times and low-frequency vibrations may render space an attractive alternative when going to higher test masses (see e.g. Ref. [28]). Over the last few years, there have been several suggestions of experiments that may (a) either provide alternatives to near-field interferometry over some of the parameter range covered by ground-based and by space-based experiments by observing orientational quantum interference[71] instead of center-of-mass interferometry, or proposals that promise allowing to overcome the limitations set by long free-fall times by (b) using electrostatic potentials to levitate charged particles [72], or (c) by using magnetic potentials and massive superconducting spheres in combination with varying magnetic fields to levitate the test particles and to accelerate their time evolution [15]. Here, we want to provide a brief overview of those proposals to illustrate how those very distinct efforts as well as center-of-mass near-field interferometry on ground and in space may complement each other to test quantum physics over an as large parameter range as possible.

9.1 Orientational quantum interference

In the course of using optically trapped particles for macroscopic quantum experiments, researchers have achieved increasing control over the center-of-mass (CM) motion of these particles to an extent that they were able to cool the CM motion close to the quantum ground state [73, 74, 75]. This success has been the goal of the optomechanics research community for the last decade. At the same time, the more control research groups achieved over the CM motion of trapped particles, the more attention was given to the other degrees of freedom. In particular, it was clear that the rotation of particles could potentially also affect the CM motion of trapped particles if they are not perfectly symmetric[76]. A high level of control over the rotation of particles was then shown by the Arndt group [77], after they aimed to develop a novel source of test particles for matter-wave interferometry [78]. In that source, a silicon substrate was patterned such that an array of thin, long silicon rods was created. Sending a strong laser pulse to the back of the substrate can then create a bulk acoustic wave inside the substrate, and that acoustic wave can then break the weak connection between some of the rods and the

substrate. The detached rods can then be slowed or even trapped as they pass through a standing wave[78]. This experiment is illustrated in Fig. 27.

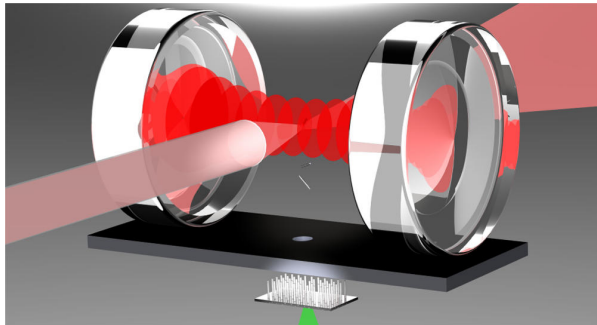


Figure 27: **Desorption of fabricated nanorods.** In an interesting new approach, the Arndt group manufactured nanorods, launched them via laser desorption and then used the light in a cavity to cool the rods' rotational degree of freedom[78].

In Ref. [77], they later trapped the released particles in an optical cavity inside a vacuum chamber at a moderate vacuum of ~ 1 mbar. By using two counter-propagating beams with well defined polarizations, the rotation of the particles could be controlled very precisely. The corresponding experimental setup is illustrated in Fig. 28. Monitoring the scattered light allowed to monitor all degrees of freedom (2 for rotation and 3 for translation).

The theoretical description of how decoherence would affect such asymmetric test particles or “nanorotors” [79] gave rise to the realization that such test particles may allow observing effects that cannot be observed in CM interferometry [80, 71]. This observation is taking advantage of the quantization of the orientational degree of freedom of asymmetric particles. The central idea is that one initially cools the rotational degrees of freedom such that the orientation of the particle is well defined. After one releases this control, the orientational distribution of the particle will quickly broaden similar to the broadening of a wavepacket after going through a single slit. Because the parameter space of orientations is limited to 2π per degree of freedom, these spreading parts will at some point overlap again and interfere. If that interference is constructive, we will have an *orientational revival*[80]. We illustrate that behaviour, and how one could realize and monitor it in an experiment in Fig. 29.

Please note that we are talking *orientational* revivals, and not about *rotational* ones. In particular, we are dealing where the rotational dynamics are restricted because of a torque that keeps an axis that is firmly related to the geometry of the body strongly aligned with an axis that is fixed in space. As an example, imagine a nanorod with its long axis at an angle θ relative to the vertical axis. Now, imagine a torque due to a trapping potential letting the nanorod sway back and forth between angles $\pm\theta$ relative

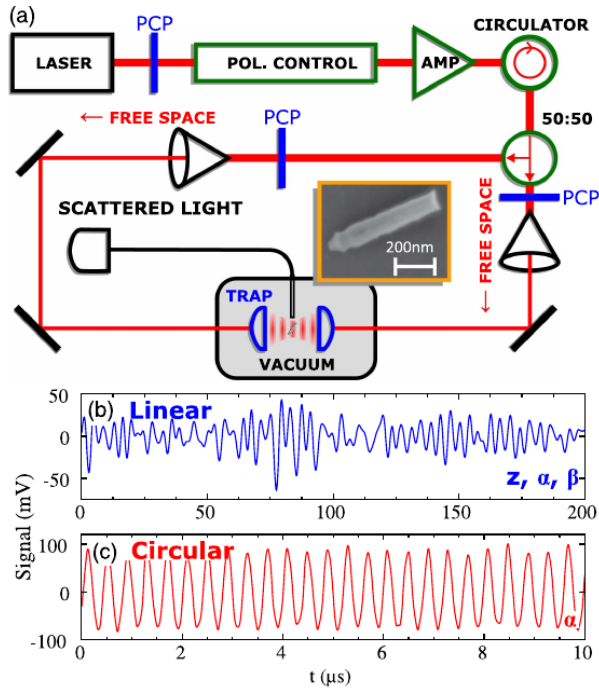


Figure 28: Counter-propagating beams are used to control the rotation of a trapped nanorod. The two counter-propagating beams trap a particle inside a vacuum chamber. The rotation of the particle is controlled by adjusting the rotations of the beams, and the various degrees of freedom of the trapped particle are monitored via the scattered light collected with a multi-mode fiber [77].

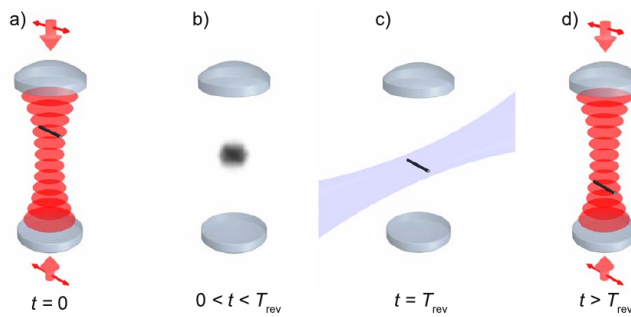


Figure 29: Orientational revival. (a) If one initially traps a particle and cools its orientation at time $T = 0$, the orientation will quickly disperse if the particle is released (b). After multiples of a time T_{rev} interference can lead to a revival of the orientation [80].

to that vertical axis. If this librational state is not pure but thermal, we can assign a librational temperature T to it and write the corresponding density matrix as[80]:

$$\rho_0 = \exp(-H/k_B T)/Z, \quad (9.1)$$

where $H = \mathbf{J}^2/2I + V(\hat{\beta})$ is the Hamiltonian, I is the moment of inertia, $\hat{\beta}$ is an angle operator, $V(\beta)$ is the potential trying to keep our test particle aligned with the z axis. The moment of inertia is given by $I = Ml^2/12$ for a linear rigid rotor of length l and mass M .

The free evolution of a nanorotor can, of course, be affected by decoherence mechanisms in an analogous way to the CM motion of test particles. For simplicity, let us take the conservative approach and assume that a single scattering event could already fully decohere the state into a fully mixed state ρ_i . This mixed state fulfils $\langle \Omega | \rho_i | \rangle = 4\pi$. The dynamics of the nanorotor can then be described by the following master equation[80]:

$$\frac{\partial \rho}{\partial t} = -i[H_0, \rho]/\hbar + \Gamma(\rho_i - \rho). \quad (9.2)$$

Here, Γ is the rate of decohering scattering events.

One can then describe the time evolution of the average alignment of the nanorotor as:

$$\langle \cos^2 \beta \rangle = \text{tr}[\rho(t) \cos^2 \hat{\beta}] = \langle \cos^2 \beta \rangle_u e^{-\Gamma t} + \frac{1}{3}(1 - e^{-\Gamma t}), \quad (9.3)$$

where the subscript u denotes the dynamics without decoherence, and we introduced the rate $\kappa = \sqrt{2k_B T/I}$.

Let us use the states $|jm\rangle$, where j denotes the total angular momentum, and m denotes the angular momentum along the field polarization to define a basis for our Hilbert space. In the absence of decoherence, we can then write the time evolution of the matrix elements of the density matrix as:

$$\langle jm | \rho_u(t) | j'm' \rangle = \sum_{j,j'=0}^{\infty} \sum_{m=-j}^j \sum_{m'=-j'}^{j'} \langle jm | \rho_0 | j'm' \rangle \exp \left[-\frac{i\hbar t}{2I} [j(j+1) - j'(j'+1)] \right]. \quad (9.4)$$

From equation 9.4, one can see that we will get the same state as the initial one after integer multiples of the *revival time*:

$$T_{\text{rev}} = \frac{2\pi I}{\hbar}. \quad (9.5)$$

The reason is that the two integer summands in the exponent in equation 9.4 are both even numbers independent of the actual values of j and j' .

From equation 9.5, and assuming a moment of inertia of $I = Ml^2/12$, we can see that the revival time will grow very quickly as we go to larger test particles. At the same

time, the duration of the revival will become very short compared to the revival time. These two facts may very quickly render it unfeasible to observe rotational revivals for increasingly massive test particles. Nevertheless, it is an intriguing idea that is worth investigating in more detail. There will very likely be a mass regime where observing rotational revivals is simpler than observing center-of-mass interferometry.

9.2 Experiments using magnetically levitated particles

Soon after the first proposals of using optically trapped particles for quantum optomechanics, it became apparent that the decoherence due to scattering of the light used for trapping could pose significant limitations. In particular, this scattering is a strong decoherence channel that will quickly decay quantum superpositions if their size is non-negligible compared to the wavelength of the trapping field. For that reason, it was proposed to instead levitate massive, superconducting test particles in a magnetic field. This is based on magnetic field being expelled from superconductors due to the Meissner effect. The idea was to use the Meissner effect to levitate superconducting spheres with a radius on the micrometer scale, and to couple their motion to a nearby qubit that could either be flux qubits or qubits based on LC circuits [81]. For this proposal, the size of the particle has to be large compared to the penetration depth of the magnetic field in order to allow magnetic levitation. For that reason, this method is not applicable to the sub-micron particles typically used in optomechanics with optically trapped particles. Because the mass density of superconducting materials is typically also higher than that of transparent dielectric media, proposals using magnetic levitation typically assume masses of at least around 10^{13} amu[81, 15].

There are, in principle, several huge advantages of magnetic levitation:

- There is no free fall, and there is no decoherence due to light scattering.
- The experiment is “automatically” at cryogenic temperatures because one typically needs that in any case to ensure that to achieve superconductivity.
- Because the trapped particles couple to magnetic fields, one can couple their motion to superconducting qubits, which allows transferring non-classical qubit states to non-classical center-of-mass states of the levitated particle via magnetomechanic coupling.

Performing matter-wave interferometry with such large superconducting particles would, of course, take very long times. Remember that we estimated around 10^2 s for near-field interferometry with 10^9 amu particles. For 10^{13} amu, we would therefore expect times on the order of 10^6 s or more for near-field interferometry – that would be more than 10 days per data point and several life times for an interferogram. For far-field interferometers like in double-slit interference, the situation is even more hopeless. To overcome that

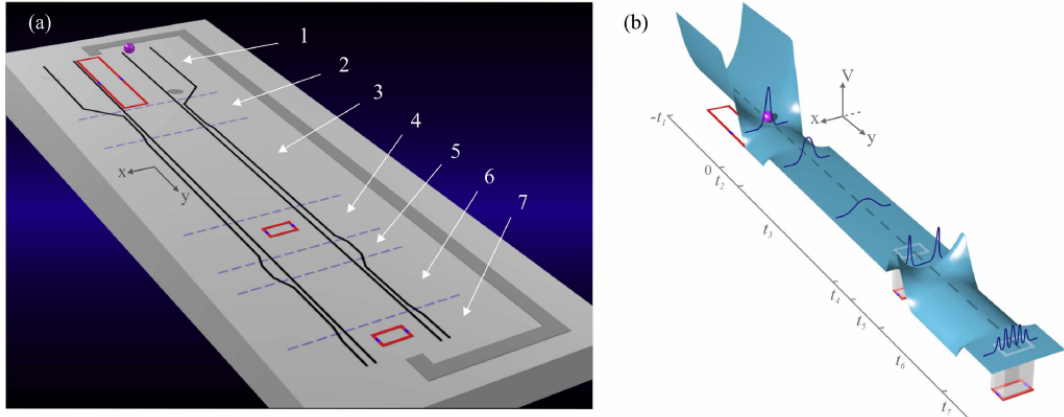


Figure 30: **Superconducting skatepark.** A particle is levitated above a superconducting chip. Persistent currents in the wires generate a magnetic potential along which the particle “skates”. After the particle has passed through the skate park, it is returned to the start along the dark-shaded path. Panel (a) illustrates the chip, and the dashed lines indicate the times indicated on the timeline in panel (b). That latter panel shows the magnetic potential, the particle encounters at different times. The figure is from Ref. [15].

limitation, O. Romero-Isart proposed to use conservative potentials to accelerate the time evolution [82].

This was also the basis for a proposal of Pino et al. [83] that was later published in Ref. [15]. There they proposed using magnetically trapped particles and accelerating potentials to observe far-field matter-wave interferometry. The central idea is that a superconducting sphere is magnetically levitated a short distance above a chip, where superconducting wires conduct persistent currents. These currents generate magnetic fields that allow (1) to guide the particles, (2) to accelerate the expansion of wavepackets, (3) to slow the expansion of wavepackets, (4) to accelerate the overlapping of different parts of the wave function to facilitate interference, and (5) to “inflate” the interference pattern to make it simpler to observe the interference. This is illustrated in Fig. 30. At various points, the levitated particle is coupled to superconducting qubits (a) to cool the motion of the particle in the initial trap, (b) to perform a squared position measurement to prepare a superposition, (c) to perform a final position measurement. After repeating the protocol many times, the measured positions should exhibit an interference pattern. Fig. 31 illustrates this protocol by showing how the Wigner function evolves in time during the various steps of the protocol. In the following, we will describe the protocol in more detail because that description will allow us to introduce a few interesting concepts.

9.2.1 Magnetomechanical cooling

For times $t < 0$, the CM motion of the test particle is first cooled using feed-back cooling by measuring the particle position using the magnetomechanic interaction with a nearby superconducting circuit containing a superconducting quantum interference device (SQUID). The measured position is used to feed back on the current generating the trapping potential. After this initial feedback cooling, the motion of the particle is coupled to a microwave resonator containing a SQUID. That coupling can be described with the following Hamiltonian[15]:

$$\frac{H_1}{\hbar} = -\Delta' \hat{a}^\dagger \hat{a} + \omega_1 \hat{b}^\dagger \hat{b} + g_l \hat{a}^\dagger \hat{a} (\hat{b} + \hat{b}^\dagger) - i E_1 E_1 (\hat{a} - \hat{a}^\dagger). \quad (9.6)$$

Here, Δ' is the detuning $\Delta' = \omega_{l_1} - \omega_{c_1}$ between the cavity driving field ω_{l_1} and the cavity resonance ω_{c_1} , E_1 is the strength of the cavity drive, ω_1 is the trap frequency, and g_l is the linear magneto-optical coupling between the motion of the sphere and the cavity field. The above Hamiltonian is given in the rotating frame around the cavity driving frequency.

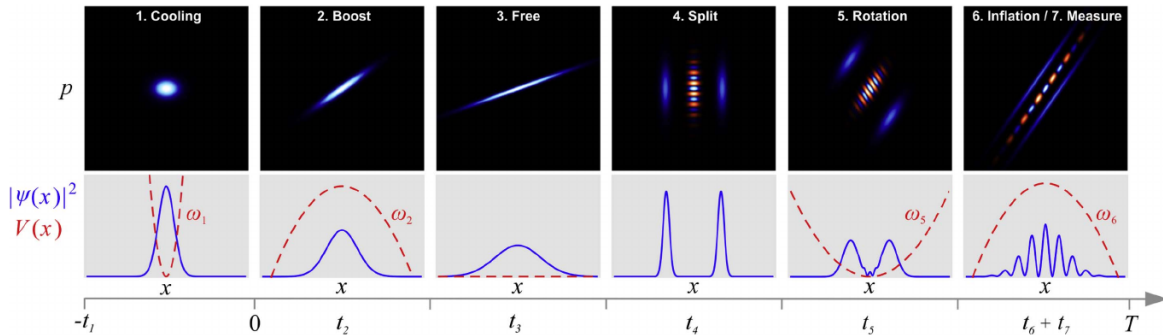


Figure 31: **Protocol for double-slit interference in the magnetomechanic skatepark.** In the beginning (for times $t < 0$) the particle is trapped and cooled in a narrow potential. Starting at $t = 0$, the wavefunction expansion is accelerated by an inverse potential (“inflation”). After that, the particle is coupled to a superconducting qubit, and the square of the position is measured to create a superposition state. For a short time, a potential is applied to give momenta of opposing sign to the two parts of the wave function to reduce the time they need to overlap and interfere. Then another potential for additional “inflation” is applied, essentially to magnify the interference pattern. The figure is from Ref. [15].

If one assume sufficiently large cavity fields and motion of the sphere, one can linearize the system by changing the operators as $\hat{a} \rightarrow \alpha_1 + \hat{a}$ and $\hat{b} \rightarrow \beta_1 + \hat{b}$. If one assumes the

proper values for α_1 and β_1 [15], and if one assumes weak coupling ($g_l|\alpha_1|/(2\kappa_1) \ll 1$), then the master equation results in the following equation for the change of the phonon number of the CM motion of the levitated sphere [15]:

$$\frac{d\langle\hat{b}^\dagger\hat{b}\rangle}{dt} = -(A_- - A_+)\langle\hat{b}^\dagger\hat{b}\rangle + A_+. \quad (9.7)$$

This also assumes, as Pino et al put it, that the thermal bath attached to the cavity mode is at zero temperature. Effectively, this means that the optical state coupled to the cavity is close to a pure state. A_\pm are damping and driving terms given by:

$$A_\mp = 2g_l^2|\alpha_1|^2 \frac{\kappa_1}{(\Delta \pm \omega_1)^2 + \kappa_1^2}. \quad (9.8)$$

Here, $\Delta = \Delta' + 2g_l^2|\alpha_1|^2/\omega_1$ is the shifted detuning to take into account the shift of the resonance frequency of the microsphere due to the optomechanical coupling.

If we have an initial thermal occupation of n_0 for the CM motion of the particle at time $t = -t_1$, then the average occupation number at time $t = 0$ will be[15]:

$$\bar{n} = \frac{A_+}{A_- - A_+} + \left(n_0 - \frac{A_+}{A_- - A_+} \right) e^{-(A_- - A_+)t_1}. \quad (9.9)$$

If there is additional heating Γ , one can include that by adding it to A_+ . The cooled state will be a Gaussian with the following moments:

$$\begin{aligned} v_x(t=0) &\equiv \text{tr}(\hat{x}^2\hat{\rho}(t=0)) = \sigma_1^2(2\bar{n} + 1), \\ v_p(t=0) &\equiv \text{tr}(\hat{p}^2\hat{\rho}(t=0)) = \frac{\hbar^2}{4\sigma_1^2}(2\bar{n} + 1), \\ c(t=0) &\equiv \text{tr}\left[\frac{1}{2}(\hat{x}\hat{p} + \hat{p}\hat{x})\hat{\rho}(t=0)\right] = 0, \end{aligned} \quad (9.10)$$

$$(9.11)$$

where $\sigma_1 = \sqrt{\hbar/(2m\omega_1)}$ is the ground-state size of the trapped particle, and m is its mass.

9.2.2 Accelerated expansion

In order to make the wavefunction expand faster, an inverted harmonic potential of frequency ω_2 is applied. This will boost the momentum variance by an exponential factor $\exp(2\omega_2 t_2)$. During expansion, of course, there may also be some additional decoherence but, theoretically, this acceleration will preserve the Gaussian nature of the state.

How this accelerated expansion affects the state can be expressed using the following

differential equations [15]:

$$\begin{aligned}\dot{v}_x(t) &= \frac{2}{m}c(t), \\ \dot{v}_p(t) &= 2m\omega_2^2 c(t) + 2\hbar^2 \Lambda_2, \\ \dot{c}(t) &= m\omega_2^2 v_x(t) + \frac{1}{m}v_p(t).\end{aligned}$$

These can easily be solved using the initial conditions in equation 9.10. The solutions for $t = t_2$ are given in Ref. [15]. After the initial cooling followed by the accelerated expansion, the particle then evolves freely for a time t_3 similar to experiments we discussed earlier.

9.2.3 The double slit

The double slit in this proposal is realized via post selection after an \hat{x}^2 measurement like it was originally proposed in 2011 for optically trapped particles (see, e.g. Ref. [39]). The central idea is simple: if we measure \hat{x}^2 , the measurement will provide us with an absolute value $|x|$ of the particle position, but the sign is missing. The state will therefore be a superposition of the two states $|\pm x\rangle$. One can then discard all particles where the $|x|$ is not within a predefined range of values. In particular, one can choose results where $|x|$ corresponds to some slit separation d . The width of the slits will be determined by the strength of the measurement because it defines the uncertainty of the outcome.

One can realize the interaction necessary for such a measurement via the quadratic coupling of the CM of the sphere to a cavity containing a SQUID. Pino et al assume that the result is read out via a homodyne measurement. This quadratic interaction is left on for a finite time t_4 between times T_3 and T_4 . While we will not reproduce the derivation, we want to briefly present the result. For simplicity, let us use the notation of Pino et al for the spatial representation of the density matrix:

$$\langle x | \hat{\rho}(t) | y \rangle = A(x, y, t) \exp[i\phi(x, y, t)], \quad (9.12)$$

where we introduce the real quantities A and ϕ to separate the amplitude from the phase.

The effect of a measurement on the density matrix can then approximately be described by the relation[15]:

$$\rho(x, y, T_4) \approx M_{\mathcal{W}}(x) M_{\mathcal{W}}(y) A(x, y, T_3), \quad (9.13)$$

where we introduced:

$$M_{\mathcal{W}}(x) = \left(\frac{2}{\pi}\right)^{1/4} \exp\left[-\left(\chi_4 x^2 - \frac{\mathcal{W}}{2\sqrt{t_4}}\right)^2\right]. \quad (9.14)$$

That means, the measurement multiplies the initial density matrix with functions whose peaks will depend on the measurement outcome. In particular, \mathcal{W} is a normally distributed random outcome. It has zero mean and a variance of t_4 . These are related to the outcome of the homodyne measurement: $p_L \equiv \mathcal{W}/(2\sqrt{t_4})$. The measurement strength λ of the continuous position-squared measurement depends on the quadratic optomechanical coupling g_q and the cavity decay rate is κ_4 . Then we have $\lambda \equiv g_q^2 |\alpha_4|^2 / \kappa_4$ [15]. We can then write the measurement strength of the position-squared measurement read out via homodyne detection as: $\chi_4 \equiv \sqrt{2\lambda t_4} = g_q |\alpha_4| \sqrt{2t_4/\kappa_4}$. Given what Pino et al call an “adiabatic elimination condition”, one can write $\chi_4 \ll 2\sqrt{t_4\kappa_4}$.

Following the measurement under the assumptions we made, the position probability distribution will be given by two Gaussian peaks that are separated by the distance:

$$D = 2\sigma_4 \sqrt{\frac{p_L \chi_4 - \mathcal{P}_3^2}{\chi_4^2}} \approx 2\sigma_4 \sqrt{\frac{p_L}{\chi_4}}. \quad (9.15)$$

The width of each slit is:

$$\sigma_d = \frac{\sigma_4}{\sqrt{8(p_L \chi_4 - \mathcal{P}_3^2)}} \approx \frac{\sigma_4}{8p_L \chi_4} = \frac{\sigma_4^2}{\sqrt{2}\chi_4 d}. \quad (9.16)$$

The approximation assumed that $p_L \chi_4 \gg \mathcal{P}_3^2$, which means that the two peaks are clearly distinguishable. \mathcal{P}_3 is the purity of the state after the expansion of the state[15]. The purity is calculated as the trace of square of the density matrix $\mathcal{P}(t) = \text{tr}(\rho^2(t))$, and the index denotes the time. For example, $\mathcal{P}_3 = \mathcal{P}(T_3)$, where T_3 denotes the time when the free expansion ends.

As we indicated earlier, the double slit in this approach is prepared in post selection. That means, one only keeps the particles where the x^2 measurement results in adequate measurement results. That means, results where the separation of the slits has values within a specified range $[d_{\min}, d_{\max}]$. Of course, this only makes sense if the probability for such measurement outcomes is sufficiently high. If the measurement strength is chosen strong enough ($p_L \chi \gg \mathcal{P}_3^2$), one can approximate that probability to be[15]:

$$\int_{d_{\min}}^{d_{\max}} dl P_s(l) \approx \text{erf}(\mathcal{P}_3) - \text{erf}\left[\frac{2\mathcal{P}_3}{\sqrt{\chi_4}}\right]. \quad (9.17)$$

Here, $P_s(d)$ is the probability that the x^2 measurement yields a slit width d :

$$P_s(d) = \frac{\chi_4 d}{2\sigma_4^2} P_o \left(\frac{\chi_4 d^2}{4\sigma_4^2} + \frac{\mathcal{P}_3^2}{\chi_4} \right). \quad (9.18)$$

$P_o(p_L)$ is the probability for a measurement outcome p_L in the homodyne measurement:

$$P_o(p_L) = \text{Tr} [\hat{\mathcal{M}}_{\mathcal{W}} \hat{\rho}(T_3) \hat{\mathcal{M}}_{\mathcal{W}}^\dagger] = \left(\frac{2}{\pi} \right)^{\frac{1}{2}} \int dx e^{-2(\chi_4 x^2 - p_L)^2} \langle x | \hat{\rho}(T_3) | x \rangle. \quad (9.19)$$

Here, $\hat{\mathcal{M}}_{\mathcal{W}} = M_{\mathcal{W}}(\hat{x})$ using the function defined in equation 9.14.

9.2.4 Rotation and acceleration of the fringe formation

Like we discussed earlier, the duration for the interference fringes to form after a grating (or double slits) can take a very long time. Because one observes far-field interferometry in a double-slit setup, it takes even longer. To keep the time to a manageable duration, Pino et al. propose to follow the double-slit measurement described above by another phase where a conservative, inverted harmonic potential accelerates the time evolution similar to the original accelerated expansion. This inverted harmonic potential is assumed to have a resonance frequency ω_6 . Before this accelerated expansion, however, the Wigner function first has to be correctly rotated such that the accelerated expansion affects the correct dimension of the Wigner function (see Fig. 31). This can be achieved by exposing the particle to a harmonic potential with resonance frequency ω_5 for a time t_5

If one chooses the frequencies $\omega_{5,6}$ and times $t_{5,6}$ such that:

$$\cos(\omega t_5) = \frac{\omega_5}{\omega_6} \sin(\omega_5 t_5), \quad (9.20)$$

then one gets:

$$\hat{x}(T_6) \approx e^{\omega_6 t_6} \hat{p}(T_4) \frac{\sin(\omega_5 t_5)}{2m\omega_5} \left[1 + \left(\frac{\omega_5}{\omega_6} \right)^2 \right]. \quad (9.21)$$

That means, that the position operator at time T_6 will be proportional to the momentum operator at time T_4 , and that the proportionality factor will grow exponentially with t_6 . A time T_6 , one will therefore see an interference pattern in position corresponding to the earlier interference in the momentum basis (see Fig. 31). The fringe spacing of that interference pattern will grow exponentially with t_6 .

Bibliography

- [1] Angelo Bassi, Kinjalk Lochan, Seema Satin, Tejinder P. Singh, and Hendrik Ulbricht. Models of wave-function collapse, underlying theories, and experimental tests. *Rev. Mod. Phys.*, 85:471–527, Apr 2013. [1](#), [9](#), [41](#), [42](#), [43](#), [44](#), [45](#), [46](#), [49](#), [50](#)
- [2] Č. Brukner. On the Quantum Measurement Problem. In R. Bertlmann and A. Zeilinger, editors, *Quantum [Un]Speakables II*. Springer, 2017. [1](#), [11](#), [12](#), [13](#)
- [3] Maximilian A. Schlosshauer. *Decoherence and the Quantum-to-Classical Transition*. Springer, Berlin, 2007. [1](#), [18](#), [26](#), [29](#), [32](#), [33](#), [34](#), [35](#), [36](#), [37](#), [41](#), [42](#), [43](#), [44](#)
- [4] M. Kumar. *Quantum: Einstein, Bohr and the Great Debate About the Nature of Reality*. Icon Books, 2000. [2](#), [9](#)
- [5] E. Schrödinger. Die gegenwärtige Situation in der Quantenmechanik. *Die Naturwissenschaften*, 23(48):807–812, 1935. [3](#)
- [6] W. H. Zurek. Pointer basis of quantum apparatus: Into what mixture does the wave packet collapse? *Phys. Rev. D*, 24:1516–1525, Sep 1981. [7](#)
- [7] W. H. Zurek. Environment-induced superselection rules. *Phys. Rev. D*, 26:1862–1880, Oct 1982. [7](#)
- [8] W. H. Zurek. Quantum Darwinism and Envariance. *arXiv:quant-ph/0308163*, August 2003. arXiv: quant-ph/0308163. [7](#)
- [9] Philip Ball. Why the Many-Worlds Interpretation Has Many Problems, October 2018. [11](#)
- [10] Robert P. Crease. The bizarre logic of the many-worlds theory. *Nature*, 573(7772):30–32, September 2019. Bandiera_abtest: a Cg_type: Books And Arts Number: 7772 Publisher: Nature Publishing Group Subject_term: Quantum physics, History. [11](#)
- [11] Simon Saunders, Jonathan Barrett, Adrian Kent, and David Wallace. *Many Worlds?: Everett, Quantum Theory, & Reality*. Oxford University Press, June 2010. Google-Books-ID: LGkVDAAAQBAJ. [11](#)
- [12] David Deutsch. Quantum theory as a universal physical theory. *International Journal of Theoretical Physics*, 24(1):1–41, January 1985. [11](#)

- [13] L. Diósi. Quantum Master Equation of a Particle in a Gas Environment. *Europhys. Lett.*, 30:63, 1995. [17](#)
 - [14] C. F. Bohren and D. R. Huffman. *Absorption and Scattering of Light by Small Particles*. WILEY-VCH Verlag, Weinheim, 2004. [25](#), [79](#)
 - [15] H. Pino, J. Prat-Camps, K. Sinha, B. Prasanna Venkatesh, and O. Romero-Isart. On-chip quantum interference of a superconducting microsphere. *Quantum Science and Technology*, 3(2):025001, January 2018. Publisher: IOP Publishing. [26](#), [85](#), [89](#), [90](#), [91](#), [92](#), [93](#), [94](#)
 - [16] Klaus Hornberger and John E. Sipe. Collisional decoherence reexamined. *Phys. Rev. A*, 68(1):012105, Jul 2003. [26](#)
 - [17] James Bateman, Stefan Nimmrichter, Klaus Hornberger, and Hendrik Ulbricht. Near-field interferometry of a free-falling nanoparticle from a point-like source. *Nature communications*, 5:4788, January 2014. [26](#), [80](#), [81](#), [82](#), [83](#), [84](#), [85](#)
 - [18] L. Hackermüller, K. Hornberger, B. Brezger, A. Zeilinger, and M. Arndt. Decoherence in a talbot-lau interferometer: the influence of molecular scattering. *Applied Physics B*, 77(8):781–787, Dec 2003. [31](#)
 - [19] Lucia Hackermüller, Klaus Hornberger, Björn Brezger, Anton Zeilinger, and Markus Arndt. Decoherence of matter waves by thermal emission of radiation. *Nature*, 427:711–714, 2004. [31](#)
 - [20] E. Joos and H. D. Zeh. The emergence of classical properties through interaction with the environment. *Zeitschrift für Physik B Condensed Matter*, 59:223–243, 1985. 10.1007/BF01725541. [31](#), [66](#)
 - [21] M. Arndt, O. Nairz, J. Voss-Andreae, C. Keller, G. Van der Zouw, and A. Zeilinger. Wave-particle duality of C₆₀ molecules. *Nature*, 401:680–682, 1999. [36](#), [71](#), [73](#)
 - [22] Peter Asenbaum, Stefan Kuhn, Stefan Nimmrichter, Ugur Sezer, and Markus Arndt. Cavity cooling of free silicon nanoparticles in high vacuum. *Nature Communications*, 4, October 2013. [38](#)
 - [23] Nikolai Kiesel, Florian Blaser, Uros Delic, David Grass, Rainer Kaltenbaek, and Markus Aspelmeyer. Cavity cooling of an optically levitated submicron particle. *Proceedings of the National Academy of Sciences of the United States of America*, 110(35):14180–14185, 2013. [38](#)
 - [24] J. Millen, P. Z. G. Fonseca, T. Mavrogordatos, T. S. Monteiro, and P. F. Barker. Cavity cooling a single charged levitated nanosphere. *Phys. Rev. Lett.*, 114:123602, Mar 2015. [38](#)
-

- [25] Uroš Delić, Manuel Reisenbauer, David Grass, Nikolai Kiesel, Vladan Vuletić, and Markus Aspelmeyer. Cavity Cooling of a Levitated Nanosphere by Coherent Scattering. *Physical Review Letters*, 122(12):123602, mar 2019. [38](#)
- [26] Dominik Windey, Carlos Gonzalez-Ballester, Patrick Maurer, Lukas Novotny, Oriol Romero-Isart, and René Reimann. Cavity-Based 3D Cooling of a Levitated Nanoparticle via Coherent Scattering. *Physical Review Letters*, 122(12):123601, mar 2019. [38](#)
- [27] Sandra Eibenberger, Stefan Gerlich, Markus Arndt, Marcel Mayor, and Jens Tüxen. Matter-wave interference of particles selected from a molecular library with masses exceeding 10,000 amu. *Physical chemistry chemical physics : PCCP*, 15(35):14696–700, September 2013. [38](#), [73](#)
- [28] Rainer Kaltenbaek, Markus Aspelmeyer, Peter F Barker, Angelo Bassi, James Bateman, Kai Bongs, Sougato Bose, Claus Braxmaier, Časlav Brukner, Bruno Christophe, Michael Chwalla, Pierre-François Cohadon, Adrian Michael Cruise, Catalina Curceanu, Kishan Dholakia, Lajos Diósi, Klaus Döringshoff, Wolfgang Ertmer, Jan Gieseler, Norman Gürlebeck, Gerald Hechenblaikner, Antoine Heidmann, Sven Herrmann, Sabine Hossenfelder, Ulrich Johann, Nikolai Kiesel, Myungshik Kim, Claus Lämmerzahl, Astrid Lambrecht, Michael Mazilu, Gerard J Milburn, Holger Müller, Lukas Novotny, Mauro Paternostro, Achim Peters, Igor Pikovski, André Pilan Zanoni, Ernst M Rasel, Serge Reynaud, Charles Jess Riedel, Manuel Rodrigues, Loïc Rondin, Albert Roura, Wolfgang P Schleich, Jörg Schmiedmayer, Thilo Schuldt, Keith C Schwab, Martin Tajmar, Guglielmo M Tino, Hendrik Ulbricht, Rupert Ursin, and Vlatko Vedral. Macroscopic Quantum Resonators (MAQRO): 2015 update. *EPJ Quantum Technology*, 3(1):5, March 2016. [39](#), [65](#), [85](#)
- [29] J. S. Bell. Against “measurement”. In Miller, A. I., editor, *Sixty-Two Years of Uncertainty*, pages 17–31. Plenum Press, 1990. [41](#)
- [30] Yaakov Y. Fein, Philipp Geyer, Patrick Zwick, Filip Kiałka, Sebastian Pedalino, Marcel Mayor, Stefan Gerlich, and Markus Arndt. Quantum superposition of molecules beyond 25 kDa. *Nature Physics*, pages 1–4, sep 2019. [41](#), [78](#), [85](#)
- [31] Philip Pearle. Reduction of the state vector by a nonlinear Schrödinger equation. *Phys. Rev. D*, 13(4):857–868, Feb 1976. [42](#)
- [32] N. Gisin. Weinberg’s non-linear quantum mechanics and supraluminal communications. *Physics Letters A*, 143(1):1 – 2, 1990. [42](#)
- [33] G. C. Ghirardi, A. Rimini, and T. Weber. Unified dynamics for microscopic and macroscopic systems. *Phys. Rev. D*, 34(2):470–491, Jul 1986. [42](#), [58](#)

- [34] Gian Carlo Ghirardi, Philip Pearle, and Alberto Rimini. Markov processes in hilbert space and continuous spontaneous localization of systems of identical particles. *Phys. Rev. A*, 42(1):78–89, Jul 1990. [43](#), [47](#)
- [35] Luca Ferialdi and Angelo Bassi. Dissipative collapse models with nonwhite noises. *Phys. Rev. A*, 86:022108, Aug 2012. [43](#)
- [36] Angelo Bassi and Davide G M Salvetti. The quantum theory of measurement within dynamical reduction models. *Journal of Physics A: Mathematical and Theoretical*, 40(32):9859–9876, jul 2007. [45](#)
- [37] Brian Collett and Philip Pearle. Wavefunction Collapse and Random Walk. *Foundations of Physics*, 33:1495–1541, 2003. 10.1023/A:1026048530567. [47](#)
- [38] Rainer Kaltenbaek, Gerald Hechenblaikner, Nikolai Kiesel, Oriol Romero-Isart, Keith C. Schwab, Ulrich Johann, and Markus Aspelmeyer. Macroscopic quantum resonators (MAQRO). *Experimental Astronomy*, 34:123–164, 2012. [47](#)
- [39] O. Romero-Isart, A. C. Pflanzer, F. Blaser, R. Kaltenbaek, N. Kiesel, M. Aspelmeyer, and J. I. Cirac. Large Quantum Superpositions and Interference of Massive Nanometer-Sized Objects. *Phys. Rev. Lett.*, 107(2):020405, Jul 2011. [47](#), [93](#)
- [40] F. Károlyházy. Gravitation and quantum mechanics of macroscopic objects. *Il Nuovo Cimento A*, 42(2):390–402, March 1966. [48](#)
- [41] L. Diósi. A universal master equation for the gravitational violation of quantum mechanics. *Physics Letters A*, 120(8):377–381, March 1987. [48](#)
- [42] L. Diósi. Gravitation and quantum-mechanical localization of macro-objects. *Physics Letters A*, 105(4–5):199 – 202, 1984. [48](#), [53](#)
- [43] Lajos Diósi. Notes on certain newton gravity mechanisms of wavefunction localization and decoherence. *Journal of Physics A: Mathematical and Theoretical*, 40(12):2989, 2007. [48](#)
- [44] Roger Penrose. On the Gravitization of Quantum Mechanics 1: Quantum State Reduction. *Foundations of Physics*, 44(5):557–575, May 2014. [48](#), [61](#)
- [45] Lajos Diósi. Intrinsic Time-Uncertainties and Decoherence: Comparison of 4 Models. *Braz. J. Phys.*, 35(2A):260, 2005. [48](#), [51](#), [52](#), [53](#), [54](#), [55](#)
- [46] G. J. Milburn. Intrinsic decoherence in quantum mechanics. *Phys. Rev. A*, 44:5401–5406, Nov 1991. [52](#), [53](#)

- [47] G. J. Milburn. Lorentz invariant intrinsic decoherence. *New Journal of Physics*, 8(6):96–96, jun 2006. [53](#)
 - [48] L. Diósi. Models for universal reduction of macroscopic quantum fluctuations. *Phys. Rev. A*, 40:1165–1174, Aug 1989. [53](#)
 - [49] R. Penrose. Gravity and quantum mechanics. In *General Relativity and Gravitation 13. Part 1: Plenary Lectures 1992*, pages 179–189. Institute of Physics Publishing, Bristol, Philadelphia, 1998. [53](#)
 - [50] Roger Penrose. On Gravity’s role in Quantum State Reduction. *General Relativity and Gravitation*, 28(5):581–600, May 1996. [53](#), [54](#)
 - [51] Igor Pikovski, Magdalena Zych, Fabio Costa, and Časlav Brukner. Universal decoherence due to gravitational time dilation. *Nature Physics*, 11(8):668–672, June 2015. [55](#), [56](#)
 - [52] Stephen L Adler. Lower and upper bounds on csl parameters from latent image formation and igm heating. *Journal of Physics A: Mathematical and Theoretical*, 40(12):2935, 2007. [58](#)
 - [53] Matteo Carlesso, Angelo Bassi, Paolo Falferi, and Andrea Vinante. Experimental bounds on collapse models from gravitational wave detectors. *Phys. Rev. D*, 94:124036, Dec 2016. [57](#), [58](#), [65](#)
 - [54] A. Vinante, M. Carlesso, A. Bassi, A. Chiasera, S. Varas, P. Falferi, B. Margesin, R. Mezzena, and H. Ulbricht. Narrowing the Parameter Space of Collapse Models with Ultracold Layered Force Sensors. *Physical Review Letters*, 125(10):100404, September 2020. [57](#)
 - [55] A. Vinante, R. Mezzena, P. Falferi, M. Carlesso, and A. Bassi. Improved noninterferometric test of collapse models using ultracold cantilevers. *Phys. Rev. Lett.*, 119:110401, Sep 2017. [59](#), [65](#)
 - [56] Sandro Donadi, Kristian Piscicchia, Catalina Curceanu, Lajos Diósi, Matthias Laubenstein, and Angelo Bassi. Underground test of gravity-related wave function collapse. *Nature Physics*, 17(1):74–78, January 2021. Number: 1 Publisher: Nature Publishing Group. [60](#), [61](#)
 - [57] GianCarlo Ghirardi, Renata Grassi, and Alberto Rimini. Continuous-spontaneous-reduction model involving gravity. *Physical Review A*, 42(3):1057–1064, August 1990. [60](#)
 - [58] Lajos Diósi. Gravity-related wave function collapse: mass density resolution. *Journal of Physics: Conference Series*, 442:012001, June 2013. [60](#)
-

- [59] Rainer Kaltenbaek. Feasibility considerations for free-fall tests of gravitational decoherence. *arXiv:2111.01483*, November 2021. [60](#), [62](#)
 - [60] Dominic Branford, Christos N. Gagatsos, Jai Grover, Alexander J. Hickey, and Animesh Datta. Quantum enhanced estimation of diffusion. *Physical Review A*, 100(2):022129, August 2019. [63](#)
 - [61] R Kaltenbaek, G Hechenblaikner, N Kiesel, F Blaser, S Gröblacher, S Hofer, W Vanner, M R Wieczorek, K C Schwab, U Johann, and M Aspelmeyer. Macroscopic quantum experiments in space using massive mechanical resonators. Technical report, Study conducted under contract with the European Space Agency, Po P5401000400, 2011–2012. [65](#)
 - [62] Rainer Kaltenbaek and Markus Aspelmeyer. Optomechanical Schrödinger cats - a case for space. In Reiter, WL and Yngvason, J, editor, *Erwin Schrödinger - 50 Years After*, volume 9 of *ESI Lectures in Mathematics and Physics*, pages 123–134. Europ. Math. Soc., 2013. International Symposium on Erwin Schrodinger - 50 Years After, ESI, Boltzmann Lect Hall, Vienna, ITALY, JAN 13-15, 2011. [65](#)
 - [63] Klaus Hornberger, Stefan Gerlich, Philipp Haslinger, Stefan Nimmrichter, and Markus Arndt. Colloquium: Quantum interference of clusters and molecules. *Rev. Mod. Phys.*, 84:157–173, 2012. [65](#)
 - [64] W. P. Schleich. *Quantum Optics in Phase Space*. WILEY-VCH Verlag, Berlin, 2001. [67](#), [68](#), [82](#)
 - [65] S. Nimmrichter and K. Hornberger. Theory of near-field matter-wave interference beyond the eikonal approximation. *Phys. Rev. A*, 78:023612, 2008. [67](#)
 - [66] Dietrich Leibfried, Tilman Pfau, and Christopher Monroe. Shadows and mirrors: Reconstructing quantum states of atom motion. *Physics Today*, 51:22–28, 04 1998. [69](#)
 - [67] William B Case, Mathias Tomandl, Sarayut Deachapunya, and Markus Arndt. Realization of optical carpets in the Talbot and Talbot-Lau configurations. *Optics express*, 17(23):20966–74, nov 2009. [71](#)
 - [68] S. Nimmrichter. *Macroscopic Matter-wave Interferometry*. PhD thesis, Univeristy of Vienna, 2013. [72](#), [73](#), [75](#), [76](#), [77](#)
 - [69] Philipp Haslinger, Nadine Dörre, Philipp Geyer, Jonas Rodewald, Stefan Nimmrichter, and Markus Arndt. A universal matter-wave interferometer with optical ionization gratings in the time domain. *Nat. Phys.*, 9:144–148, February 2013. [72](#), [74](#), [75](#)
-

- [70] Klaus Hornberger, Stefan Gerlich, Hendrik Ulbricht, Lucia Hackermüller, Stefan Nimmrichter, Ilya V Goldt, Olga Boltalina, and Markus Arndt. Theory and experimental verification of Kapitza–Dirac–Talbot–Lau interferometry. *New Journal of Physics*, 11(4):043032, apr 2009. [73](#)
- [71] Benjamin A. Stickler, Klaus Hornberger, and M. S. Kim. Quantum rotations of nanoparticles. *Nature Reviews Physics*, pages 1–9, June 2021. [85](#), [86](#)
- [72] Lukas Martinetz, Klaus Hornberger, James Millen, M. S. Kim, and Benjamin A. Stickler. Quantum electromechanics with levitated nanoparticles. *npj Quantum Information*, 6(1):1–8, December 2020. Number: 1 Publisher: Nature Publishing Group. [85](#)
- [73] Uroš Delić, Manuel Reisenbauer, Kahan Dare, David Grass, Vladan Vuletić, Nikolai Kiesel, and Markus Aspelmeyer. Cooling of a levitated nanoparticle to the motional quantum ground state. *Science*, page eaba3993, jan 2020. [85](#)
- [74] Lorenzo Magrini, Philipp Rosenzweig, Constanze Bach, Andreas Deutschmann-Olek, Sebastian G. Hofer, Sungkun Hong, Nikolai Kiesel, Andreas Kugi, and Markus Aspelmeyer. Real-time optimal quantum control of mechanical motion at room temperature. *Nature*, 595(7867):373–377, July 2021. Bandiera_abtest: a Cg_type: Nature Research Journals Number: 7867 Primary_atype: Research Publisher: Nature Publishing Group Subject_term: Quantum mechanics;Quantum optics Subject_term_id: quantum-mechanics;quantum-optics. [85](#)
- [75] Felix Tebbenjohanns, M. Luisa Mattana, Massimiliano Rossi, Martin Frimmer, and Lukas Novotny. Quantum control of a nanoparticle optically levitated in cryogenic free space. *Nature*, 595(7867):378–382, July 2021. [85](#)
- [76] D. E. Chang, C. A. Regal, S. B. Papp, D. J. Wilson, J. Ye, O. Painter, H. J. Kimble, and P. Zoller. Cavity opto-mechanics using an optically levitated nanosphere. *Proceedings of the National Academy of Sciences of the United States of America*, 107(3):1005–1010, 2010. [85](#)
- [77] Stefan Kuhn, Alon Kosloff, Benjamin A. Stickler, Fernando Patolsky, Klaus Hornberger, Markus Arndt, and James Millen. Full rotational control of levitated silicon nanorods. *Optica*, 4(3):356, mar 2017. [85](#), [86](#), [87](#)
- [78] Stefan Kuhn, Peter Asenbaum, Alon Kosloff, Michele Sclafani, Benjamin A. Stickler, Stefan Nimmrichter, Klaus Hornberger, Ori Cheshnovsky, Fernando Patolsky, and Markus Arndt. Cavity-Assisted Manipulation of Freely Rotating Silicon Nanorods in High Vacuum. *Nano Letters*, 15(8):5604–5608, aug 2015. [85](#), [86](#)
-

- [79] Benjamin A. Stickler, Birthe Papendell, and Klaus Hornberger. Spatio-orientational decoherence of nanoparticles. *Physical Review A*, 94(3):033828–033828, September 2016. [86](#)
- [80] Benjamin A Stickler, Birthe Papendell, Stefan Kuhn, Björn Schrinski, James Millen, Markus Arndt, and Klaus Hornberger. Probing macroscopic quantum superpositions with nanorotors. *New Journal of Physics*, 20(12):122001, dec 2018. [86](#), [87](#), [88](#)
- [81] O. Romero-Isart, L. Clemente, C. Navau, A. Sanchez, and J. I. Cirac. Quantum magnetomechanics with levitating superconducting microspheres. *Phys. Rev. Lett.*, 109:147205, Oct 2012. [89](#)
- [82] Oriol Romero-Isart. Coherent inflation for large quantum superpositions of levitated microspheres. *New Journal of Physics*, 19(12):123029, December 2017. [90](#)
- [83] H. Pino, J. Prat-Camps, K. Sinha, B. P. Venkatesh, and O. Romero-Isart. Quantum Interference of a Microsphere. *arXiv:1603.01553*, pages 20–20, March 2016. [90](#)